STRENGTH DEGRADATION OF PRE-FATIGUED GFRP COMPOSITES UNDER HYGROTHERMAL LOADING CONDITIONS

A
Thesis Report

submitted in partial fulfilment of the requirement for the award of degree

MASTER OF ENGINEERING
IN
CAD/CAM & ROBOTICS

Submitted by
ABHINEET SAINI
Roll No. 800881002

Under Guidance of

Dr. ABHIJIT MUKHERJEE
Director
Thapar University, Patiala

Dr. RAHUL CHHIBBER
Assistant Professor
Deptt. Of Mechanical Engg.
Thapar University, Patiala

DEPARTMENT OF MECHANICAL ENGINEERING
THAPAR UNIVERSITY
PATIALA-147004, INDIA

July 2010

CERTIFICATE

This is to certify that the work done in this thesis report titled "**Strength Degradation of Pre-fatigued Glass Fibre Reinforced Polymer Composites under Hygrothermal Loading Conditions**" submitted in partial fulfilment of requirement for the award of **Master of Engineering Degree in CAD/CAM/Robotics** in the Mechanical Engineering Department of Thapar University, Patiala, is an authentic record of work carried out by me under the guidance of **Dr. Abhijit Mukherjee, Director, Thapar University, Patiala and Dr. Rahul Chhibber, Assistant Professor, Mechanical Engineering Department, Thapar University, Patiala.**

The matter embodied in this report has not been submitted in part or full to any other university or institute for the award of any degree.

Dated: 15 July 2010 **(Abhineet Saini)**

This is to certify that above declaration made by the student concerned is correct to the best of my knowledge & belief.

Dr. Abhijit Mukherjee
Director
Thapar University, Patiala

Dr. Rahul Chhibber
Assistant Professor
Deptt. of Mechanical Engg.
Thapar University, Patiala

Dr. S.K. Mohapatra
Professor & HOD
Deptt. of Mechanical Engg.
Thapar University, Patiala

Dr. R.K. Sharma
Dean
Deptt. of Academic Affairs
Thapar University, Patiala

ACKNOWLEDGEMENT

I am highly grateful to the authorities of Thapar University, Patiala for providing this opportunity to carry out the seminar work. I would like to express a deep sense of gratitude and thank profusely to my thesis guide Dr Abhijit Mukherjee & Dr Rahul Chhibber for their sincere & invaluable guidance, suggestions and attitude which inspired me to submit seminar report in the present form.

I am very thankful to all the staff members of mechanical workshop for their timely guidance and help for the work being done.

I am also thankful to other faculty members of Mechanical Department, TU, Patiala for their intellectual support.

My special thanks are due to my family members and friends who constantly encouraged me to complete this study.

Abhineet Saini

ABSTRACT

Composite materials are engineered materials made from two or more constituent materials with significantly different physical or chemical properties which remain separate and distinct on a macroscopic level within the finished structure.
Glass fibre-reinforced polymer (GFRP) have been used as an alternative to steel in concrete due to high strength-to-weight ratio, high stiffness-to-weight ratio, and corrosion and fatigue resistance.

GFRP's have been found attractive in the Asian region due to their cost competitiveness in comparison. Wide-spread use of fibre-reinforced polymers (FRP) in construction is hampered in this part of world due to lack of long-term durability and performance data, especially in a tropical environment.

The main environmental factors for the deterioration of GFRP are temperature, sunshine, water/moisture, alkalinity and load. Most of the early durability tests were carried out with reference to application of FRP (Fibre Reinforced Polymer) in aerospace.

With the consideration of the above points an experimental study was conducted to perform the pre-fatigue of GFRP specimen and then placing them in water at different temperatures i.e. 45°C and 55°C for one month and two month and observing the degradation in tensile strength for the specimen under investigation.
Simultaneously macroscopic and microscopic behavior of the specimen were also studied at regular intervals and results were drawn graphically.
In the end comparison for specimen exposed to different conditions of pre-fatigue load, time and temperature was done and different macroscopic and microscopic behaviors were observed and compared one on one in the graphical manner.

TABLE OF CONTENTS

LIST OF FIGURES

LIST OF TABLES

CHAPTER 1 INTRODUCTION

1.1 COMPOSITE[2]

Composite materials are engineered materials made from two or more constituent materials with significantly different physical or chemical properties which remain separate and distinct on a macroscopic level within the finished structure.

Composites are made up of individual materials referred to as constituent materials. There are two categories of constituent materials: **matrix and reinforcement**. At least one portion of each type is required. The matrix material surrounds and supports the reinforcement materials by maintaining their relative positions. The reinforcements impart their special mechanical and physical properties to enhance the matrix properties.

Usually composites have these two phases:

- **MATRIX PHASE**

The primary phase, having a continuous character, is called matrix. Matrix is usually more ductile and less hard phase. It holds the dispersed phase and shares a load with it.

- **DISPERSED (REINFORCING) PHASE**

The second phase (or phases) is imbedded in the matrix in a discontinuous form. This secondary phase is called dispersed phase. Dispersed phase is usually stronger than the matrix, therefore it is sometimes called reinforcing phase.

Properties of composites depend on

- properties of phases
- geometry of dispersed phase (particle size, distribution, orientation)
- amount of phase

1.2 CLASSIFICATION OF COMPOSITE[2]

Composites can be broadly classified in to two groups. They are

1.2.1 NATURAL COMPOSITES: Several natural materials can be grouped under natural composites. Eg. Bones, wood, shells, pearlite (steel which is a mixture of a phase and Fe_3C) etc.

1.2.2 MAN-MADE COMPOSITES: Man-made composites are produced by combining two or more materials in definite proportions under controlled conditions. Eg. Mud mixed straw to

produce stronger mud mortar and bricks, Plywood, Chipboards, Decorative laminates, Fibre Reinforced Plastic (FRP),Carbon Composites, Concrete and RCC, Reinforced Glass etc

Classification of Composites I

(Based on matrix material)

Metal Matrix Composites (MMC)

Metal Matrix Composites are composed of a metallic matrix (aluminum, magnesium, iron, cobalt, copper) and a dispersed ceramic (oxides, carbides) or metallic (lead, tungsten, molybdenum) phase.

Ceramic Matrix Composites (CMC)

Ceramic Matrix Composites are composed of a ceramic matrix and embedded fibers of other ceramic material (dispersed phase).

Polymer Matrix Composites (PMC)

Polymer Matrix Composites are composed of a matrix from thermo set (Unsaturated Polyester (UP), Epoxy (EP)) or thermoplastic (Polycarbonate (PC), Polyvinylchloride, Nylon, Polystyrene) and embedded glass, carbon, steel or Kevlar fibers (dispersed phase).

Classification of composite materials II[33]

(Based on reinforcing material structure)

Particulate Composites

Particulate Composites consist of a matrix reinforced by a dispersed phase in form of particles as shown in fig. 1.1.

1. **Composites with random orientation of particles.**
2. **Composites with preferred orientation of particles.** Dispersed phase of these materials consists of two-dimensional flat platelets (flakes), laid parallel to each other.

Fibrous Composites

1. **Short-fiber reinforced composites.** Short-fiber reinforced composites consist of a matrix reinforced by a dispersed phase in form of discontinuous fibers (length < 100 diameter) (Fig. 1.1).
    1. **Composites with random orientation of fibers.**

2. **Composites with preferred orientation of fibers.**

2. **Long-fiber reinforced composites.** Long-fiber reinforced composites consist of a matrix reinforced by a dispersed phase in form of continuous fibers.
    1. **Unidirectional orientation of fibers.**
    2. **Bidirectional orientation of fibers (woven).**

Laminate Composites

When a fiber reinforced composite consists of several layers with different fiber orientations, it is called **multilayer (angle-ply) composite**.

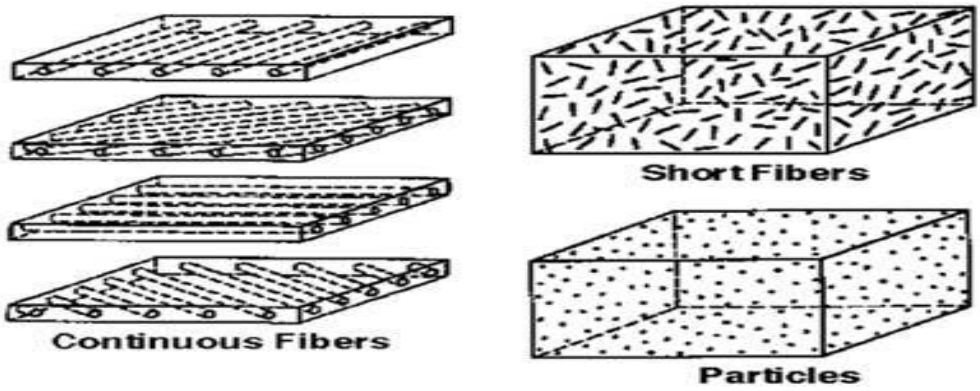

Fig. 1.1 Types of composites[33]

1.3 ADVANTAGES OF USING COMPOSITES OVER METALS

- Very high specific strength. Which means very high strength and low weight
- Great freedom of shape. Double curved and complex parts can be simple produced.
- High degree of integration possible. Which means simple integration of stiffeners, inserts, cores, and production of self supporting structures in one or two production cycles?
- Material can be tailored. Which means fit for the loads / performance the end product has to perform during its lifetime
- Excellent fatigue endurance concerning number of load cycles (many times higher than with metals) and residual fatigue strength *(*aramide and carbon epoxy laminates retain more than 60% of their residual static strength, which is far more higher than is possible with metals*).*
- Excellent chemical resistance against acids, chemicals etc.
- Excellent weather/water resistance. Material has almost no corrosion, takes on little water which leads to low maintenance cost especially on the long run.
- Composites have excellent RAM features (Radar absorbing materials). It's also possible to make special laminates which are radar and sonar transparent.
- Excellent impact habits

- Excellent electrical habits, concerning isolation but also conduction, dielectric habits, EMS shielding etc. Structures can be tailored on RF transparency but can also be made RF reflecting. Great for telecom especially UMTS frequencies.
- Great thermal isolation habits, fire retardant habits, and high temperature performance.

1.4 USES OF COMPOSITE MATERIALS

1. Extensively used in space technology and production of Aerospace Components (tails, wings etc.)
2. Used in the production of sport goods e.g. racing car bodies and bicycle frames etc.
3. Used for general industrial and engineering structures
4. Used in high speed and fuel efficient transport vehicles
5. The shell composed of CosmoLite, a thermoplastic fibre-reinforced composite and the exterior surface SpectraLite which incorporates DuPont Surlyn, an impact-resistant coating found on golf balls.
6. Carbon composite is a key material in today's launch vehicles and spacecraft. It is widely used in solar panel substrates, antenna reflectors and yokes of spacecraft. It is also used in payload adapters, inter-stage structures and heat shields of launch vehicles.

1.5 INTRODUCTION TO FIBRE REINFORCED POLYMERS (FRP)

Fibre-reinforced polymer (**FRP**) (also fibre-reinforced plastic) is a composite material made of a polymer matrix reinforced with fibres. The fibers are usually fiberglass, carbon (Fig. 1.2), or aramid, while the polymer is usually an epoxy, vinyl ester or polyester thermosetting plastic. FRPs are commonly used in the aerospace, automotive, marine, and construction industries.

Fig. 1.2 Link made of carbon fibre[30]

The strength properties of FRP collectively make up one of the primary reasons for which civil engineers select them in the design of structures. A material's strength is governed by its ability to sustain a load without excessive deformation or failure. When an FRP specimen is tested in axial tension, the applied force per unit cross-sectional area (stress) is proportional to the ratio of change in a specimen's length to its original length (strain). When the applied load is removed, FRP returns to its original shape or length. In other words, FRP responds linear-elastically to axial stress. The response of FRP to axial compression is reliant on the relative proportion in volume of fibres, the properties of the fibre and resin, and the interface bond strength.
FRP's response to transverse tensile stress is very much dependent on the properties of the fiber and matrix, the interaction between the fiber and matrix, and the strength of the fiber-matrix interface. Generally, however, tensile strength in this direction is very poor.

According to orientation of fibre (Fig.1.3) they can be categorized as:

1. Unidirectional
2. Bidirectional
   - Cross Ply
   - Angle Ply

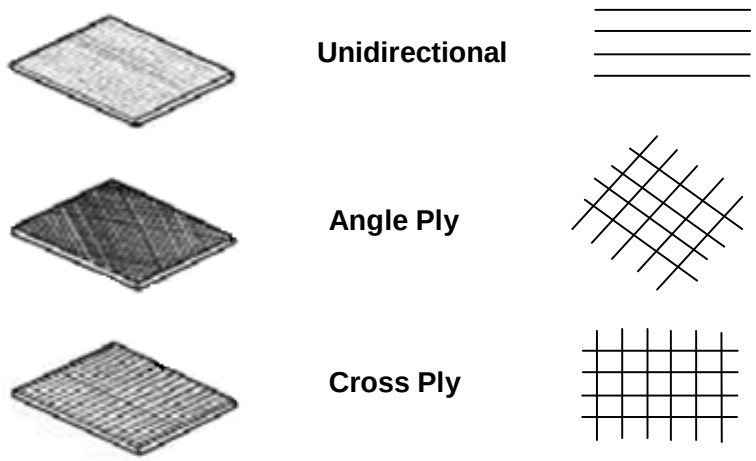

Fig. 1.3 Fibre orientation types[33]

1.6 ADVANTAGES OF FRP:

1. High strength to weight ratio
2. Corrosion resistant
3. Can be tailored for the application (both shape and type of FRP)
4. FRP has a low cost considering other materials
5. Cost of installation versus replacement is low
6. Cost of installation time (both direct and indirect) is also low.

1.7 TYPES OF FIBER

A. Carbon Fibre

Carbon fibres are created when polyacrylonitrile fibres (PAN), Pitch resins, or Rayon are carbonized (through oxidation and thermal pyrolysis) at high temperatures. Through further processes of graphitizing or stretching the fibers strength or elasticity can be enhance respectively. Carbon fibers are manufactured in diameters analogous to glass fibers with diameters ranging from 9 to 17 µm. These fibers wound into larger threads for transportation and further production processes. Further production processes include weaving or braiding into carbon fabrics, cloths and mats analogous to those described for glass that can then be used in actual reinforcement processes (Fig.1.4).

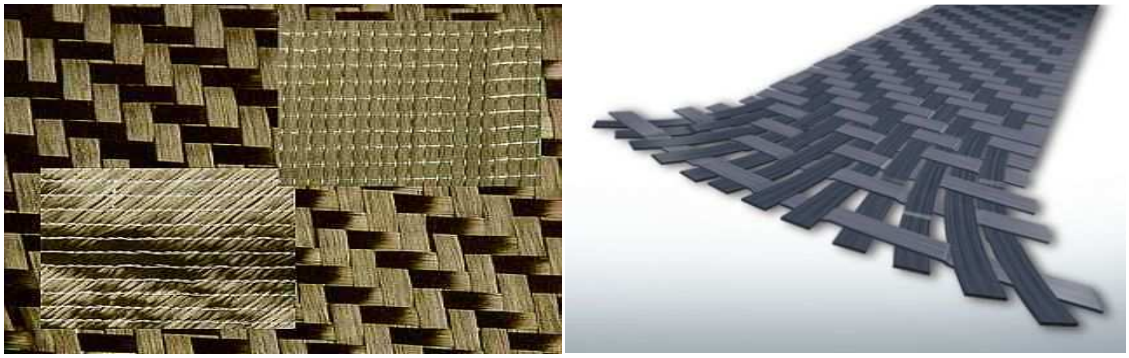

Fig. 1.4 Different types of matted carbon fibres[10]

B. Glass Fibre

FRP plastics use textile glass fibers; textile fibers are different from other forms of glass fibers used for insulating applications. Textile glass fibers begin as varying combinations of SiO_2, Al_2O_3, B_2O_3, CaO, or MgO in powder form. These mixtures are then heated through a direct melt process to temperatures around 1300 degrees Celsius, after which dies are used to extrude filaments of glass fiber in diameter ranging from 9 to 17 µm. These filaments are then wound into larger threads and spun onto bobbins for transportation and further processing. Glass fiber is by far the most popular means to reinforce plastic and thus enjoys a wealth of production processes, some of which are applicable to aramid and carbon fibers as well owing to their shared fibrous qualities. Different types of glass fibre are shown in the Fig.1.5.

Fig. 1.5 Commercially available glass fibres[10]

The types of glasses used for structural reinforcements are as follows:

1) **E-glass** (electrical) - lower alkali content and stronger than A glass (alkali). Good tensile and compressive strength and stiffness, good electrical properties and relatively low cost, but impact resistance relatively poor. E-glass is the most common form of reinforcing fibre used in polymer matrix composites.

2) **C-glass** (chemical) - best resistance to chemical attack. Mainly used in the form of surface tissue in the outer layer of laminates used in chemical and water pipes and tanks.

3) **R, S or T-glass** – manufacturers' trade names for equivalent fibres having higher tensile strength and modulus than E glass, with better wet strength retention. Higher ILSS and wet out properties are achieved through smaller filament diameter. Developed for aerospace and defence industries, and used in some hard ballistic armour applications. This factor, and low production volumes mean relatively high price.

Glass fibre is available in the following forms as shown in Fig.1.6:

A. Continuous Fibre
B. Chopped strands
C. Woven Fabric.

Continuous Fibre Chopped Fibre Woven Fibre

Fig. 1.6 Types of glass fibre[3]

C. Aramid (Kevlar) Fibre

Aramid fibre is a man-made organic polymer (an aromatic polyamide) produced by spinning a solid fibre from a liquid chemical blend. The bright golden yellow filaments produced can have a range of properties, but all have high strength and low density giving very high specific strength. All grades have good resistance to impact, and lower modulus grades are used extensively in ballistic applications. Compressive strength, however, is only similar to that of E glass. Although

most commonly known under its Dupont trade name 'Kevlar', there are now a number of suppliers of the fibre, most notably Akzo Nobel with 'Twaron'. Each supplier offers several grades of aramid with various combinations of modulus and surface finish to suit various applications. As well as the high strength properties, the fibres also offer good resistance to abrasion, and chemical and thermal degradation. However, the fibre can degrade slowly when exposed to ultraviolet light. Aramid fibres are usually available in the form of rovings, with texes ranging from about 20 to 800.

1.8 FIBRE TYPE COMPARISONS:

Materials	Density (g/cm^3)	Tensile Strength (MPa)	Young modulus (GPa)
E-Glass	2.55	2000	80
S-Glass	2.49	4750	89
Alumina (Saffil)	3.28	1950	297
Carbon	2.00	2900	525
Kevlar 29	1.44	2860	64
Kevlar 49	1.44	3750	136

Fig. 1.7 Comparison of typical properties for some common fibres[2]

1.9 TYPES OF FIBRE REINFORCED POLYMERS[18]:

- Carbon Fibre Reinforced Polymer (CFRP)
- Glass Fibre Reinforced Polymer (GFRP)
- Boron Fibre Reinforced Polymer (BFRP)
- Aramid Fibre Reinforced Polymer (AFRP)

Glass Fibre Reinforced Polymer (GFRP)

Glass fibre reinforced polymer is a material made of a plastic reinforced by fine fibres made of glass. Like carbon fibre reinforced plastic, the composite material is commonly referred to by the name of its reinforcing fibres (for properties of different glass fibres refer Fig.1.7). The plastic is thermosetting, most often polyester or vinyl ester, but other plastics, like epoxy, are also used. An individual structural glass fibre is both stiff and strong in tension and compression—that is, along its axis. On the other hand, the glass fibre is unstiff and unstrong in shear—that is, across its axis. Therefore if a collection of fibres can be arranged permanently in a preferred direction within a material, and if the fibres can be prevented from buckling in compression, then that material will become preferentially strong in that direction.

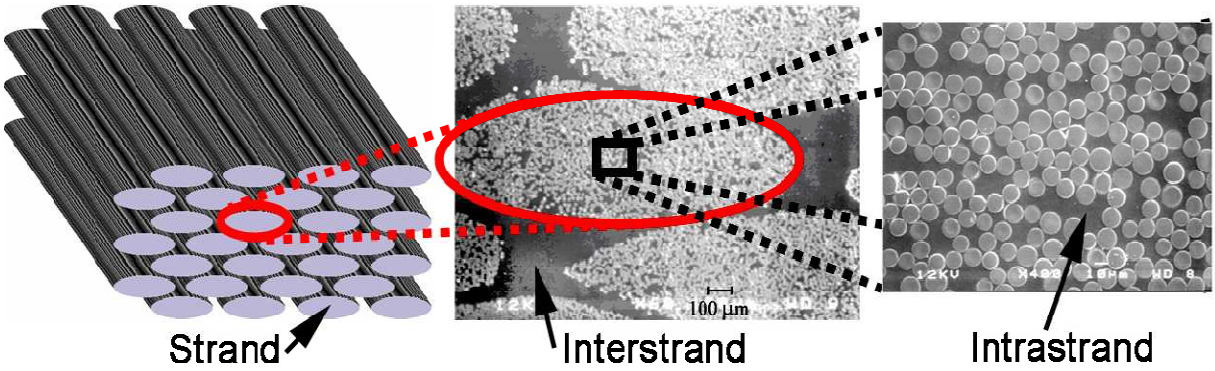

Fig. 1.8 GFRP Microstructure[5]

1.10 APPLICATIONS OF GLASS FIBRE REINFORCED POLYMERS[18]

- Sailplanes, sports cars, karts, body shells, boats, kayaks, flat roofs, lorries, wind turbine blades.
- Pods, domes and architectural features where a light weight is necessary.
- Bodies for automobiles.
- FRP tanks and vessels: FRP is used extensively to manufacture chemical equipments and tanks and vessels.
- UHF-broadcasting antennas are often mounted inside a glass-reinforced plastic cylinder on the pinnacle of a broadcasting tower.
- Engine intake manifolds are made from glass fiber reinforced PA 66.

  Advantages this has over caste aluminum manifolds are:

  - Up to a 60% reduction in weight
  - Improved surface quality and aerodynamics
  - Reduction in components by combining parts and forms into simpler molded shapes.
- Automotive gas and clutch pedals made from glass fiber reinforced PA 66 (DWP 12-13)

  Advantages over stamped aluminum are:

  - Pedals can be molded as single units combining both pedals and mechanical linkages simplifying the production and operation of the design.

- Fibers can be oriented to reinforce against specific stresses, increasing the durability and safety.

1.11 ENVIRONMENTAL EFFECTS ON FIBRE COMPOSITES [27]:

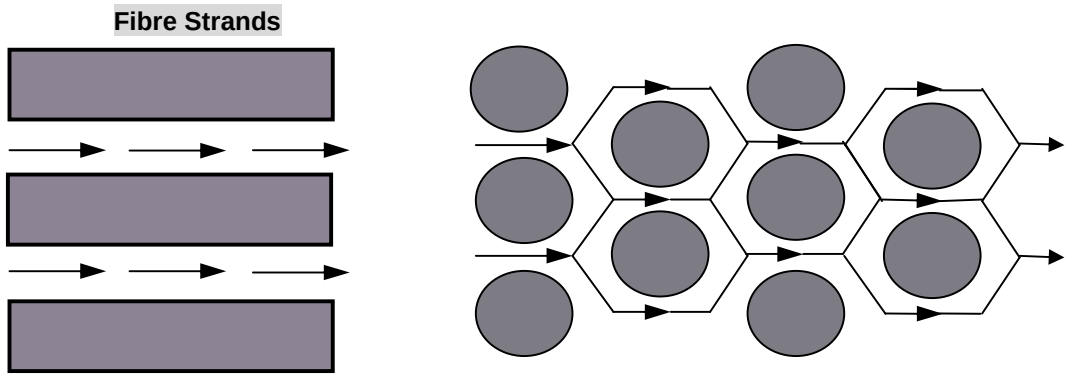

Fig. 1.9 Diffusion path of moisture into composite laminate in the thickness direction[27]

Fibrous composites, especially carbon fibre reinforced epoxy are increasingly being used in military and aerospace applications owing to several desirable properties including high specific strength, high specific stiffness and controlled anisotropy. Despite these advantages over conventional structural materials such as metals, composites are susceptible to heat and moisture when operating in harsh and changing environmental conditions. When exposed to humid environments, carbon–epoxy composites absorb moisture and undergo dilatational expansion (refer Fig. 1.9).

The presence of moisture and the stresses associated with moisture induced expansion can result in lowered damage tolerance, with an adverse effect on long-term structural durability. The amount of moisture absorbed by the epoxy matrix is significantly greater than that by the carbon fibres, which absorb very little or no moisture. This result in a significant mismatch in the moisture induced volumetric expansion between the matrix and the fibres, and thus leads to the evolution of localized stress and strain fields in the composite. Additionally, moisture absorption leads to changes in the thermo physical, mechanical and chemical characteristics of the epoxy matrix by plasticization and hydrolysis. These changes in the polymer structure lower both the elastic modulus and the glass transition temperature. At the same time, moisture wicking along the fibre matrix interface degrades the fibre matrix bond, resulting in loss of micro structural integrity. The net effect of moisture absorption is the deterioration of matrix-dominated properties such as compressive strength, interlaminar shear strength, fatigue resistance and impact tolerance .These factors lead to reduced damage tolerance and lack of long-term durability.

When the humid environmental condition is combined with UV exposure, its detrimental effect on the composite becomes obvious. A significant amount of the epoxy matrix is eroded after repeated exposures to humidity and UV. Such degradation decreases the transverse strength and

inter-laminar toughness. Moisture absorption characteristics of composites have been the subject of considerable investigation where transient moisture diffusion under normal environmental conditions is approximated as a Fickian process. In homogeneous materials, the kinetics of moisture diffusion is governed by the maximum moisture content and the diffusivity. The maximum moisture content is defined by the net amount of moisture that a fully saturated material contains under steady state equilibrium when exposed to a given environmental condition. It is usually expressed as the ratio of the increase in weight per unit dry weight at the point of saturation.

The time variation of relative weight gain can be measured as

$$w_t = \frac{W(t) - W_0}{W_0}$$

Here $W(t)$ is the total weight at time t and W_0 is the reference dry weight of the specimen. The relative weight gain approaches the maximum moisture content of composite at infinite time. It has been shown that the maximum moisture content strongly depends on the relative humidity of the exposure environment. Usually the maximum moisture content is determined by exposing the material to a humid environment for a long duration of time until steady state equilibrium is attained. This process often takes several months, which makes the procedure cumbersome and time consuming. Also the rate of moisture diffusion is governed by the diffusivity. In general, the diffusivity is a strong function of the ambient temperature and a weak function of the relative humidity. In the case of composites, the diffusion process is more complex. It depends on the diffusivities of the individual constituents, their relative volume fractions, constituent arrangement and morphology. Traditionally, effective diffusivity has been used to predict the amount of moisture content. The effective diffusivity can be estimated either using a rule-of-mixtures approach or numerical analyses. While the effective or average property is appropriate for conditions under *equilibrium* or *steady-state*, its applicability for transient moisture transport is, at best, questionable. More specifically, under transient condition, the effective or average property may not accurately describe the time variation of moisture content. An additional concern with the homogenized rule-of-mixtures approach is that it ignores the micro structural heterogeneity of a fibre-reinforced composite.

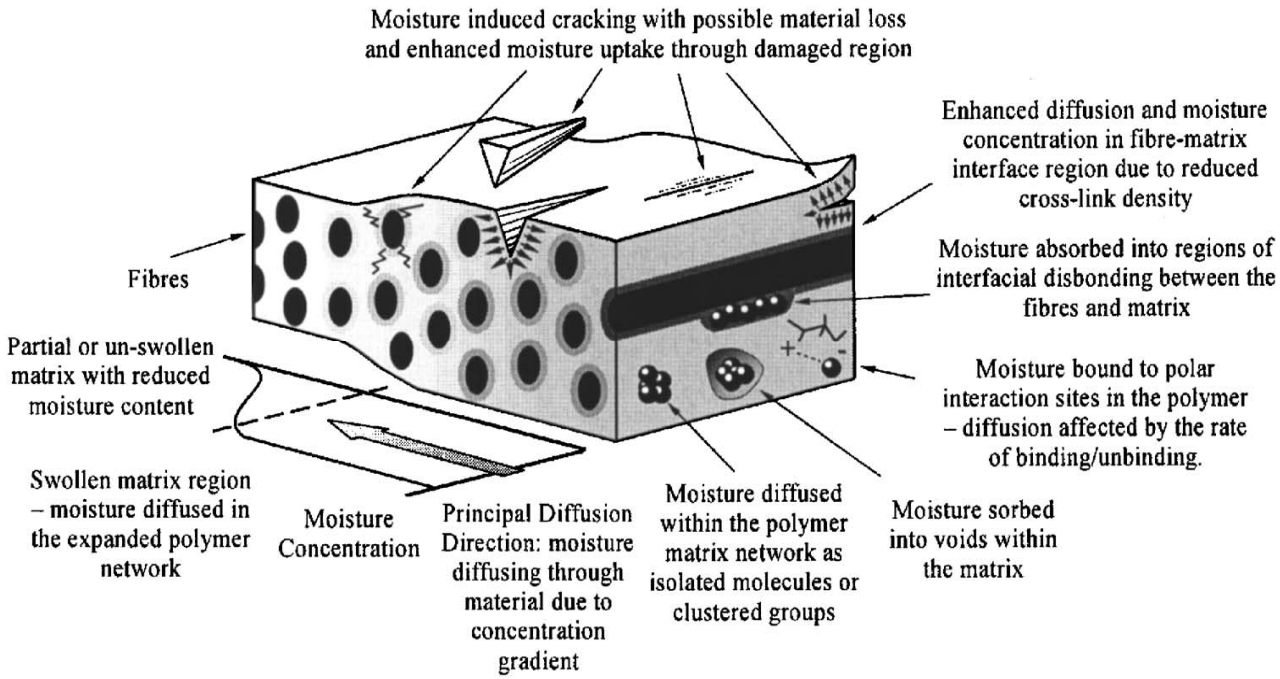

Fig. 1.10 Deteriorated fibre specimen under moist environmental condition[27]

When a fibre-reinforced composite material is exposed to a hygrothermal environment and mechanical loads, changes in material properties are expected (refer Fig. 1.10). These changes in material properties are connected to an irreversible material degradation. The moisture may affect the laminates through chemical changes such as relaxation and oxidation of the matrix material. A cyclic moisture environment exposed to a laminate may cause damage such as *debonding* at fibre/matrix interfaces and continuous cracks. Other damage modes that can occur in a fibre-composite laminate are transverse matrix cracks, delamination and fibre fracture. The results of chemical changes and mechanical damage in general affect the overall material properties, e.g. elastic modulus, hygrothermal expansion coefficients, diffusion coefficients.

Usually one of the first observed damage modes in a laminated composite is *matrix cracking*. These cracks are in general not critical for final failure, but if they are connected to a surrounding moisture environment more rapid moisture absorption may be expected for the cracked laminate. The accelerated moisture absorption in a cracked material exposed to humid air is a result of the faster diffusion in air compared to the diffusion speed in the composite material. Faster moisture uptake may also develop a faster material degradation. This makes it important to know the moisture absorption behaviour in a cracked laminate. For an undamaged material, well-accepted moisture transportation models are available. The most common models for the transportation of moisture in undamaged polymeric composite materials are *Fickian diffusion and Langmuir diffusion*. If the material contains cracks that significantly affect the moisture uptake, then the original laws of Fickian and Langmuir are no longer valid for the whole laminate, but locally they still work. The influences of matrix cracks on moisture uptake in glass-fibre/epoxy laminates have been studied.

CHAPTER 2 LITERATURE REVIEW

[1] A. Mukherjee, S.J. Arwikar (ACI Structural Journal) Part1-Title No. 102-S76 [2006]

A set of accelerated aging and natural environment tests has been carried out to evaluate performance of glass fibres reinforced polymer (GFRP) sheets bonded on concrete in tropical environment. Plain concrete beams were cast and externally reinforced by bonding with E-glass GFRP sheets. The beams were immersed in a 60^{o}C water bath for varying durations. The novelty of the experiment was that the environmental exposure was given while they were subjected to service loads. This load helped in seeping sheet exposed to hot water under stressed condition. Thus field environment very similar to tropical climate was simulated. The loaded specimen were also subjected to natural weathering for 6 and 12 months duration. The sheets were removed from the specimen and the tensile strength and modulus were determined to assess the degradation, if any. In the first part of the paper the structural level studies are discussed. In Part 2 the micro structural investigation is reported.

[2] A. Mukherjee, S.J. Arwikar (ACI Structural Journal) Part2- Title No. 102-S82 [2006]

In the first part of the paper the structural scale tests on the synergistic effects of moisture, temperature, alkalinity and stress level on the performance and durability of GFRP sheet bonded externally on concrete have been discussed. This part describes the micro structural studies to find out the nature, quantum and mechanism of deterioration in the conditioned sheets. Micrographic investigations were carried out using a scanning electron microscope (SEM) to visualize the changes in the microstructure. The other tests are energy dispersive X-ray analysis (EDX) and inductively coupled plasma mass spectrometry (ICP-MS) to determine the chemical changes in the composite.

[3] Abhijit Mukherjee and S. J. Arwikar-Part1 [2007]

A set of accelerated aging and natural environment tests has been carried out to evaluate performance of glass fibre-reinforced polymer (GFRP) reinforcing bar in a tropical environment. Beams were cast with the GFRP reinforcing bars as internal reinforcement. They were immersed in a 60 °C water bath for varying durations. The novelty of the experiment was that the environmental exposure was given to the beams while they were subjected to service loads. These loads kept the cracks open for reinforcing bars to remain exposed to hot water. Thus, a field environment very similar to a tropical climate was created. The loaded specimen were also subjected to natural weathering for 18 and 30 months duration. The reinforcing bars were removed from the specimen and investigated at both structural and micro structural scale to assess the degradation, if any.

[4] Abhijit Mukherjee and S. J. Arwikar-Part 2 [2007]
In the first part of this study, the structural scale tests on the synergistic effects of moisture, temperature, alkalinity, and stress level on the performance and durability of glass fibre-reinforced polymer (GFRP) reinforcing bars in concrete have been discussed. In this part, investigations on micro structural studies, carried out to find out the nature, quantum, and mechanism of deterioration in the conditioned reinforcing bars, are reported. Micrographic investigations were carried out using a scanning electron microscope (SEM) to visualize thechanges in the microstructure. The other tests that have been carried out are energy-dispersive x-ray analysis (EDX) and inductively coupled plasma mass spectrometry (ICPMS) to determine the chemical changes in the composite. Observations of the fracture surfaces by optical and scanning electron microscopes showed typical damage mechanisms for laminates [0/0]s and [0/90]s.

[5] D. Olmos, R. Lo´pez-Moro´ n, J. Gonza´lez-Benito[2006]
The effect of the nature of glass fibre surface in the water absorption of glass fibres/epoxy composites was studied. Three different silane coatings were used to change the nature of the surface of the glass fibre. Aqueous solutions of dansyl labelled silanes (5-dimethylamino-1-naphthalene sulfonylchloride): (i) 3-aminopropyltriethoxysilane, APTES; (ii) 3-aminopropylmethyldiethoxysilane, APDES and (iii) 3-aminopropyldimethylmonoethoxysilane, APMES were used to get respectively three different coatings. Gravimetry and FTNIR measurements were used to complementary study the water absorption process in the whole composites systems. Besides, to locally study the ingress of water exactly at the interfaces of the composites the fluorescence from dansyl label was used. The presence of the silanized fibres seems to induce changes in the water absorption process of the epoxy resin decreasing the relative gain of mass at equilibrium and suggesting that the glass fibre surface may induce a change in the structure of the epoxy matrix in comparison with this polymer without reinforcement. Besides, the fluorescence measurements point out that the water accessibility to the interface is delayed respect to the water absorption of the polymer matrix and the relative amount of water absorbed by the interface depends on the nature of the glass fibre surface, being absorbed less water the lower the functionality of the silane was.

[6] Beckry Abdel-Magid , Saeed Ziaee , Katrina Gass , Marcus Schneider [2005]
The properties of an E-glass/epoxy composite were examined before and after mechanical loading and moisture conditioning. Preliminary results indicate that the modulus, strength, and strain of the E-glass/epoxy composite material are affected by the presence of moisture and mechanical loading when compared to control specimen. At shorter durations of conditioning at room temperature, a slight increase in strength and a slight decrease in modulus were observed; and at longer durations, 3000 h, a noticeable reduction in strength and strain-to-failure was observed. Specimen conditioned under stress, in water at 65 °C for 1000 h exhibited higher loss in modulus. It is speculated that constant stress may have a positive effect in short-term, and that

extended exposure to moisture at room temperature leads to brittle failure while exposure at high temperatures may lead to ductile failure of E-glass/epoxy composites.

[7] J.M. Ferreira, J.T.B. Pires , J.D. Costa , O.A. Errajhi , M. Richardson [2005]
Aluminized glass fiber composites in a polyester matrix were used in this work in an attempt to study their fatigue resistance under both dry and water saturated ambient conditions (compared to conventional glass fiber composites). These composites, containing specially modified fibers, exhibit increased thermal and electrical conduction properties whilst still being potentially adequate for many structural applications. The fatigue tests were performed in tension at ambient temperature and a frequency of 10 Hz. The fatigue damage of aluminized composites are described and evaluated in under environmental conditions and compared to the performance of uncoated fiber composites.

[8] Tong Yuanjian, D. H. Isaac [2007]
The low velocity impact and tension–tension fatigue behavior of glass fiber reinforced polyester resin composites have been investigated. Two fiber geometries, namely [±45°]4 and [0/90°]2s stitch bonded glass fibers were studied. The results revealed that even low energy impact could seriously impair the tensile properties of [±45°]4 composites. For the [0/90°]2s glass fiber composites, a critical impact energy was found. Below this energy level the tensile properties were hardly affected by the impact but above it the tensile properties reduced with increasing energy. Low velocity impact also reduced the fatigue lives of the composites and this reduction could be related to the degradation in tensile strength. By normalizing the fatigue stress against the post-impact residual tensile strength of the composite, it was found that for each fiber geometry a single S–N curve could be drawn, which encompassed both undamaged and impacted specimen. This implies that fatigue lifetimes of impact damaged composites can be predicted from measurement of the residual tensile strength of impacted specimen and the S–N curve of undamaged specimen.

[9] J.F. Laliberte´, C. Poon , P.V. Straznicky , A. Fahr [2002]
Fiber–metal laminates (FMLs) are a family of hybrid materials currently being considered for use in airframe structural applications. Post-impact fatigue strength tests were carried out on several varieties of Glass Reinforced (GLARE) aluminum laminates. The panels were impacted in a drop weight impact tower located at the Institute for Aerospace Research of the National Research Council of Canada. Observations made by other researchers that the internal impact damage in FMLs is confined to the immediate impact site were confirmed. The impacted specimen were cycled in tension–tension fatigue until failure. Cracks developed alongside the dent and also at the edges of the gauge section of the specimen. Aluminum baseline specimen had significantly lower fatigue lives than the FML specimen. The stress-state surrounding the dent is complicated and contributed to unusual fatigue crack initiation behavior in some GLARE variants.

[10] Keiji Ogi , Tetsuro Shiraishi , Hideki Murayama [2006]

This paper presents effect of temperature and after-cure on fatigue fracture behavior in a glass fibre reinforced phenolic resin composite. Firstly, monotonic tensile tests were conducted to measure the stress–strain curves and acoustic emission (AE) behavior. Secondly, fatigue tests at room temperature were performed for the virgin and two kinds of after-cured specimen. Thirdly, S–N curves are measured for the specimen with and without a hole at various temperatures. Fourthly, fatigue crack propagation (FCP) tests and in situ microscopic observation under tensile loading were conducted using notched specimen to investigate crack propagation behavior. Finally, fracture surfaces after the tests were observed by means of scanning electron microscopy (SEM). It is found that final failure abruptly takes place for the monotonic and fatigue tests without showing visible damage on the surface of the specimen while permanent strain and cumulative AE events increase just before fracture. The short-term after-cure process increases fatigue strength as well as static strength while the long-term after-cure process degrades the static strength and fatigue life. Fatigue strength decreases with increasing temperature for the virgin specimen without a hole. Fatigue life of open-holed specimen slightly decreases with increasing ambient temperature up to 200 _C. The FCP tests and in situ observation under loading revealed that fracture takes place in a brittle manner although stable crack propagation is observed in a few specimen. The SEM fractography indicates that pull-out of fibres was observed in all the specimen and that small resin particles were generated on the fibre surfaces of the specimen after the fatigue tests.

[11] Ying Shan, Kin Liao [2002]

Unidirectional glass fiber reinforced and glass–carbon fiber reinforced epoxy matrix composite specimen were subjected to tension–tension fatigue in air and in distilled water at 25 °C. While no significant change in fatigue life was observed for both types of specimen tested in air and in water when cyclically tested at 85% of average ultimate tensile strength (UTS), the detrimental effect of water becomes apparent at lower stress levels of 65 and 45% UTS. Compared to specimen tested in air, cyclic loading in water results in shorter fatigue lives for both glass and hybrid specimen. While all of the glass fiber specimen did not survive to 106 cycles when cyclically loaded in water, hybrid specimen (with 25% carbon fiber (by volume), 75% glass fiber (by volume), 30% total fiber volume fraction) showed better retention in structural integrity under environmental fatigue, for fatigue lives up to 107 cycles, a consequence of the corrosion resistant of carbon fiber. Thus it is shown, by incorporating appropriate amount of carbon fibers in glass fiber composite, a much better performance in fatigue can be achieved for glass–carbon hybrid composite. A simple life prediction model for the hybrid composite is proposed. Model predictions are compared with experiments results from both laminated interply and intermingled intraply hybrid composites. Results suggest that synergistic effect of the reinforcing fibers is critical in governing the fatigue behavior of intraply hybrid composite.

[12] Ashcroft et al [2003]

In this paper, a method of predicting failure in bonded composite joints subjected to combined mechanical loading and environmental degradation is described. The technique is based on a coupled mechanical-diffusion finite-element analysis combined with an appropriate failure criterion. The method is evaluated by predicting the fatigue thresholds of epoxy-CFRP lap-strap joints preconditioned and tested in dry and wet environments. The coupled stress-diffusion method was shown to be capable of predicting correctly the effect that different environments would have on the fatigue resistance of the joints. Both elastic and elastoplastic fracture criteria were then used to quantitatively predict the fatigue thresholds. The elastoplastic fracture criterion was the most suitable when moisture was encountered at elevated temperatures and was capable of predicting fatigue thresholds within the experimental scatter range. It is concluded that the technique described is a powerful and flexible way to predict failure in bonded joints subjected to a wide variety of loads and environmental conditions. The method does, however, rely on material data not commonly available, and reasonable simplifying assumptions should be made to make the method cost effective.

[13] L.W. Davies, R.J. Day, D. Bond, A. Nesbitt, J. Ellis, E. Gordon [2006]

This paper assesses the use of the Quickstep method for the processing of an epoxy/carbon fibre aerospace material and compares this to equivalent composites produced using an autoclave process. Higher process ramp rates, achievable using Quickstep, have been shown to reduce resin viscosity thus facilitating void removal. Manipulation of the Quickstep cure cycle, while the resin is at low-viscosity, has significant effects on the mechanical properties of the product whilst simultaneously reducing the cure cycle time. Using Quickstep curing, specimen were produced exhibiting comparable interlaminar properties but lower flexural strength as compared to those produced using the autoclave. However, normalisation of the data to a common fibre volume fraction showed that better interlaminar shear strengths could be obtained using Quickstep. This improvement in specific interlaminar shear strength was postulated to be due to the lowering of the resin viscosity over the duration of the cure, resulting in better wet through of fibres by resin and improved interfacial adhesion between fibre and matrix. This study identifies key parameters associated with the Quickstep process, providing a basis for further optimisation.

[14] Botelho et al [2006]

The environmental factors, such as humidity and temperature, can limit the applications of composites by deteriorating the mechanical properties over a period of time. Environmental factors play an important role during the manufacture step and during composite's life cycle. The degradation of composites due to environmental effects is mainly caused by chemical and/or physical damages in the polymer matrix, loss of adhesion at the fibre/matrix interface, and/or reduction of fibre strength and stiffness. Composite's degradation can be measure by shear tests because shear failure is a matrix dominated property. In this work, the influence of moisture in shear properties of carbon fibre/epoxy composites (laminates [0/0]s and [0/90]s) have been

investigated. The interlaminar shear strength (ILSS) was measured by using the short beam shear test, and Iosipescu shear strength and modulus (G12) have been determined by using the Iosipescu test. Results for laminates [0/0]s and [0/90]s, after hygrothermal conditioning, exhibited a reduction of 21% and 18% on the inter laminar shear strength, respectively, when compared to the unconditioned specimen. Shear modulus follows the same trend. A reduction of 14.1 and 17.6% was found for [0/0]s and [0/90]s, respectively, when compared to the unconditioned specimen.Micro structural observations of the fracture surfaces by optical and scanning electron microscopes showed typical damage mechanisms for laminates [0/0]s and [0/90]s.

[15] V. M. Karbhari and S. Zhang [2002]

2- and 4-layered specimen of E-Glass/Vinylester fabricated from uniaxial, biaxial, and triaxial, non-woven fabrics processed using the resin infusion process are immersed in deionized water at 23°C and 60°C, and a potassium based pH 10 buffer at 23°C, for a period of 57 weeks in order to investigate durability in aqueous environments. It is shown that the coefficients of apparent diffusion and levels of moisture gain are the highest for the deionized water immersed specimen at 60°C, and this results in the highest levels of tensile strength and modulus degradation. Tensile tests show the presence of an aqueous medium based post-cure that competes with the conventionally recognized mechanisms of deterioration in the resin, at the level of the fiber-matrix interface, and in the fiber, resulting in a retardation of absolute level of effects. It is also shown that effects of the immersion are different in the warp and fill directions and can in fact be affected by intricacies of the fabric architecture and thickness. It is shown that damage takes place through interface debonding and degradation as well as fiber pitting, and cracking, each of which serve as the means for renewed absorption of water resulting in moisture uptake at levels above the initial plateau. Effects of immersion on short-beam-shear strength and glass transition temperature are also elucidated.

[16] Amit Sharma [2009]

The environmental degradation of single layered GFRP specimen was studied for specimen at different water temperatures and effect of alkali material NaOH on strength and life of the material. Further microscopic as well as macroscopic properties of the GFRP specimen was also studied at regular intervals.

[17] **Leon L. Mishnaevsky Jr. [2004]**

Three-dimensional finite element (FE) simulations of the deformation and damage evolution of SiC particle reinforced Al composites are carried out for different microstructures of the composites. A program for the automatic generation and the design of FE meshes for different 3D microstructures of composites is developed. Numerical testing of composites with random, regular, clustered and gradient arrangements of spherical particles is carried out. The fraction of failed particles and the tensile stress–strain curves were determined numerically for each of the

microstructures. It was found that the strain hardening coefficient increases with varying the particle arrangement in the following order: gradient<random<clustered<regular microstructure. The variations of the particle sizes causes strong decrease in the strain hardening rate of the composite, and leads to the quicker and earlier damage growth in the composites.

[18] Benkhedda et al. [2007]

Polymer matrix composites are relevant materials for future supersonic aircraft due to their high specific properties. However, in such aeronautical applications, the material is exposed to severe environmental conditions. The present paper aims at assessing an approximate model to evaluate hygrothermoelastic stress in composite laminated plates during moisture desorption taking into account the change of mechanical characteristics induced by the variation of temperature and moisture. The developed method permits us to calculate such stresses during desorption phase without the computation of the moisture concentration, through laminated plates. It observed through this study that the variation of elasticity modulus due to the temperature causes a stress relaxation. These stresses have to be taken into account for the design of composite structures submitted to a moist environment. Through the presented study, it is hoped to contribute to the understanding of hygrothermal behaviour of composite laminated plates.

[19] V.Alvarez & A.Vazquez [2005]

In this work, the cycling diffusion behaviour of glass-fibre/VE matrix composites was studied. It was shown that glass fibres act as inert in the water absorption process of VE matrix and their main effect is the loss of the interfacial adhesion. Composites absorb less water than matrix and, for both, the amount of water increased with the temperature increase and cycle. On the other hand, diffusion coefficients were similar for composites and matrix. Temperature affects the diffusion coefficient values and the obtained values were fitted by an exponential equation. It was possible to observe, from SEM micrographs, that the adhesion at the fibre–matrix interface decreased as temperature increased. The cycle affects the composites exposed at a high temperature more when loss of adhesion was observed at the fibre–matrix interface. The flexural modulus did not change after water exposure, but the loss of strength was related to the poorer interface. The diffusion coefficients are calculated by using the simplest Fick's equation.

[20] E. Ahci , R. Talreja [2006]

This paper describes a thermodynamics based model for viscoelastic composites with damage and illustrates its use in characterization of viscoelastic response of polymer matrix woven fabric composites subjected to loading at high temperatures. The characterization is conducted by an experimental method aided by finite element (FE) modelling. The experimental characterization is based on creep data obtained under constant loads of different magnitudes and at different temperatures, and on recovery data collected after unloading. A carbon fibre/polyamide resin woven composite with glass transition temperature of around 380^{o}C was used in the experimental program. A FE model was developed to determine the non-linear viscoelastic

response by implementing incremental constitutive relations into an ABAQUS code. The laminate viscoelastic properties were obtained by finite element micromechanics analysis using the neat resin data as input. Comparing its results with creep-recovery test data at different temperature and stress levels validated the FE model. There are several factors affecting the viscoelastic behaviour of polymer matrix composites such as temperature, moisture and stress level. Accordingly, a large number of tests need to be performed to characterize the viscoelastic response experimentally for each fibre matrix combination. For this purpose an efficient and systematic experimental procedure was used to understand the effects of temperature and stress level on the viscoelastic response, to clarify the damage-viscoelasticity coupling and to determine the viscoelastic properties of the material system.

CHAPTER 3 PROBLEM FORMULATION

Glass Fibre Reinforced Polymer (GFRP) is an immensely versatile material which combines light weight with inherent strength to provide a weather resistant finish, with a variety of surface texture and an unlimited colour range available. GFRP was developed in the UK during the Second World War as a replacement for the moulded plywood used in aircraft radomes (GFRP being transparent to microwaves). Its first main civilian application was for building of boats, where it gained acceptance in the 1950s. Its use has broadened to the automotive and sport equipment sector.

From the previous studies done so far on GFRP following gaps were highlighted:

- Lack of availability of data on dynamic behaviour of GFRP materials.
- Lack of availability of literature on Environmental degradation of pre-fatigued GFRP material.
- Different mechanical parameters like fatigue, bending, creep etc. need to be studied by laboratory scale experimentation for knowing the exact performance parameters in real time situations.
- Lack of simulations and analysis designing software for modelling and simulation of real time conditions in environmental degradation of composites.

So, in this thesis work, it was decided to conduct an experimental study on pre-fatigue testing of GFRP materials and then expose them to hygrothermal conditions at different temperatures i.e. 55°C and 45°C for duration of 30 and 60 days time period and study the strength degradation occurring in these conditions. Meanwhile the other macroscopic parameters like diffusivity, weight gain, capacitance and microscopic properties like area fraction of fibres and epoxy, circularity of fibres and micro-hardness were also calculated at regular time intervals.

Finally, the modeling and analysis using Abaqus software was done from the experimental data thus collected and stress distribution for the GFRP specimen were studied.

CHAPTER 4 EXPERIMENTATION

4.1 WORK PLAN

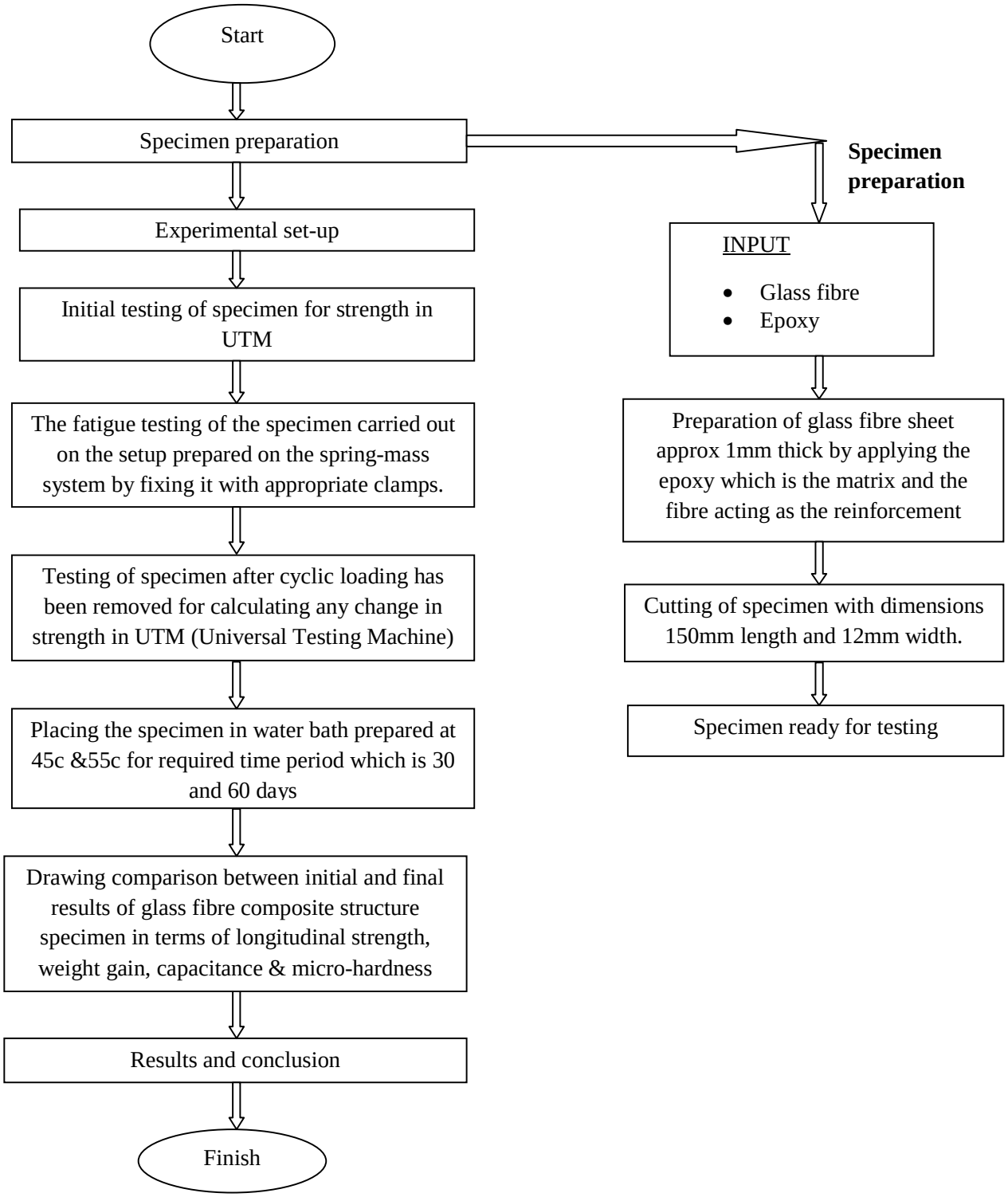

Following is the detail of the experimentation work done according to the work plan flow-chart 4.1

4.2 EXPERIMENTAL SETUP:

A set of accelerated aging tests had been carried out to evaluate performance of pre-stretched glass fibres reinforced polymer (GFRP) sheets embedded in epoxy matrix. The field environment very similar to that of tropical climate had been simulated.

The specimen were immersed in various baths for different time durations. The novelty of the experiment was that the accelerated environmental exposure had been given to specimen while they were pre-stretched to different service loads. The specimen were removed from the bath after decided time period. The tensile strength is measured and a SEM (Scanning Electron Microscope) image was obtained to check the condition of composite material.

Fig. 4.1 Setup view of the water baths

4.3 SETUP FABRICATION:

The setup (Fig.4.1) basically consists of following main items:

	ITEM NAME	QTY.
1	Water Tanks	- 03
2	Specimen	- 68
3	Heating Elements	- 02
4	RTD Sensors	- 02
5	Temperature Controllers	- 02
6	Solid State Relays	- 02

1) Water Tanks:

The experimental setup consists of three well insulated tanks (Fig. 4.1). The tank was of cylindrical shape made out of plastic. The approximate capacity of the tank was 60 litres. All tanks were filled totally with tap water and set at a temperature of 45°C ,55°C and at natural temperature respectively (refer Test Matrix -Table 4.2, 4.3). The water which evaporated from the tank was replenished on daily basis during experimentation. Each tank was labelled as per details of experimentation.

2.) Specimen

The following were the specifications of the specimen (refer Fig. 4.2):

Length of specimen	:	150 mm
Breadth of specimen	:	12 mm
Thickness of specimen	:	1 mm (approx.)

The specimen were having “tabs” at both sides only up to a length of 45 mm from respective ends. This left an “effective length” of about 60 mm in centre (refer Fig. 4.2, 4.3).

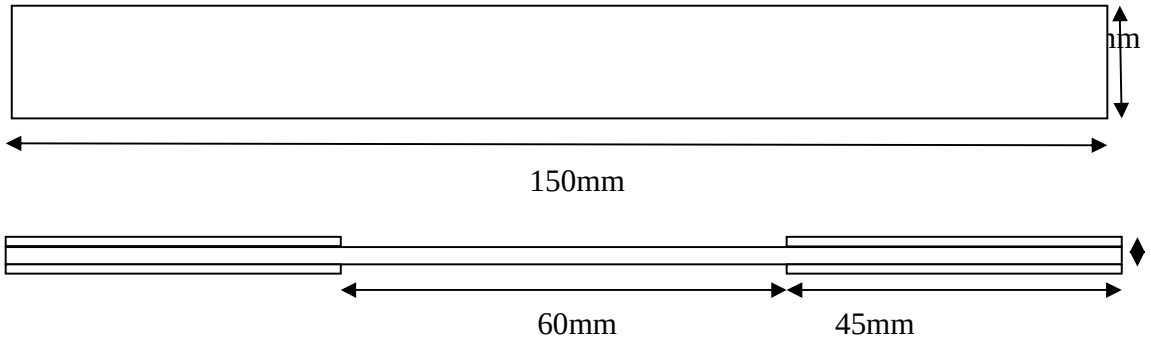

Fig. 4.2 Specimen specifications

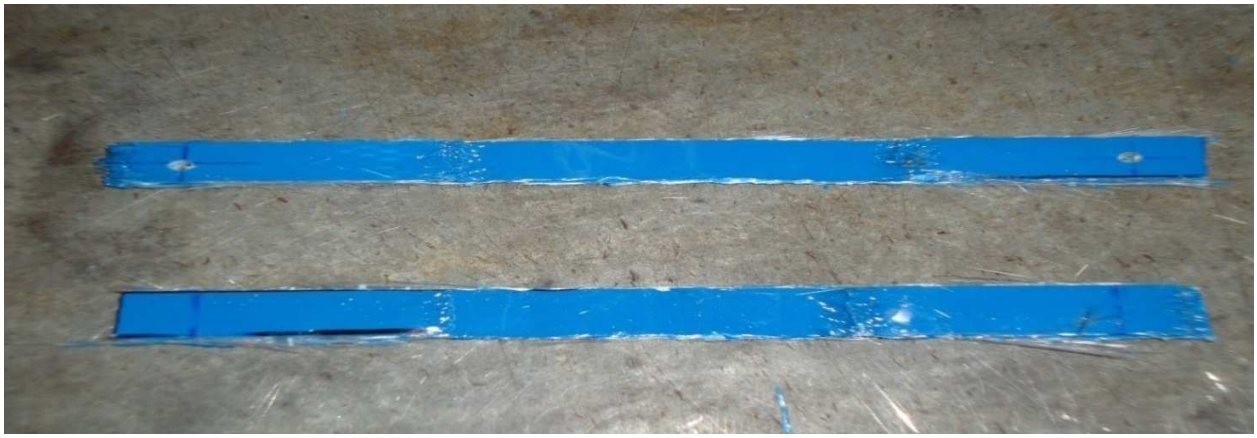

Fig. 4.3 Actual image of the specimen

3) Heating Element:

The setup was heated with help of commercially available heating rod elements (Fig. 4.4). Each bath was having its own heating rod connected via temperature controller (Fig.4.5). The wattage of rod was 1000KW with single phase connection. As the temperature reached the required value the power supply of rods were cut off by controllers.

Fig. 4.4 Heating Element and RTD sensor in a tank

4) RTD (Resistance temperature detector) Sensors:

Each of the tank was provided with separate RTD sensors (Fig.4.4). It senses process value of temperature (value at given time) of the bath and input was send to the controller which controlled the system as per set value.

5) Temperature Controller:

The objective of this set up was to maintain the bath temperature at specified value till the duration of experiment for day and night on daily basis. So a temperature controller (Fig.4.5) was connected with each of the bath along with relays cut off. The controller used the proportional-integral-derivative (PID) control to maintain the temperature. On the controller display the “Set Value” was given which was the temperature indicated in green and the “Process Value” of temperature was indicated in the red (refer Fig.4.5), which was the output from the RTD sensor. For the very first time the controller was set to auto-tune mode so that it could adjust itself according to the input variables. Once the bath had attained the set value the controller cut off its supply and after sometime it sensed the temperature if it had gone below set value, it again started heating to obtain the set value. The dimensions of the controller and actual panel used are shown in Fig.4.6 and Fig. 4.7 respectively.

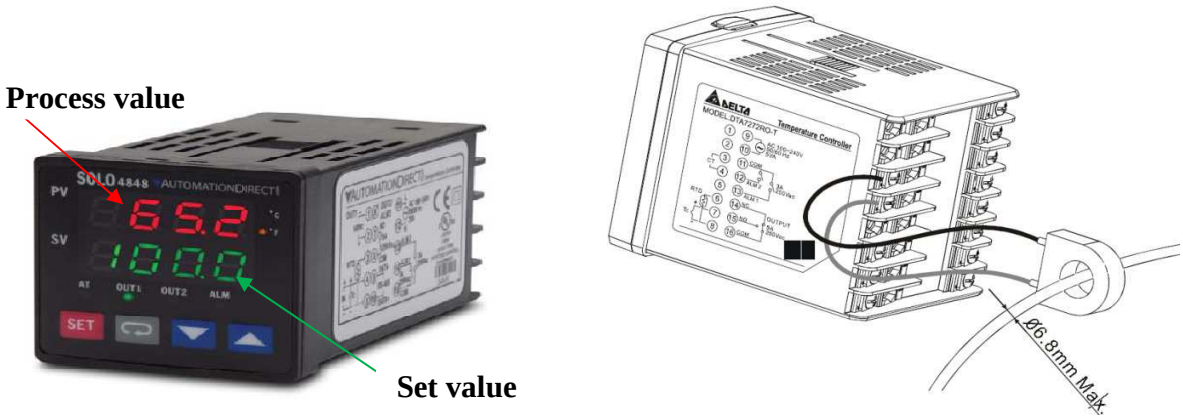

Fig. 4.5 Actual image of the temperature controller showing front and back side

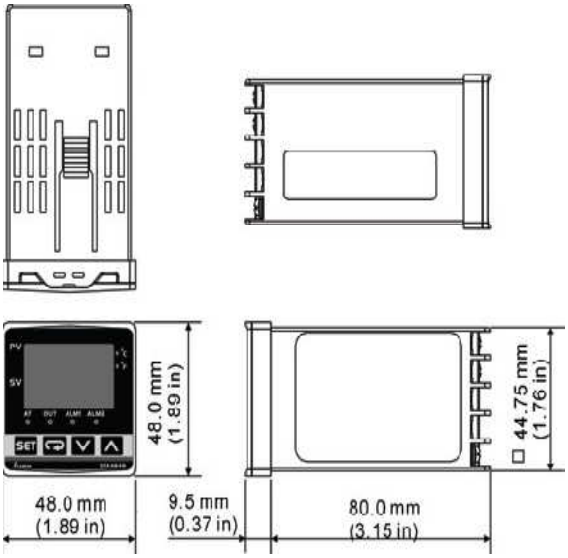

Fig. 4.6 Dimensions of controller

Fig. 4.7 Temperature display panel with controllers

6) Solid State Relays (SSR):

The solid state relay was required to break the circuit in case of overloading. It controlled the switching of the heating element and acted as a switch. It helped in protecting controller for any kind of overload or short circuiting.

4.4 FABRICATION OF SPECIMEN:

Fig. 4.8 Uncoated GFRP sheet used for making specimen

A) Cutting GFRP Sheet

For the experimentation unidirectional woven fabric roll of GFRP was purchased (Fig.4.8) of 50cm width having 0^o fibre orientation woven with polymer fibres. The sheets were initially cut from roll in length of 550mm. The reason for overcutting was that after its curing it had to be trimmed of the edges in order to remove flaws at end.

B) Mixing of Epoxy

The sheets were epoxy coated in order to make a composite material. In this case the epoxy resin (by M Brace) was used which basically consists of two parts (refer Fig. 4.9):

a) Base

b) Hardener

Base is thick blue liquid which was considered as the main ingredient and golden coloured hardener was added to it for helping it to settle down by starting the exothermic reactions. Both base and hardener were mixed (by weight) in a container in ratio of 100: 40 respectively.

Fig. 4.9 Base (blue colour container) and Hardener (white bottle) used for coating

Fig. 4.10 Hand mixing of both base and hardener

After putting the base and hardener in required quantity, the mixture was stirred continuously by manual process (Fig.4.10) so that the mixing takes place in proper manner. If mixing was not done properly the material would not settle well. Also if the ratio of the hardener was more than the pot life of the material would have been lesser. The amount prepared was consumed in 20-30 min. otherwise the epoxy would have settled in container itself. Approx. 300gms of epoxy was needed to apply to both side of sheet in this case.

C) Applying resin on sheet

The epoxy was applied on sheet using a steel scrapper (Fig. 4.11) by carefully spreading it evenly on all sides of sheet. It was made sure that there is no air bubbles present entrapped inside the epoxy applied on sheet otherwise it would create a flaw there. After applying epoxy the sheet took overnight to dry and now the coat could be applied on other side if required. The full curing of sheet (Fig.4.12) was done by leaving it under ambient temperature for at least seven days before processing further.

Fig. 4.11 GFRP sheet being resin coated

Fig. 4.12 The fully cured sheet with epoxy coating

The thing to note here was that two types of sheet were made:
One with epoxy coating on both sides - it's used to make actual specimen
Other with epoxy coating on one side only - it's used to make Tab

D) Sizing of sheet for specimen and tabs

Once the epoxy was fully cured, the sheet was cut to actual specimen size using the Treadle shearing machine (Fig.4.13) which would shear it into required size of 150mm x 12mm. After obtaining the long cured strips of the resin coated GFRP sheet, they were further tabbed on each side of either ends. The tabs were cut in size of 45mm x 12mm with same Treadle shearing machine.

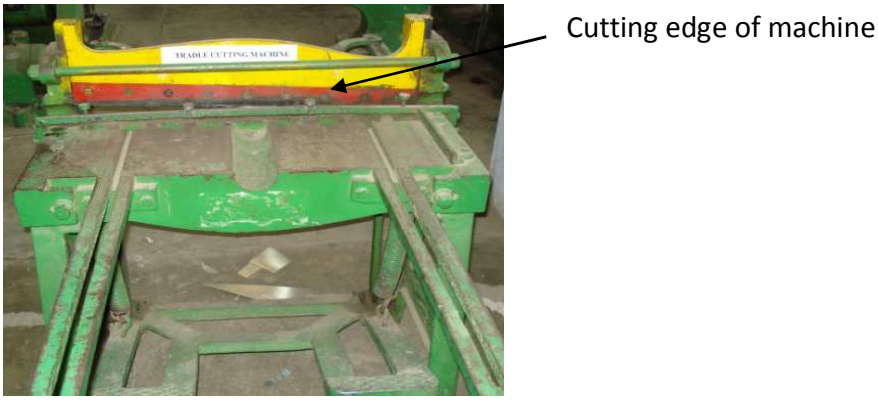

Fig. 4.13 Treadle Shearing Machine

E) Placing tabs on specimen

The specimen had to be tabbed on either side on two ends. The mixture of epoxy was again prepared as discussed before and carefully applied on to the either side of specimen. The tabs were now placed on either side of epoxy pasted specimen (with epoxy coated side of tab on upper side). The epoxy would act as binder between tab and actual specimen. Two paper clamps (Fig.4.14) were placed on either tabbed side to hold tabs in place and also to apply pressure while epoxy between them was getting dried.

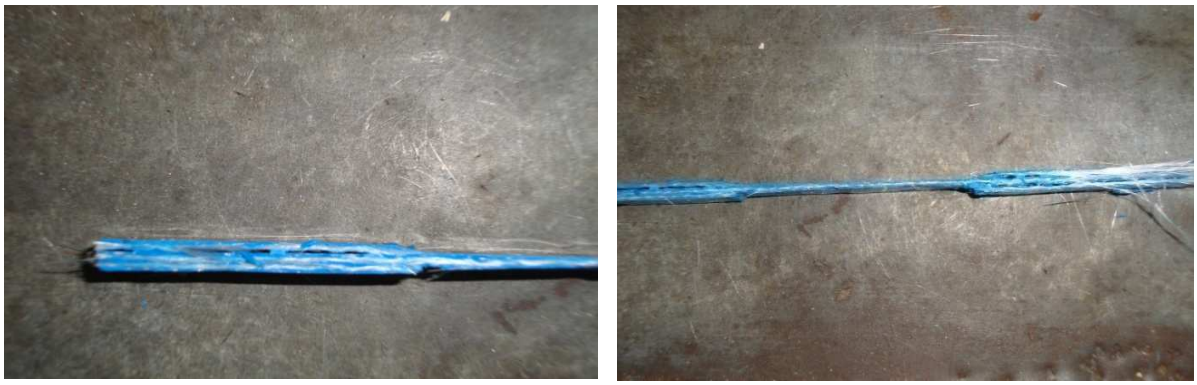

Fig. 4.14 Actual Specimen tabbed and ready for drilling

F) Drilling holes on the tabbed surface

The tabbed specimen were dried for 5 days and then holes of 3mm approx. diameter were drilled on both ends for appropriate clamping of the specimen (fig. 4.15) and now the specimen were ready for testing (Fig. 4.16).

Fig. 4.15 Drilling operation for clamping

Fig. 4.16 Specimen ready after drilling

The whole process can be summarised as mentioned below:

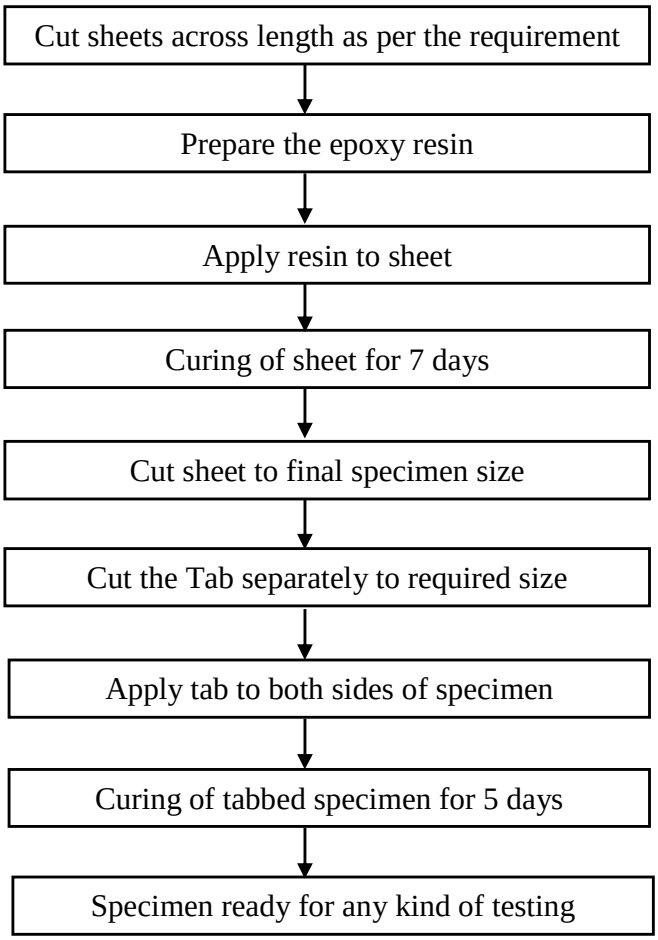

4.5 TEXT MATRIX

Table 4.1 GFRP Specimen for Fatigue loading

Cycle Fraction for 20% loading of Ultimate tensile strength	No. of Specimen for Testing
	Strength test, Micro-hardness, Capacitance, Weight gain & SEM
60% cycles (A)	32
40% cycles (B)	32
0% cycles (C)	8
Total Specimen	**72**

Table 4.2 Distribution of above GFRP specimen for Accelerated Degradation in 45°C Water Bath

Specimen	Tensile strength & SEM		For Micro-hardness, Capacitance &weight gain	For tensile strength, Micro-hardness, Capacitance & weight gain						Total
	30 days	60 days	3-day alternate	10 days	20 days	30 days	40 days	50 days	60 days	
A	3	3	1	1	1	1	1	1	1	13
B	3	3	1	1	1	1	1	1	1	13
C	1	1	0	0	0	0	0	0	0	2
Total Specimen										**28**

Table 4.3 Distribution of above GFRP specimen for Accelerated Degradation in 55°C Water Bath

Specimen	Tensile strength & SEM		For Micro-hardness, Capacitance &weight gain	For tensile strength, Micro-hardness, Capacitance & weight gain						Total
	30 days	60 days	3-day alternate	10 days	20 days	30 days	40 days	50 days	60 days	
A	3	3	1	1	1	1	1	1	1	13
B	3	3	1	1	1	1	1	1	1	13
C	1	1	0	0	0	0	0	0	0	2
Total Specimen										**28**

Table 4.4 Distribution of above GFRP specimen for Accelerated Degradation in Natural Water Bath

Specimen	Tensile strength & SEM		For Micro-hardness, Capacitance &weight gain	Total
	30 days	60 days	3-day alternate	
A	2	2	1	5
B	2	2	1	5
C	1	1	0	2
Total Specimen				**12**

4.6 FATIGUE TESTING OF GFRP

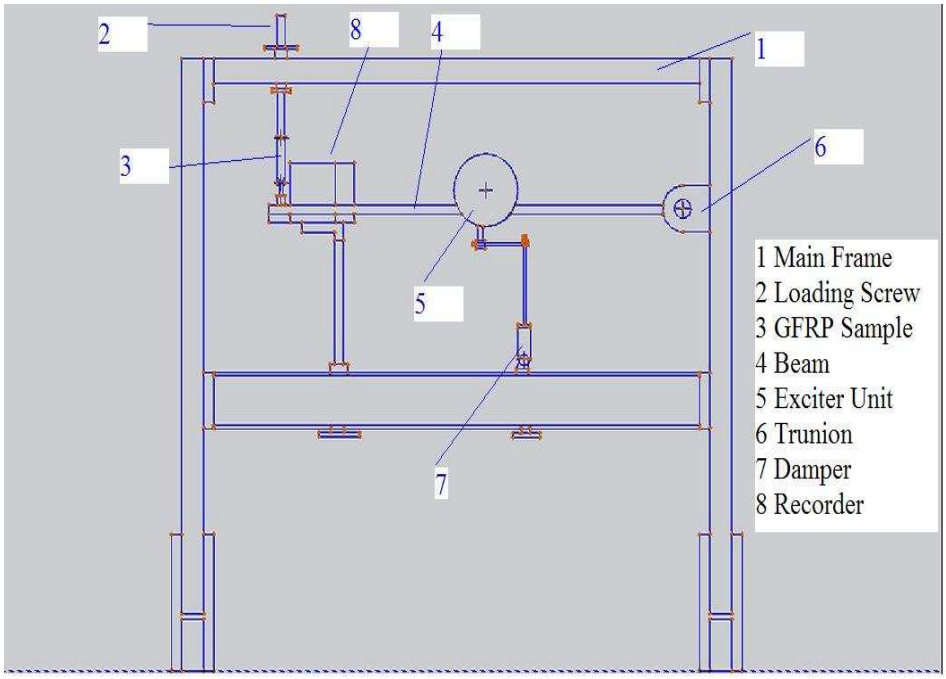

Fig. 4.17 Line diagram of the setup for fatigue testing of GFRP

Fig. 4.18 Actual picture of Fatigue Testing Setup

First of all fatigue testing of GFRP was carried out in the given machine setup refer Fig. 4.17. This machine setup is basically a mass-spring-damper system which is used for carrying out experiments based on forced vibration (Fig.4.18). Here the spring is replaced with the GFRP specimen which can be fixed on both ends by using appropriate clamps.
The exciter motor excited the bar giving cyclic load to the specimen due to unbalanced mass in the rotor of the motor which resulted in buckling of the specimen.
The load was changed by applying more moment i.e. by increasing the rpm of the motor or by placing more weight on the bar. The centrifugal force exerted by the unbalanced mass gave the linear force exerted on the specimen.

Following formulas were used for calculating the required rpm of the motor for 20% cyclic load:

Basically the setup being used for the fatigue loading is actually a cantilever which is fixed at one end and supported by a prop on the other end (Fig. 4.19). The calculations thus related are done below.

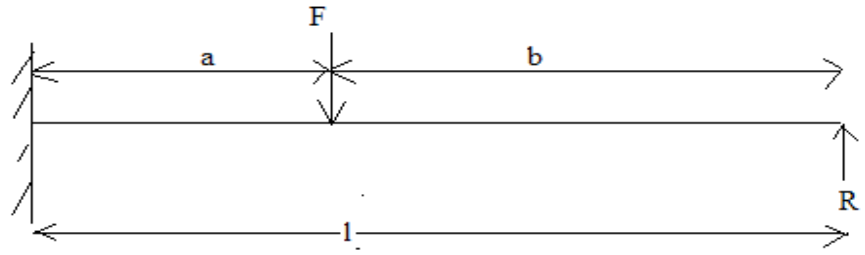

Fig. 4.19 Cantilever supported by a prop on one end

$$Y_{AB}=\frac{Fbx^2}{12EIl^3}[3l(b^2-l^2)+x(3l^2-b^2)]$$

$$R=\frac{Fa^2}{2l^3}(3l-a)$$

$$Y_0=\frac{Fba^2}{12EIl^3}[3l(b^2-l^2)+a(3l^2-b^2)]$$

$$k_0=\frac{F}{Y_0}=\frac{12EIl^3}{a^2b[3l(b^2-l^2)+a(3l^2-b^2)]}$$

$$T=\frac{\sqrt{1+(\frac{2\xi\omega}{\omega_n})^2}}{\sqrt{(1-\frac{\omega^2}{\omega_n{}^2})^2+(\frac{2\xi\omega}{\omega_n})^2}}$$

$$F_{tr}=kx\sqrt{1+\left(\frac{2\xi\omega}{\omega_n}\right)^2}=\frac{k}{M}(m_u e)\frac{\frac{\omega^2}{\omega_n{}^2}\sqrt{1+\left(\frac{2\xi\omega}{\omega_n}\right)^2}}{\sqrt{\left(1-\frac{\omega^2}{\omega_n{}^2}\right)^2+\left(\frac{2\xi\omega}{\omega_n}\right)^2}}$$

Where $X=m_u e/M$

$$F_{tr}=m_u e\omega^2\frac{\sqrt{1+\left(\frac{2\xi\omega}{\omega_n}\right)^2}}{\sqrt{\left(1-\frac{\omega^2}{\omega_n{}^2}\right)^2+\left(\frac{2\xi\omega}{\omega_n}\right)^2}}$$

Where
Y= Deflection at given point
R= Reaction at free end
k_o= stiffness
T= Transmissivity
$F_{tr=}$ Transmitted force
ω= Angular velocity of rotating mass
ω_n= Angular velocity corresponding to natural frequency
M= Mass of rotating object (motor)
m_u= Unbalanced mass
e= eccentricity
E= Young's Modulus
I= Moment of Inertia

Calculations:

Parameters known:
l= 95 cm.
a= 57 cm.
b= 38cm.
e= 6.5 cm.
E= 210 GPa
I= 3.67e-9 m^4
Ultimate Tensile load= 5000N
20% of Ultimate Tensile load= 1000N

After calculations from the above formulas the value for transmitting 1000N force, the no. of rpm came out to be **598.74 rpm** and at this rpm the cycle time for the failure of specimen came out to be **16min**.

Following is the data and graph showing the different fractions of 20% load and the cycles for obtaining that load (Fig.4.20 & Fig.4.22). Also given below is the s-n curve for the same (Fig.4.21).

Ultimate tensile load(N)	Fraction of cycle time of applied loading (20% UTL)
5000	0
4800	20
4650	30
4100	40
3800	60
3150	70
2350	80

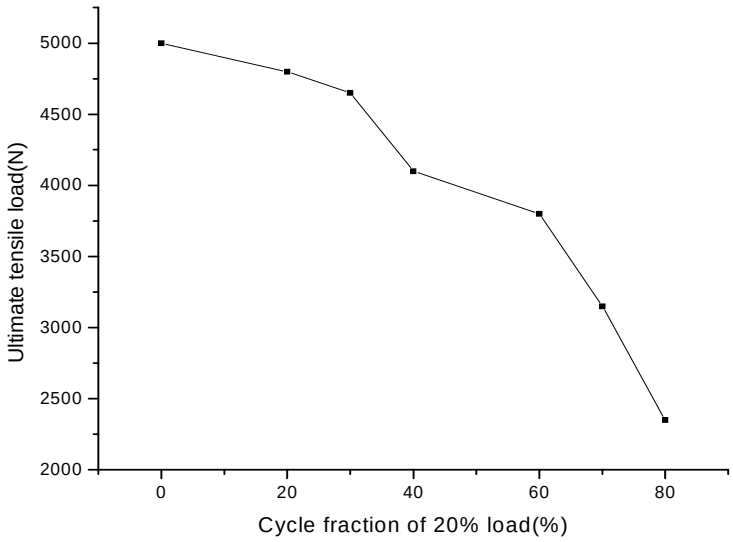

Fig. 4.20 Decrease in ultimate tensile load with change in cycle time of applied fatigue load (20% UTL)

Ultimate tensile load(N)	No. of cycles(at 20% loading)
5000	0
4800	1915.968
4650	2873.952
4100	3831.936
3800	5747.904
3150	6705.888
2350	7663.872
0	9579.84

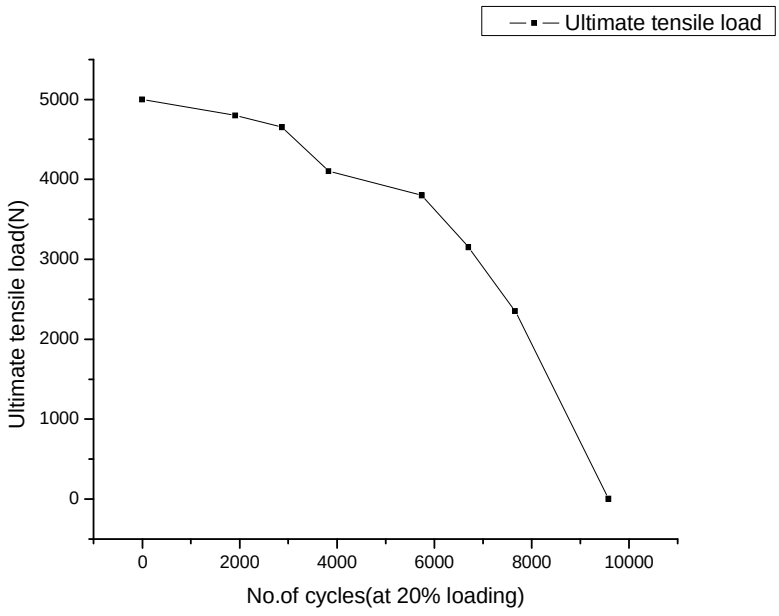

Fig. 4.21 UTL vs. No. of cycles

No. of cycles (at 20% loading)	Fraction of cycle time of applied loading (20% UTL)
0	0
1915.968	20
2873.952	30
3831.936	40
5747.904	60
6705.888	70
7663.872	80
9579.84	100

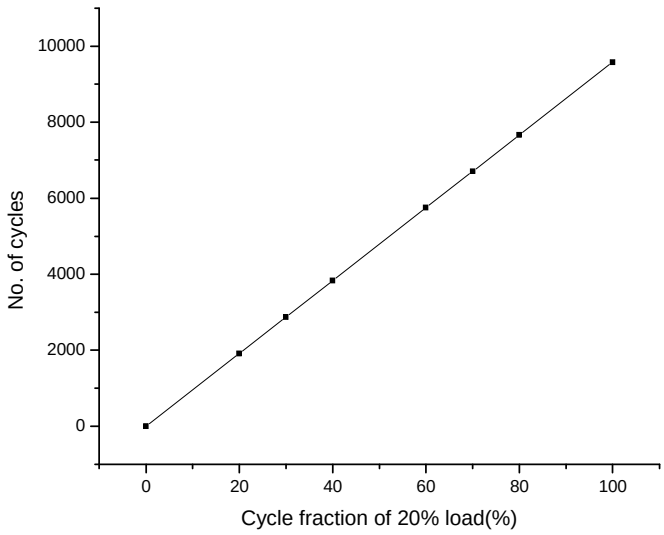

Fig. 4.22 No. of cycles for given fraction of cycle time of applied fatigue load (20% UTL)

CHAPTER 5 FINITE ELEMENT MODELLING

5.1 FINITE ELEMENT METHOD:

Finite Element Method is a very versatile method. It can also be seen from the fact that it has been used as an important tool for analyses and design in almost every industry. Finite element method not only give the behavioural insight of the different part of the structure but it also analyze the structure taking the individual behaviour of these parts into consideration and because of this fact it is becoming popular with the engineering field.

Finite Element Method can be divided into several distinctive steps. Theoretical approach to the method and its different steps are as:

- **Discretization:**

Discretization is the process of dividing domain of problem into small regions or sub domains known as elements. Corner points of elements are called nodes. Figure 5.1 below shows the most used elements:

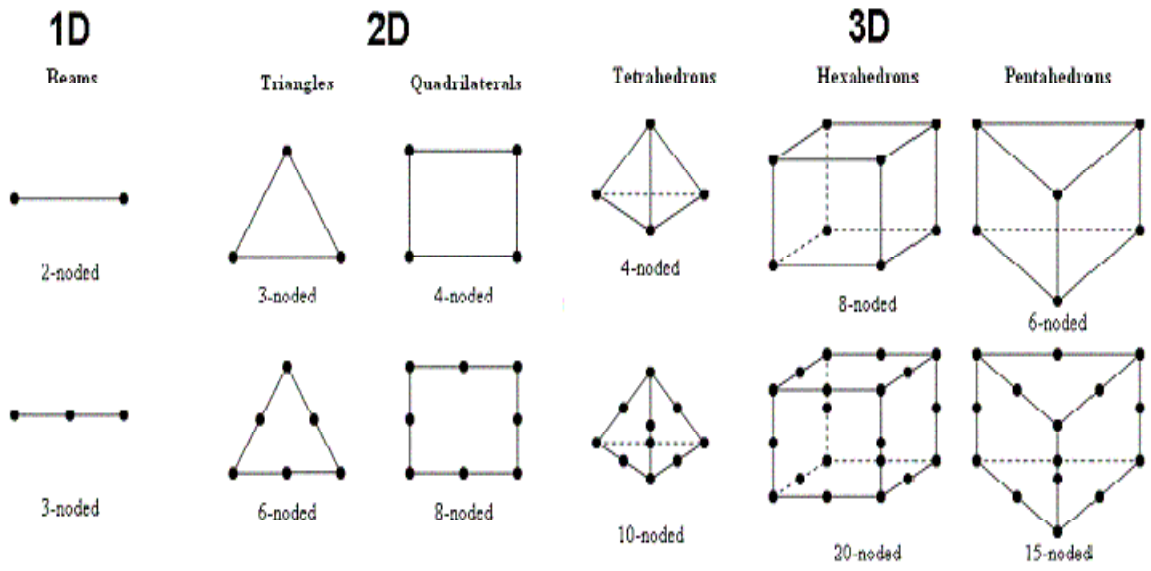

Fig. 5.1 Different types of elements

- **Element analysis / Element stiffness matrix:**

The element analysis has two key components, expressing the variable within the elements, and maintaining equilibrium of the elements.

The governing equation is converted to algebraic form which is represented in matrix form and is called element equation or element stiffness matrix. This enables solution by computer. Element stiffness matrix represents the response of elements according to its property in the system for the parameters. Same matrix can be used for all elements of same type.
For conversion of governing equation (differential or integral) into algebraic form following steps are required:

- **Construction of trial solution**: It is a cyclic process by hit trial. The equation with certain degree of freedom is taken, which is solved by applying boundary condition either at the starting for manual processing or after formulation of system stiffness matrix for solution through computer.
- **Application of optimization criteria**: Optimization criteria are used to find the values of trial function. Two methods for optimization are:
  - Method of weighted residual (differential equation) e.g. Least square Method
  - RITZ variation method (integral equation with some limitation).
- **Estimation of accuracy**: - The accuracy of solution is checked for closeness to exact solution. Also accuracy can be checked by checking the reducing difference of the consecutive solutions obtained by increasing degree of freedom known as property of convergence.

  Sources of error in FEM are:
  - Domain Error - Discretization of domain is approximate.
  - Computational Error - Integration and differentiation induce error.
  - Approximation Error - Assumption of degree of freedom makes the solution approximate.

- **System analysis / system stiffness matrix**

The matrix equations for the individual elements are combined to form the Matrix equations for the entire system called system stiffness matrix. It gives the response of the parameters on the entire system.

- **Incorporation of boundary and loading conditions**

The system stiffness matrix is modified according to the overall boundary conditions. This reduces calculation work and saves time.

- **Solving of the system equations**

The system equations can be solved to give the unknown values at the nodes. If the problem is of an equilibrium nature, then the solution is obtained by solving a set of linear or non-linear equations. System equations can be solved by number of available solvers like gauss elimination or gauss siedel etc.

- **Post processing / Display**

The post processing stage deals with the representation of results. Typically, the deformed configuration, mode shapes, temperature, and stress distribution are displayed at this stage.

5.2 MODELLING PROCEDURE:

The modelling work will be done using Abaqus software (version 6.8) and in Abaqus/CAE module. The step by step procedure of modelling is explained below with all the specifications included in that step. The procedure is explained below as per actual method of preparation of model.

1) CREATING MODEL: Firstly a 3-D part was created with given dimensions of the specimen. Then a composite part was created by splitting the cells into three parts and assigning different properties for the fibre and epoxy layers (Fig. 5.2).

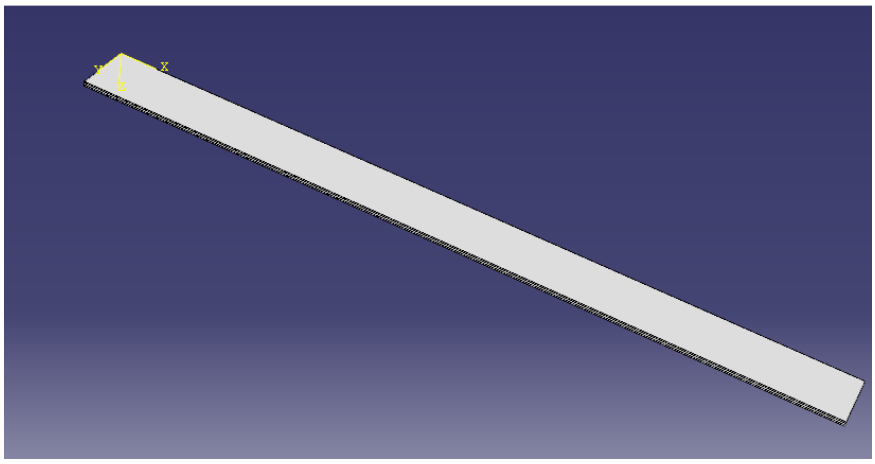

Fig. 5.2 Model of GFRP specimen

The dimensions of above model are 150x12mm as length and width and 1mm thickness.

2) CREATING MATERIAL: The composite considered here was a glass fiber-polymer matrix composite made up of E-glass fiber and epoxy matrix. So three materials were defined, one for fiber, other for matrix and for whole section assignment properties of GFRP were used. The various properties used are mentioned in the tables 5.1 and 5.2 below:

Table 5.1 Mechanical and Thermal properties of material

Material	Density (gm/cm^3)	Poisson's Ratio	Thermal conductivity (W/m-per ^0K)	Young's Modulus of Elasticity (MPa)
E-glass	2.54	0.2	3.23	74000
Epoxy	1.38	0.3	0.346	3440
GFRP	2.36	0.4	3.842	125000

Table 5.2 Properties of mass diffusion of material

Material	Temperature (^oC)	Diffusivity Coefficient (mm^2/sec)	Concentration (%)
Epoxy	37	$41x10^{-8}$	100
	50	$102x10^{-8}$	100

3) CREATING & ASSIGNING SECTION: In Abaqus, section was defined in order to assign properties to particular part. Firstly two sections each for fibre and matrix were created. Then for the whole section the properties of GFRP were assigned to create a third section. Then a "Generalised Plane Strain" section was created. After sections were created, they were assigned along with material properties to the parts mentioned above i.e. fibre, matrix and GFRP respectively.

4) ASSEMBLY OF MODELS: Once section was created, the instance option in assembly section was selected and the section was made independent.

5) APPLYING LOAD: Then tensile load was applied on one end equivalent to the ultimate tensile load from the experimental results and on the other end boundary condition was applied by constraining the end in each direction (Fig. 5.3).

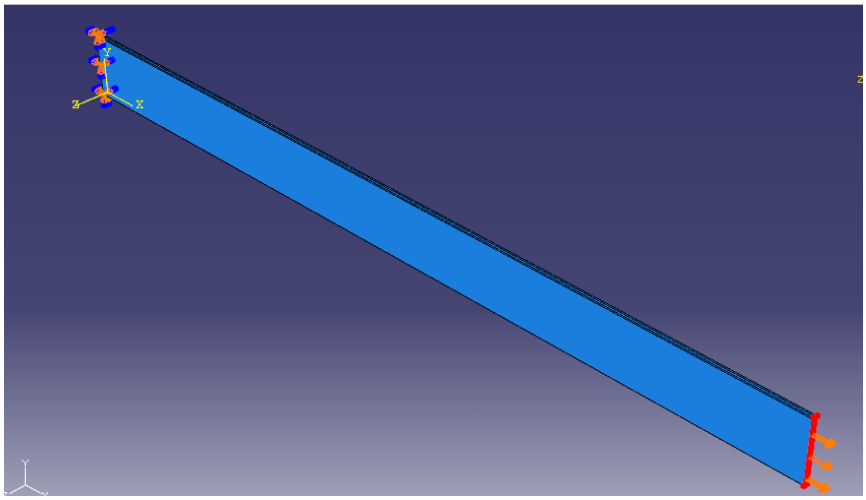

Fig. 5.3 Load applied on the specimen

5) MESHING: Once the load was applied it was needed to mesh the model in order to analyze it. Here seeding was required before meshing in order to decide the size of meshing. Once model was seeded the part got meshed automatically as shown in Fig.5.4.
The **hexagonal** element was selected and **structured** technique was used for meshing. In the element type option **standard element library** was selected with **3-D stress family**. The approximate global size of elements was taken to be **2.5**.

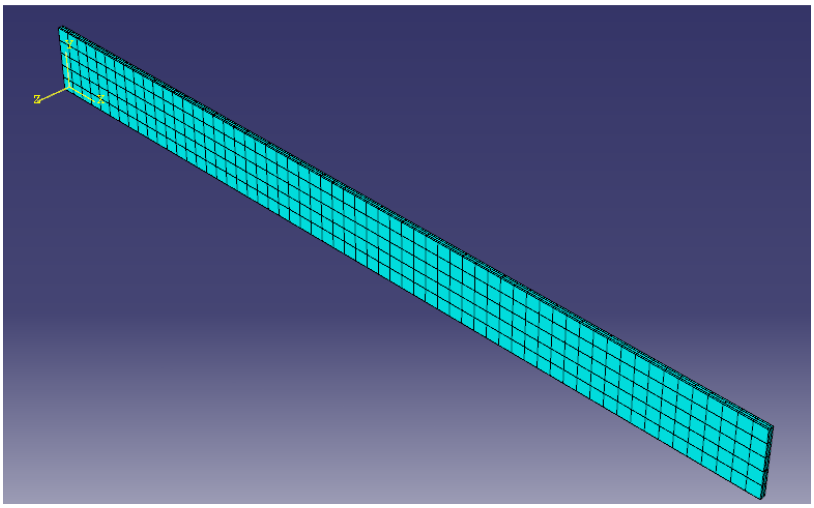

Fig. 5.4 Meshed part

6) RESULTS: After meshing, the job was submitted and the results in the form of Von-Mises stress distribution was displayed, which is discussed in detail for different specimen used:

5.3 MODELING RESULTS AND DISCUSSION:

- Results are shown in terms of Von-Mises stress for different loading conditions taken at different temperatures for a time period of one and two months.
- The stress distribution chart is shown on the top left side of the screen of abaqus as shown in the following figures and different stress levels are indicated by different colors.

5.3.1 At initial level (Fig. 5.5):

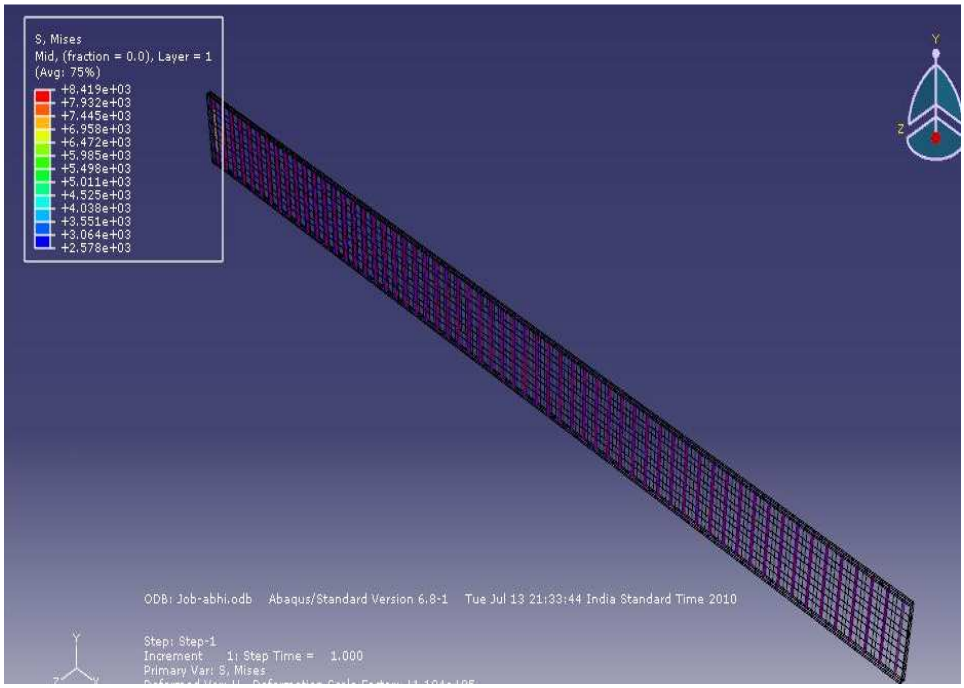

Fig. 5.5 Von-Mises stress distribution using Abaqus for initial specimen

5.3.2 For 40% pre-fatigue loading cycles (Fig. 5.6):

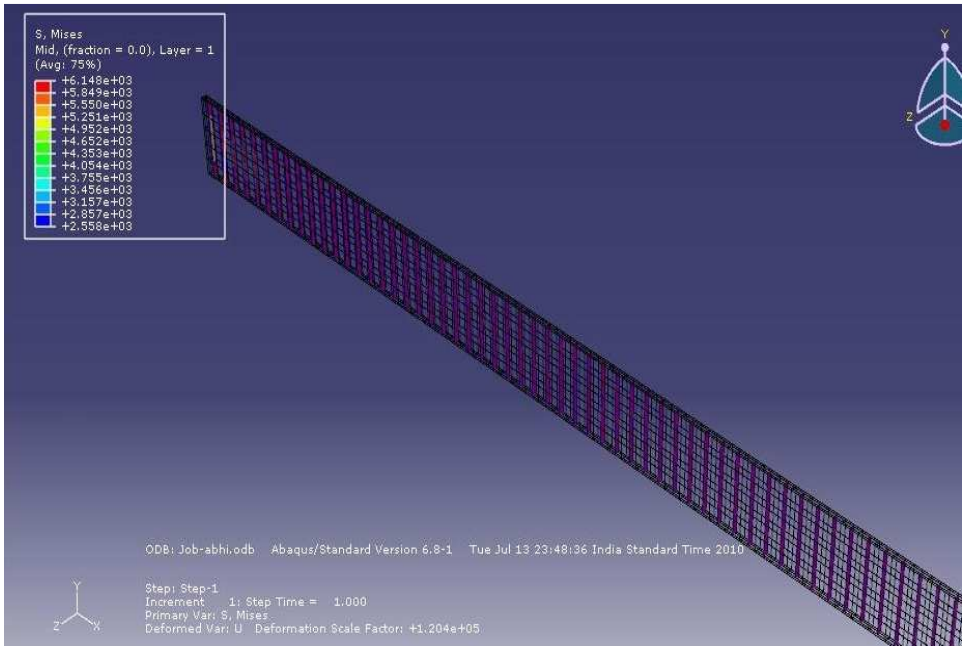

Fig. 5.6 Von-Mises stress distribution for 40% pre-fatigue loading cycle specimen

5.3.3 For 60% pre-fatigue loading cycles (Fig. 5.7):

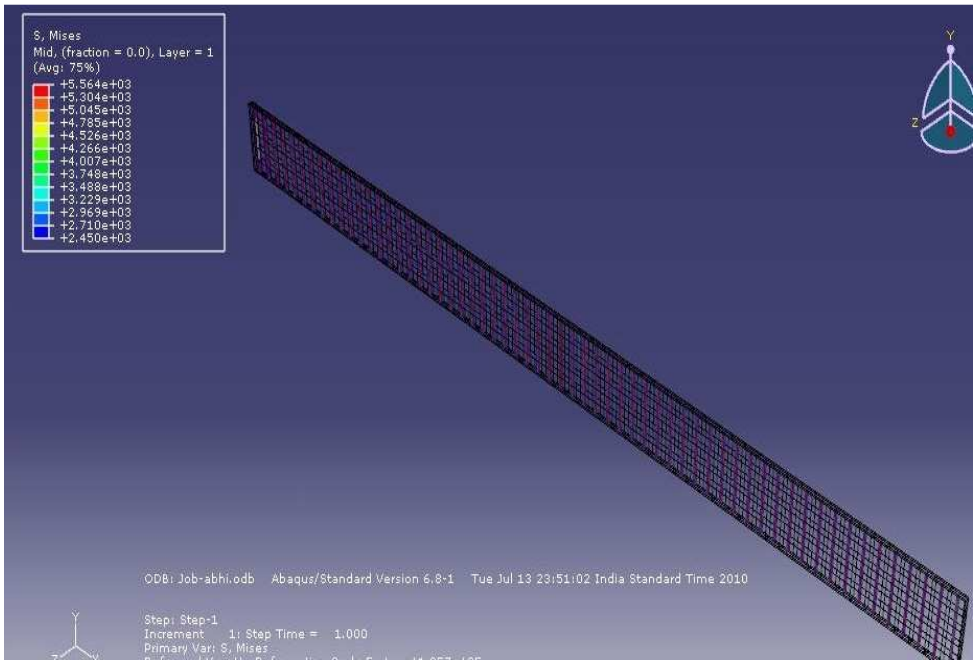

Fig. 5.7 Von-Mises stress distribution for 60% pre-fatigue loading cycle specimen

5.3.4 For 40% loading cycle in 45°C bath for one month (Fig. 5.8):

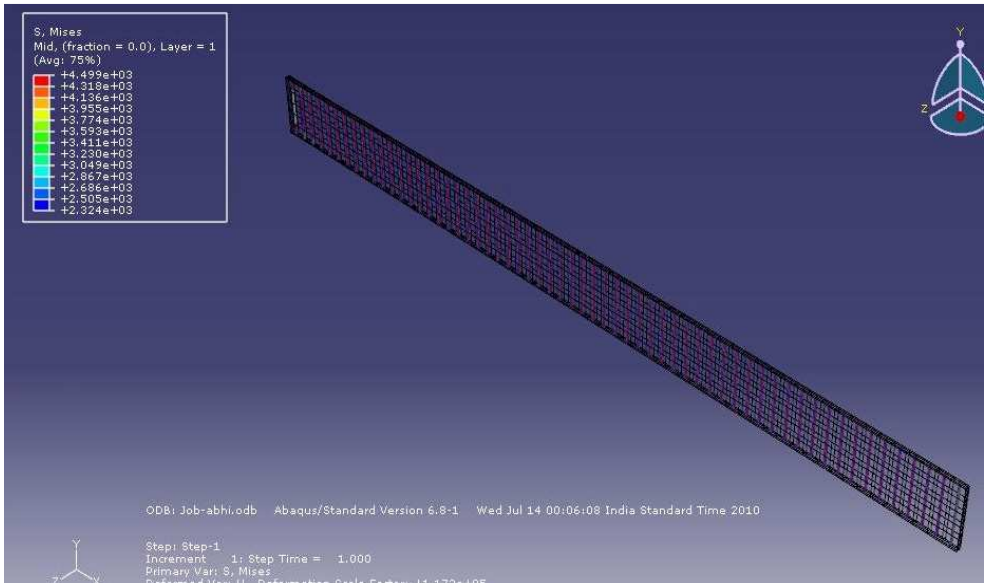

Fig. 5.8 Von-Mises stress distribution for 40% loading cycle specimen kept in 45°C bath for 1 month

5.3.5 For 60% loading cycle in 45°C bath for one month (Fig. 5.9):

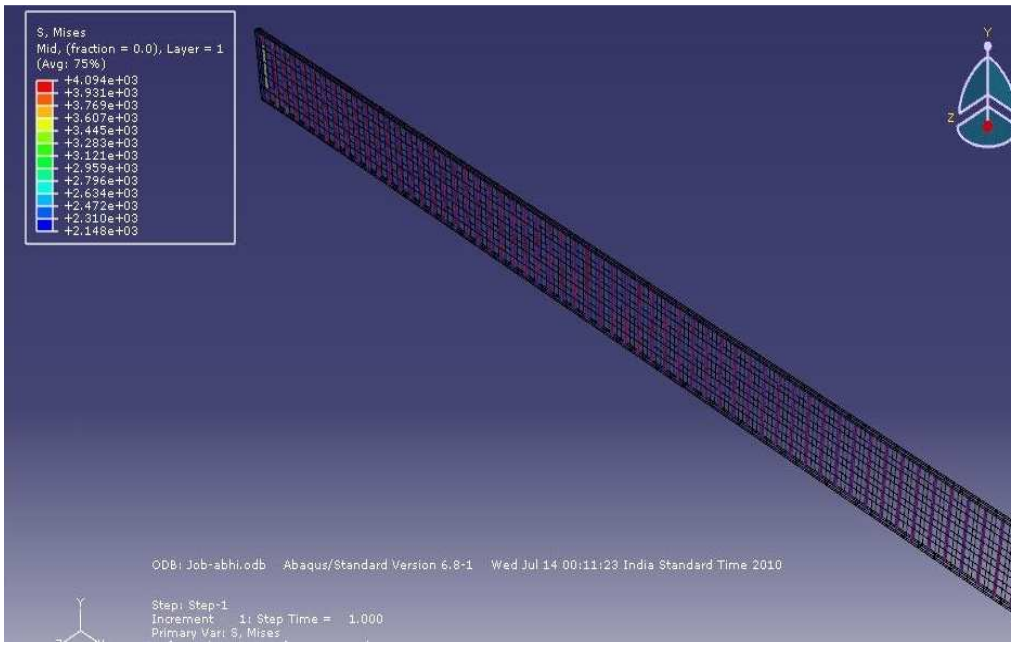

Fig. 5.9 Von-Mises stress distribution for 60% loading cycle specimen kept in 45°C bath for 1 month

5.3.6 For 40% loading cycles in 55°C bath for one month (Fig. 5.10):

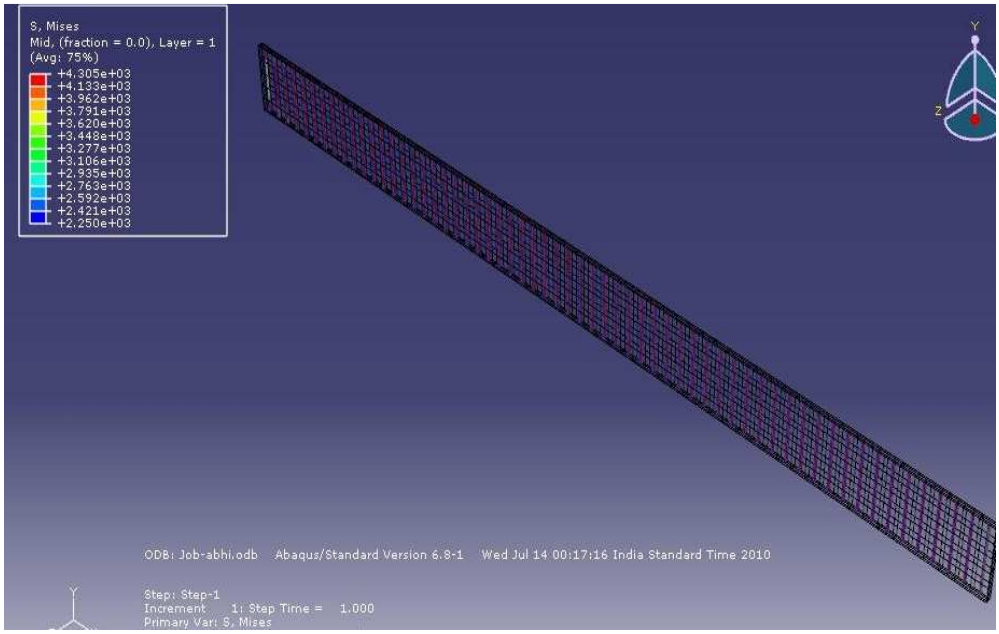

Fig. 5.10 Von-Mises stress distribution for 40% loading cycle specimen kept in 55°C bath for 1 month

5.3.7 For 60% loading cycles in 55°C bath for one month (Fig. 5.11):

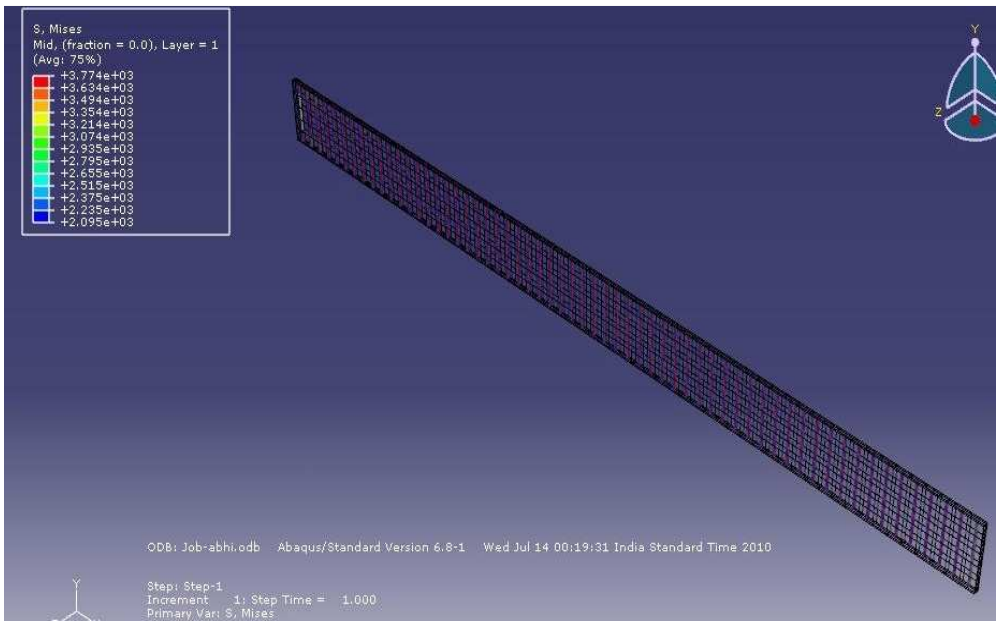

Fig. 5.11 Von-Mises stress distribution for 60% loading cycle specimen kept in 55°C bath for 1 month

5.3.8 For 40% loading cycles in 45°C bath for two month (Fig. 5.12):

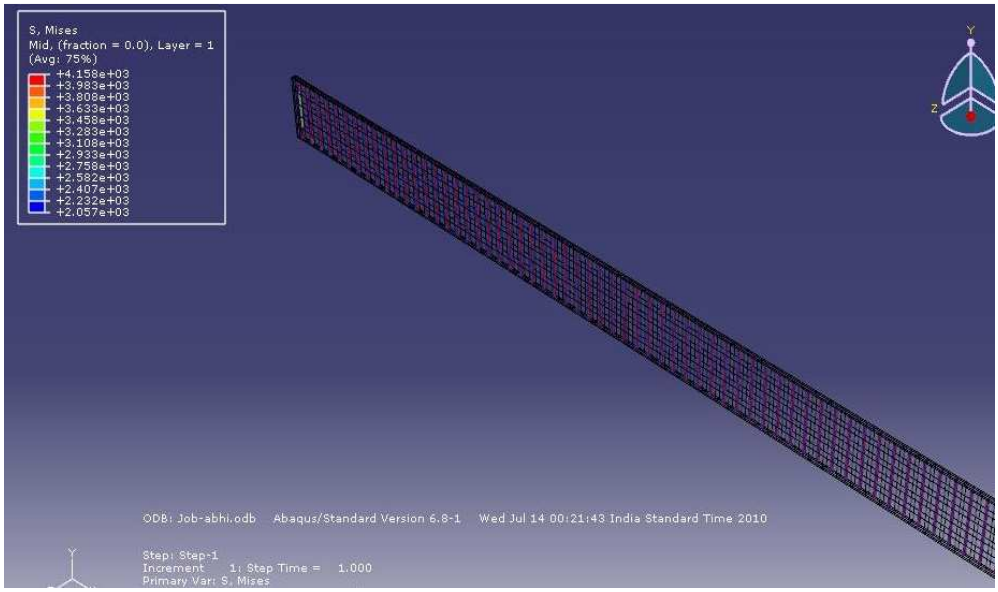

Fig. 5.12 Von-Mises stress distribution for 40% loading cycle specimen kept in 45°C bath for 2 month

5.3.9 For 60% loading cycles in 45°C bath for two month (Fig. 5.13):

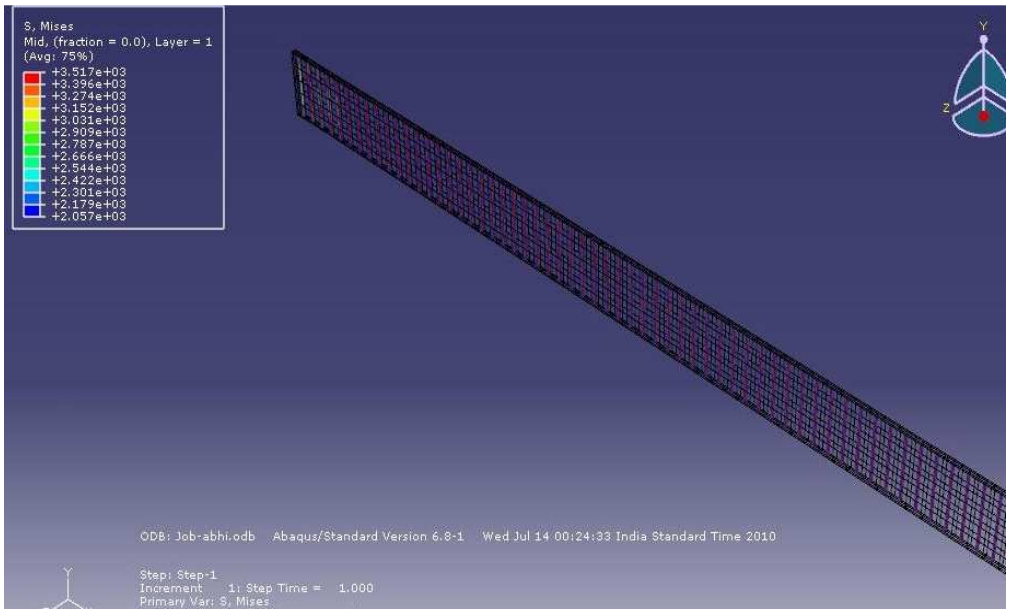

Fig. 5.13 Von-Mises stress distribution for 60% loading cycle specimen kept in 45°C bath for 2 month

5.3.10 For 40% loading cycles in 55°C bath for two month (Fig. 5.14):

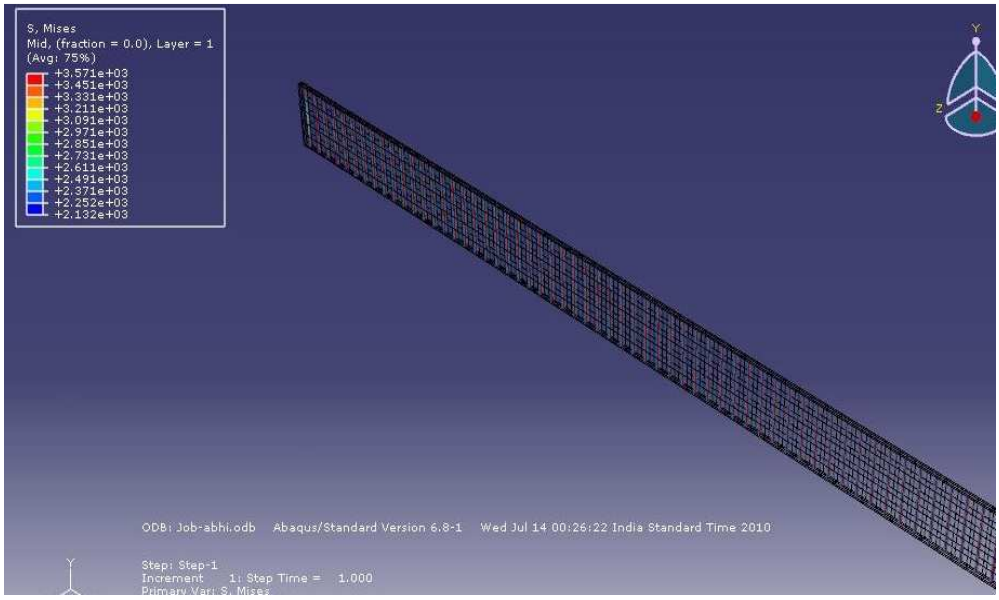

Fig. 5.14 Von-Mises stress distribution for 40% loading cycles specimen kept in 55°C bath for 2 month

5.3.11 For 60% loading cycles in 55°C bath for two month (Fig. 5.15):

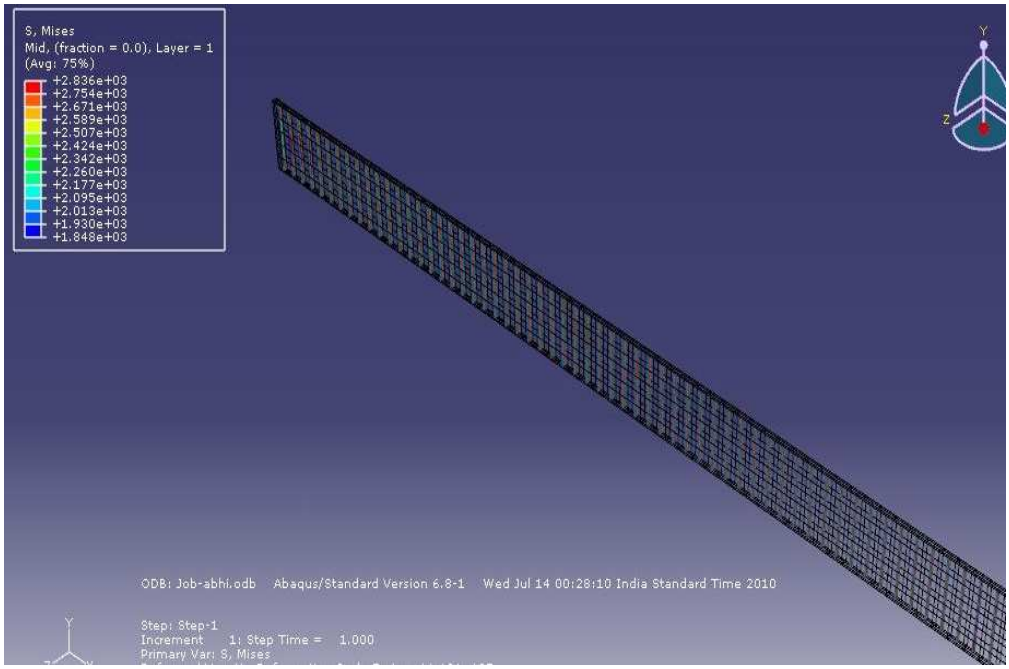

Fig. 5.15 Von-Mises stress distribution for 60% loading cycles specimen kept in 55°C bath for 2 month

Table 5.3 Maximum and Minimum Stress values for different specimen:

Stress Values	Initial specimen (1)	Fatigue loading(fraction of cycles of 20% loading)		45°C bath(1 month)		55°C bath(1 month)		45°C bath(2 month)		55°C bath(2 month)	
		40% (2)	60% (3)	40% (4)	60% (5)	40% (6)	60% (7)	40% (8)	60% (9)	40% (10)	60% (11)
MAX. (MPa)	8.419e3	6.148e3	5.564e3	4.494e3	4.094e3	4.305e3	3.774e3	4.158e3	3.317e3	3.571e3	2.836e3
MIN. (Mpa)	2.578e3	2.558e3	2.450e3	2.324e3	2.148e3	2.250e3	2.095e3	2.057e3	2.057e3	2.132e3	1.848e3

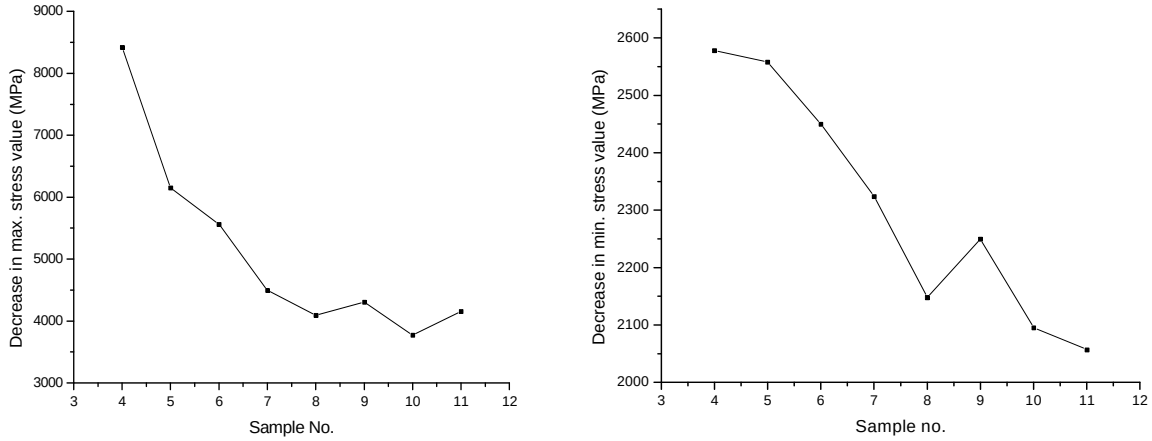

Fig. 5.16 Graphs showing max. & min. stress value trends for different specimen

Discussion:

- The values obtained from finite element analysis indicate the trend of decrement of stress values at different nodal points as shown in table 5.3 and it is shown clearly that with decreasing strength, the maximum stress it can bear is also decreasing but there is not much decline in the minimum stress value for the specimen (refer Fig. 5.16).
- Also it is clearly visible that the stress distribution for the GFRP material is almost uniform as there is not much difference in the maximum and minimum stress values.
- So, it indicates the uniform load bearing property of GFRP materials.

CHAPTER 6 RESULTS AND DISSCUSSION

6.1 MACROSCOPIC BEHAVIOR

6.1.1 Mode of Failure (Macroscopic Visual Observations)

As per the visual observation the initial specimen had fine shiny epoxy coating and the failure of such specimen under uniaxial tensile load showed an abrupt type and shear type failure.
After 1 month of exposure in water baths there was heavy visible scale formation on all the specimen (refer Fig. 6.1 and Fig. 6.2). Surface observation showed that epoxy had lost its shine and outer edges on either side showed little fanning out. But still after bending (by hands) the specimen showed considerable strength and flexibility. Abrupt type failure was visible for the initial as well as for one month duration specimen (Fig. 6.3 and 6.5).
After 2 months of environmental exposure in water baths observations of degradation and heavy scaling were noted with more scale formation on water immersed specimen as compared to first month observations for water immersed specimen (Fig.6.1 and Fig.6.2). Shear type failure after two months in water for 60% loading cycles was seen in the specimen as shown in Fig. 6.3 and Fig. 6.6.

(a) **(b)**

Fig. 6.1 Shows condition of specimen taken out after (a) one month (b) two month for 40% loading cycles at 55°C.

(a) **(b)**

Fig. 6.2 Shows condition of specimen taken out after (a) one month (b) two month for 60% loading cycles at 55°C.

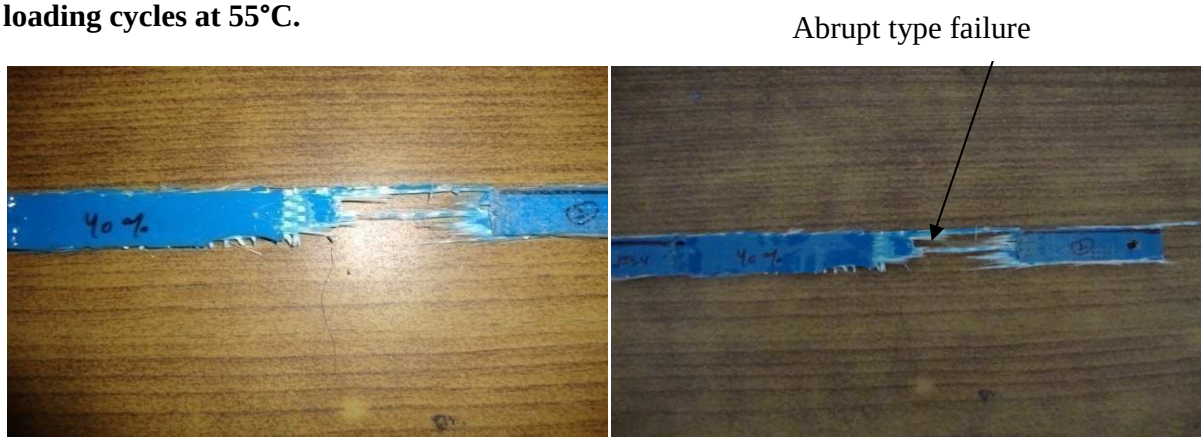

(a) **(b)**

Fig. 6.3 Shows abrupt type failure in tensile testing after (c) one month (d) two month for 40% loading cycles at 45°C

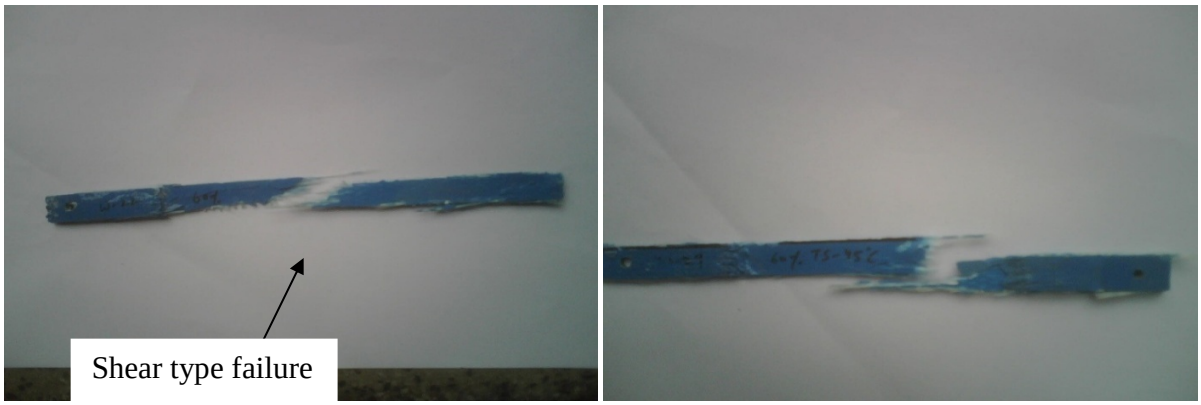

(a) **(b)**

Fig. 6.4 Shows abrupt type failure in tensile testing after (c) one month (d) two month for 60% loading cycles at 45°C

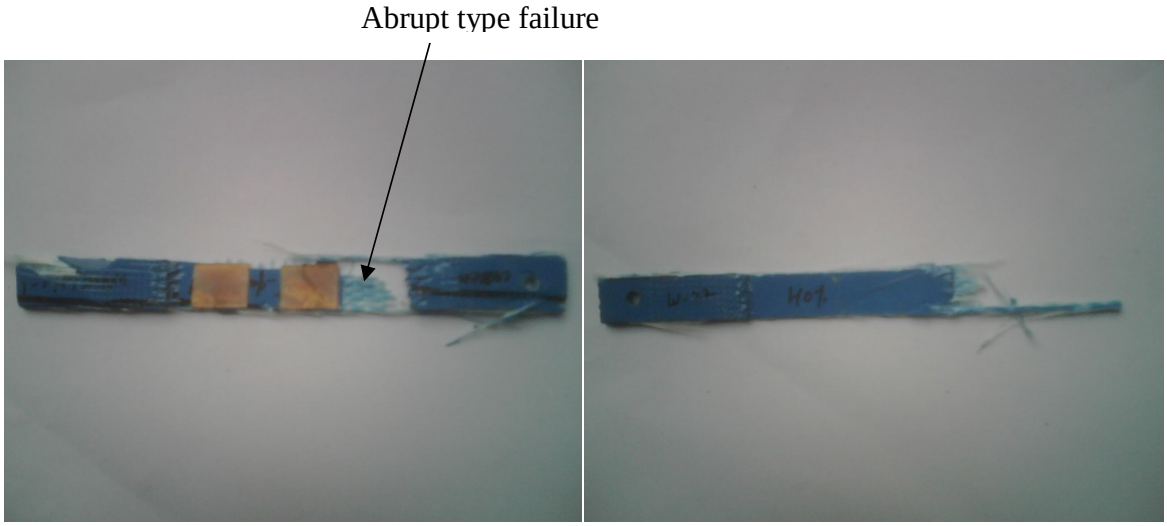

(a) **(b)**

Fig. 6.5 Shows abrupt type failure in tensile testing after (a) one month (b) two month for 40% loading cycles at 55°C

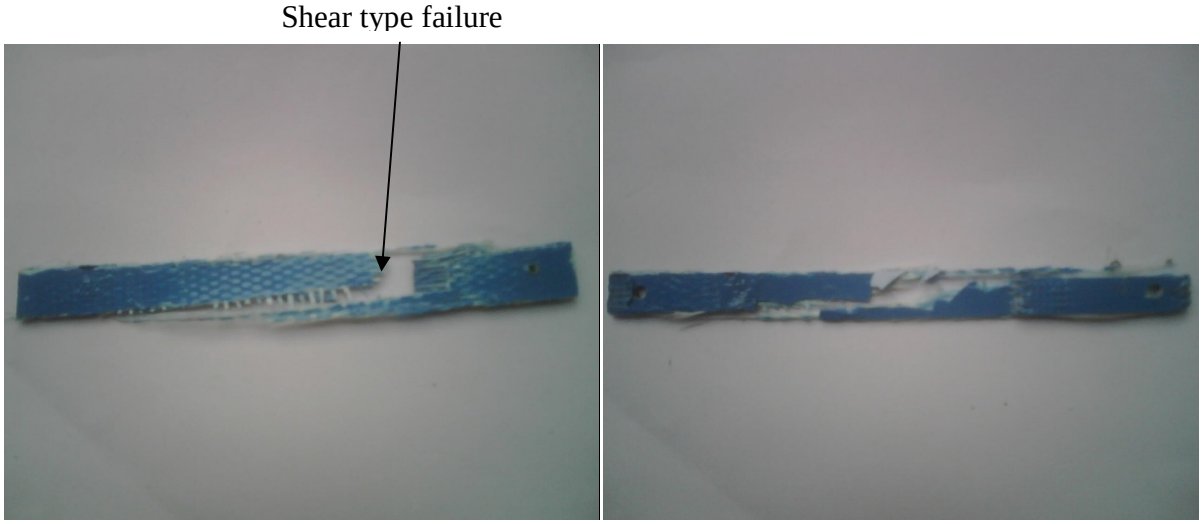

(a) **(b)**

Fig. 6.6 Shows abrupt type failure in tensile testing after (a) one month (b) two month for 60% loading cycles at 55°C

6.1.2 Ultimate Tensile Strength

Fig. 6.7 Tensile testing machine used for testing **Fig. 6.8 Gripped specimen on the machine**

A Universal Tensile testing machine (Fig.6.7) was used for the testing of the GFRP specimen for its tensile strength. All the pre-fatigued specimen (Fig. 6.8) as well as specimen at different conditions were tested until they break.

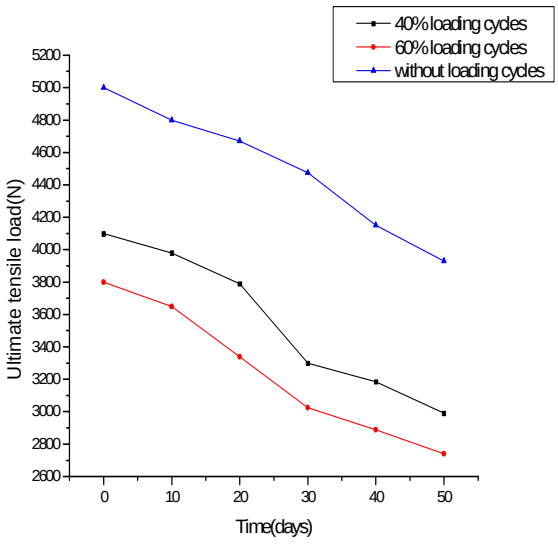

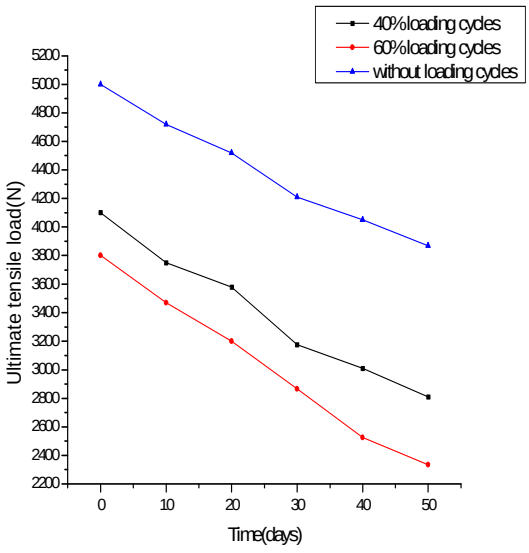

Fig. 6.9 For 45°C Bath **Fig. 6.10 For 55°C Bath**

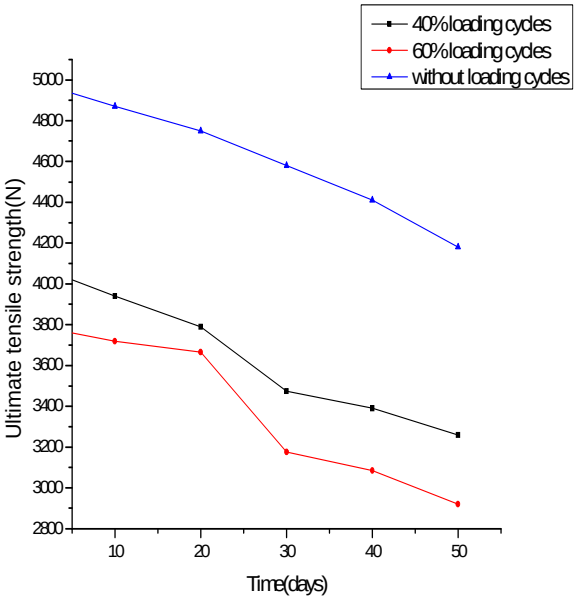

Fig. 6.11 For Natural Bath

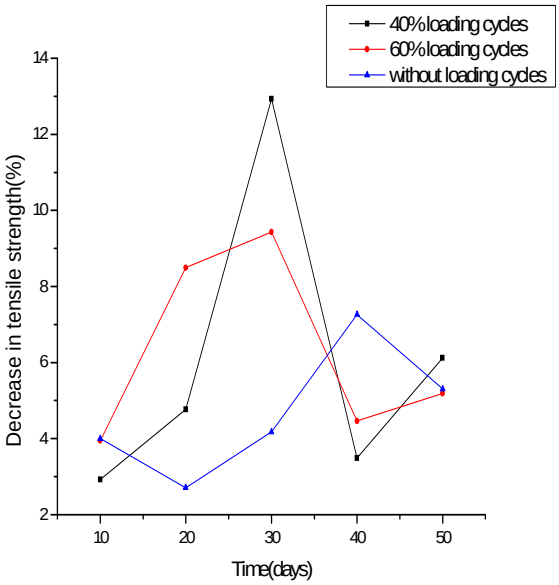

Fig. 6.12 For 45°C Bath

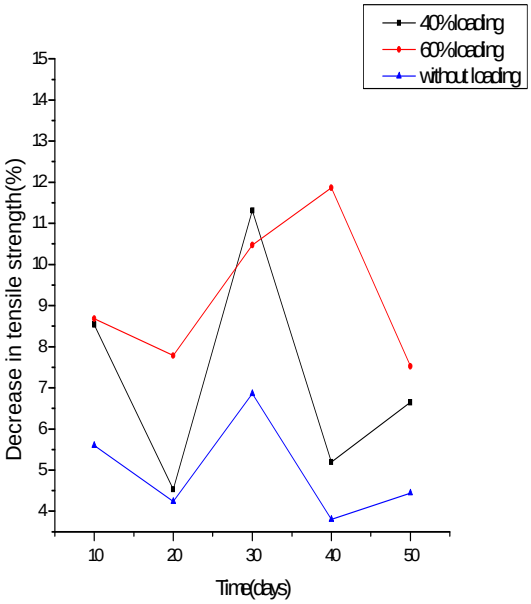

Fig. 6.13 For 55°C Bath

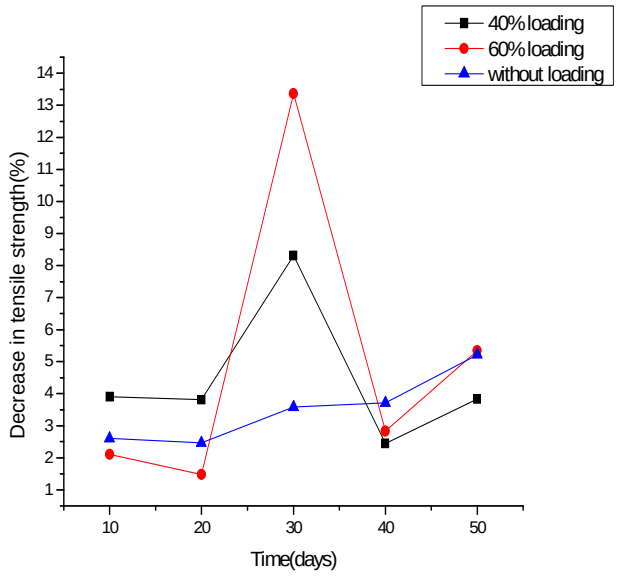

Fig. 6.14 For Natural Bath

Table 6.1 Discussion on the Ultimate Tensile Strength of the specimen (refer Fig. 6.9 to 6.14):

Loading (%)	Slope (Rate of decrease in tensile strength)			Drop (N)		
	55°C bath	45°C bath	Natural bath	55°C bath	45°C bath	Natural bath
60	29.3	23.4	17.6	1465	1170	880
40	25.8	22.2	16.8	1290	1110	840
0	22.6	21.4	16.4	1130	1070	820

From the above table 6.1 it is clear that the rate with which the tensile strength is decreasing is more for 55°C bath as compared to 45°C bath and minimum in case of natural degradation for each type of loading.

For different loadings it is seen that for a given temperature maximum decrease in tensile strength has occurred in case of 60% loading cycles as compared to 40% loading cycles and minimum for the specimen which are without fatigue loading cycles.

6.1.3 Percentage Weight gain

The time variation of percentage weight gain (w_t) can be measured as:

$$w_t = \frac{(W(t)-Wo)}{Wo} \text{x} 100$$

Here *W(t)* is the total weight after time *t*

W_0 is the reference dry weight of the specimen before immersion in medium

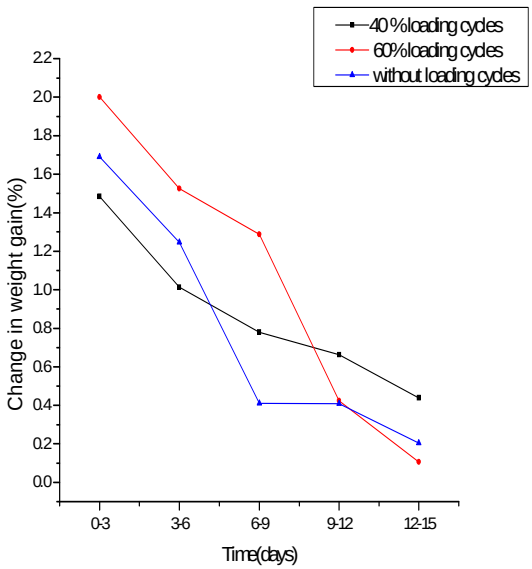

Fig. 6.15 For 45°C Bath (3-day alt.)

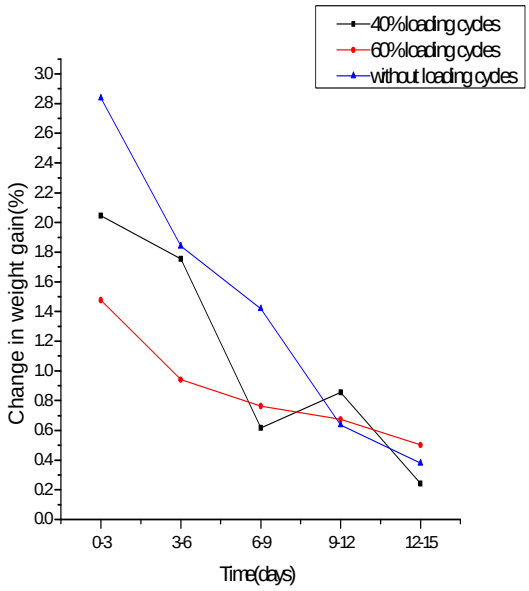

Fig. 6.16 For 55°C Bath (3-day alt.)

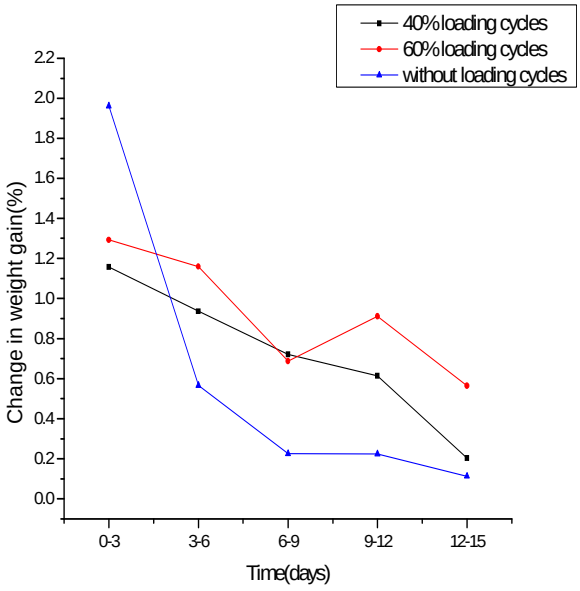

Fig. 6.17 For Natural Bath (3-day alt.)

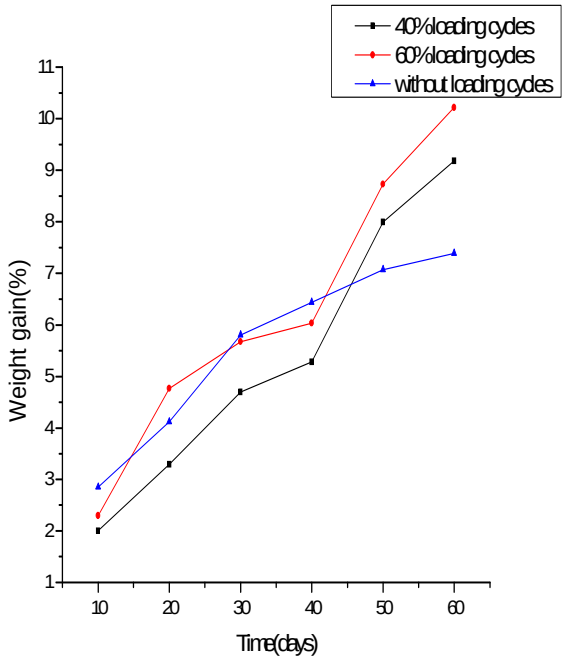

Fig. 6.18 For 45°C Bath

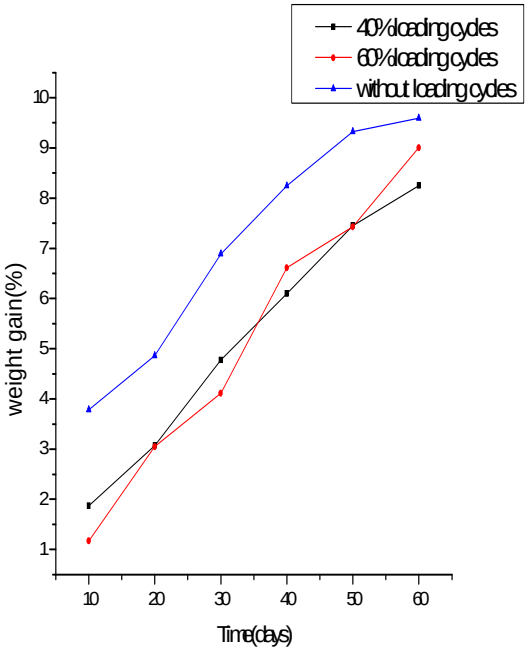

Fig. 6.19 For 55°C Bath

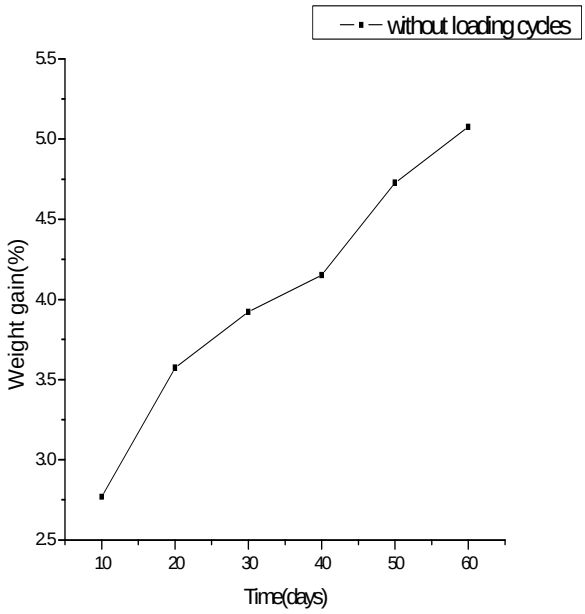

Fig. 6.20 For Natural Bath

Table 6.2 Discussion on the percentage weight gain of specimen of the specimen (refer Fig. 6.15 to 6.20):

Loading (%)	Slope (Rate of change of weight gain percentage)		Drop (%)	
	55°C bath	45°C bath	55°C bath	45°C bath
60	0.134	0.132	7.927	7.9213
40	0.116	0.1197	6.977	7.182
0	0.097	0.076	5.81	4.541

The percentage weight gain for different loaded specimen at different time period were compared at two different temperatures i.e. at 55°C and 45°C as shown in table 6.2. It could be easily noticed that at higher temperatures the weight gain is more effective in comparison to the lower temperatures.

Similarly for different water tanks the percentage weight gain is increasing with respect to time indicating that more moisture is absorbed after two months compared to first month in all the specimen with different loads.

Also specimen which are in the same bath show greater percentage of weight gain in case of specimen with increasing cyclic loading.

6.1.4 Diffusivity

Diffusivity for the specimen is calculated by using the formula:

$$D=\pi\left(\frac{h}{4M_m}\right)^2\left(\frac{M_2-M_1}{\sqrt{t_2}-\sqrt{t_1}}\right)^2(1+\frac{h}{L_e}+\frac{h}{w})^2$$

Where Le, W, and h are the length, width and thickness of the test specimen, respectively, and M1 and M2 are moisture contents at times t1 and t2, respectively.

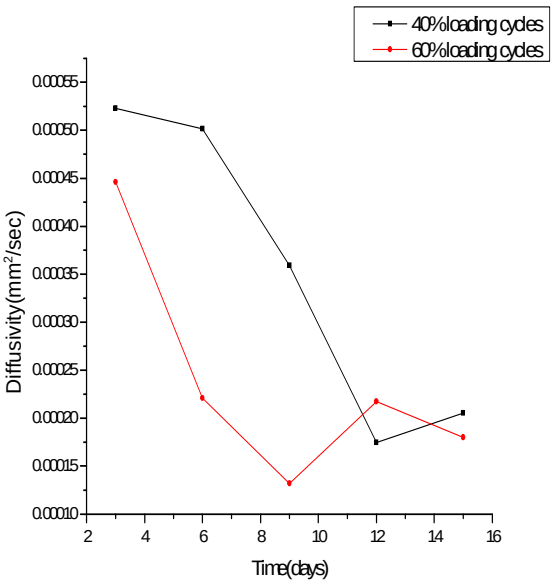

Fig. 6.21 For 45°C Bath (3-day alt.)

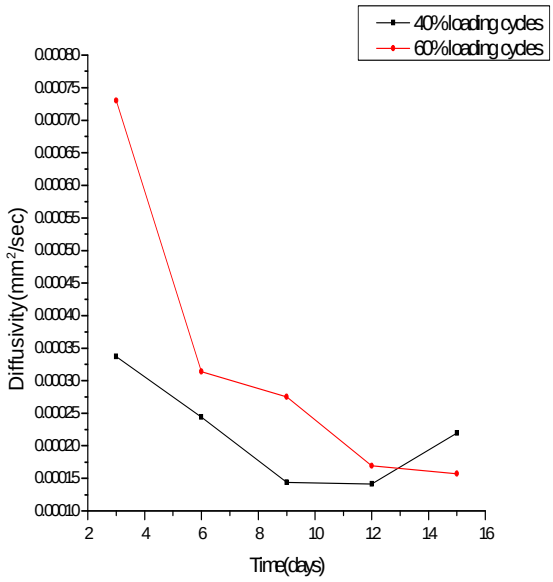

Fig. 6.22 For 55°C Bath (3-dat alt.)

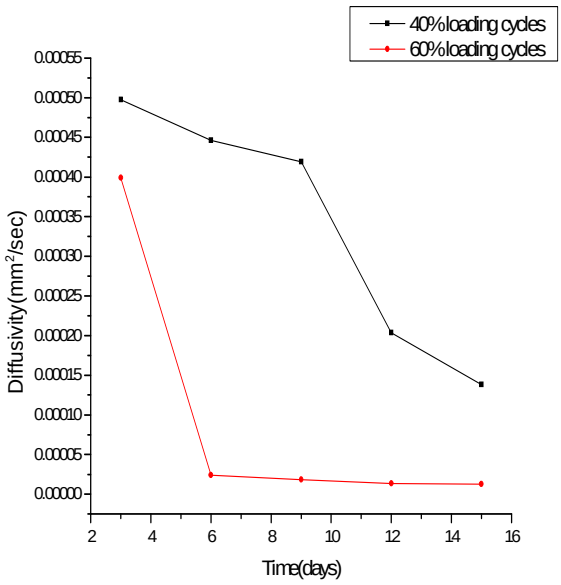

Fig. 6.23 For Natural Bath (3-day alt.)

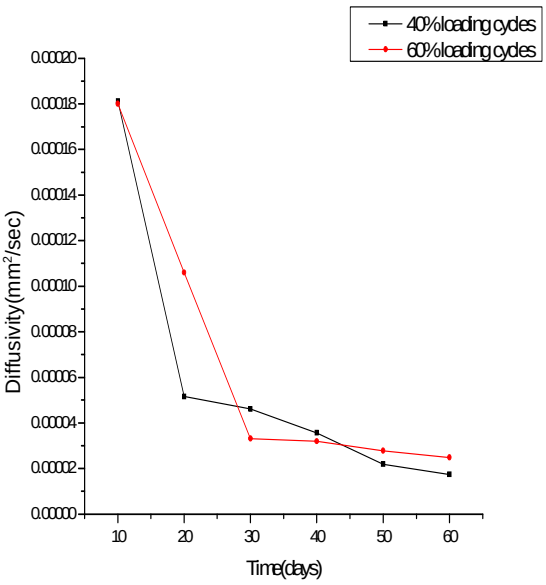

Fig. 6.24 For 45°C Bath

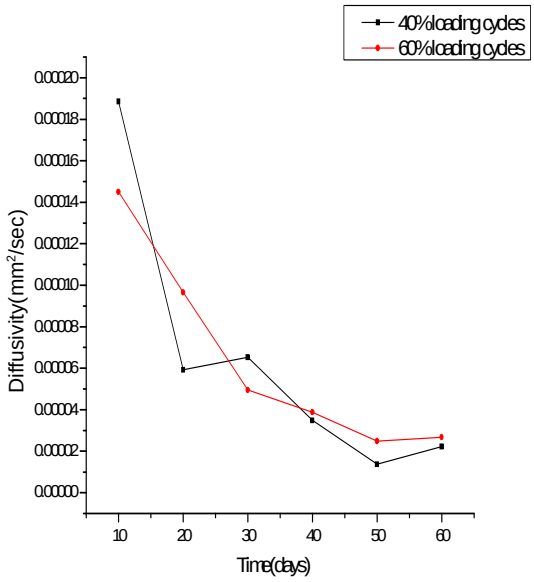

Fig. 6.25 For 55°C Bath

Table 6.3 Discussion on diffusivity rate of the specimen (refer Fig. 6.21 to 6.25):

Loading (%)	**Slope (Rate of change of diffusivity)**		**Drop (mm^2/sec)**	
	55°C bath	**45°C bath**	**55°C bath**	**45°C bath**
60	-1.97E-06	-2.58E-06	-1.18E-04	-1.55E-04
40	-2.77E-06	-2.73E-06	-1.66E-04	-1.64E-04

The above data from table 6.3 for the diffusivity shows that there is a decrease in the diffusivity for all specimen at different temperatures with time i.e. the diffusivity at initial stage is maximum which keeps on decreasing with time i.e. at one month record and minimum for two month.

Also it is clear from the data that for 55°C bath the rate of diffusivity as well as the diffusivity value is much larger as compared to specimen at 45°C bath.

The loading parameters also show that for given time and temperature the specimen with 60% loading cycles have higher diffusivity compared to specimen with 40% loading cycles.

6.1.5 Capacitance

The capacitance of the specimen is calculated at following parameters (refer Fig. 6.26):

Circuit:	Series
Lock:	C
Parameter:	Impedance
Reference:	none
Speed:	Normal
Mode:	Cont.
Delay:	1 s
Frequency:	50 Hz
Level:	1.00 V
DC-Bias:	Off
Fixture-Set:	0
Contact Check:	Off
Scan:	Freq. log
From:	50 Hz
To:	1 MHz
Step:	1

Fig. 6.26 RCL Meter used for capacitance test

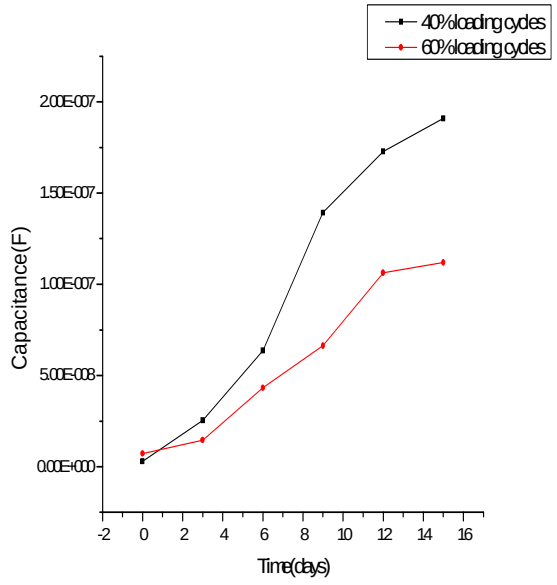

Fig. 6.27 For 45°C Bath (3-day alt.)

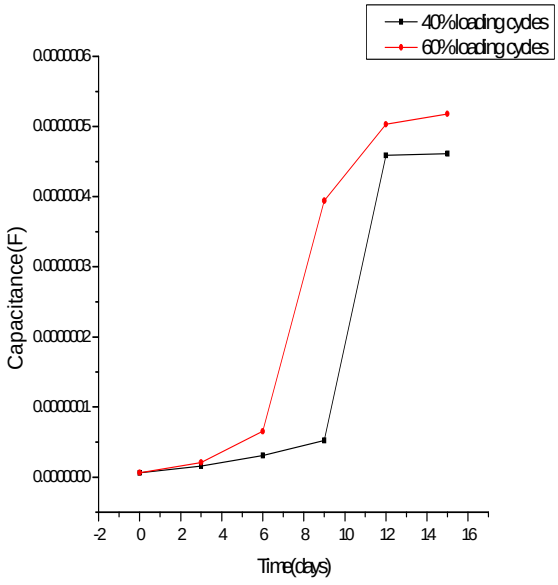

Fig. 6.28 For 55°C Bath (3-day alt.)

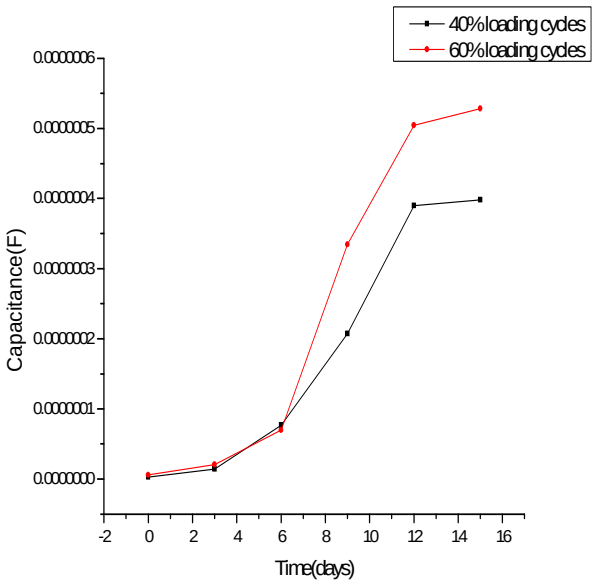

Fig. 6.29 For Natural Bath (3-day alt.)

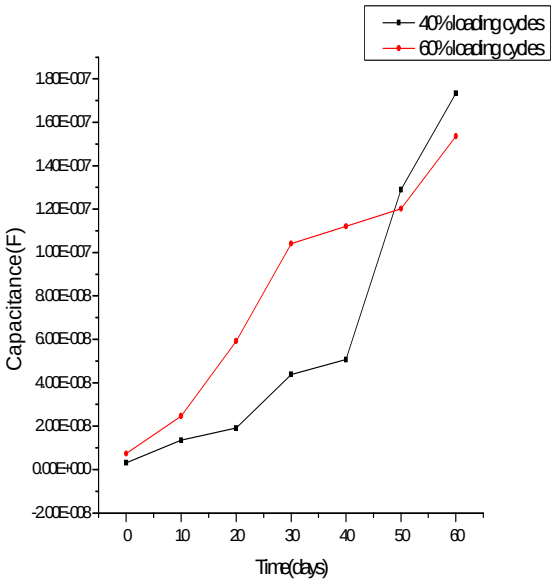

Fig. 6.30 For 45°C Bath

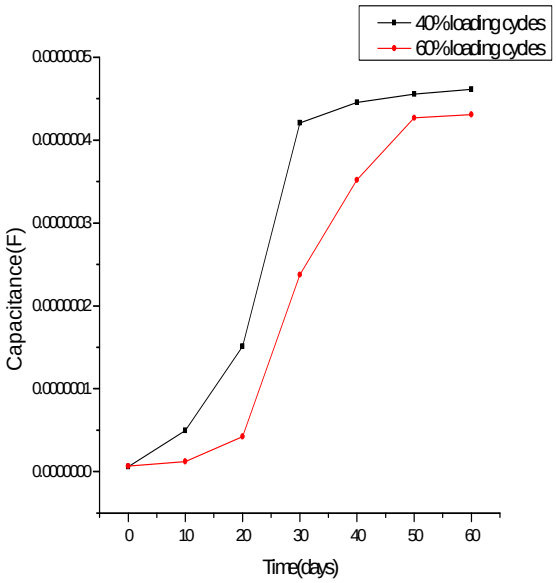

Fig. 6.31 For 55°C Bath

Table 6.4 Discussion on capacitance change of the specimen (refer Fig. 6.27 to 6.31):

Loading (%)	Slope (Rate of change of capacitance)		Drop (F)	
	55°C bath	45°C bath	55°C bath	45°C bath
60	7.57E-09	2.4365E-09	4.55E-07	1.46E-07
40	7.09E-09	2.83811E-09	4.24E-07	1.70E-07

From above data shown in table 6.4, it is clear that the rate of increase of capacitance is larger in case of water bath with temperature 55°C as compared to the 45°C bath.

Also with the data collected at one month and two month time period it is evident that the rate of increase for first month is high as compared to the increase in second month.

The increase for higher loading cycle specimen i.e. 60% is slightly higher than the less loading cycle specimen i.e. 40%.

The above graph pattern is comparable to the increase in weight gain.

So it clearly shows that the weight gain nature can be easily predicted with the capacitance increase data in GFRP specimen.

6.2 MICROSCOPIC BEHAVIOR

6.2.1 Micro-hardness

The micro-hardness data was collected at following parameters (refer Fig.6.32):

Load applied: 200 gm.

Magnification used: 10X

Dwell time 20 sec.

Fig 6.32 Micro-hardness testing machine

The micro-hardness for specimen in each bath was measured at regular intervals. The setup consists of a computer attached to the micro-hardness testing machine as shown in the Fig.6.32. Firstly an indent is made on the surface (Fig.6.33) of the specimen and then the micro-hardness estimation is made by the software employed for the same purpose (Fig.6.34).

The study is helpful for developing a relationship between micro-hardness change and change in tensile strength.

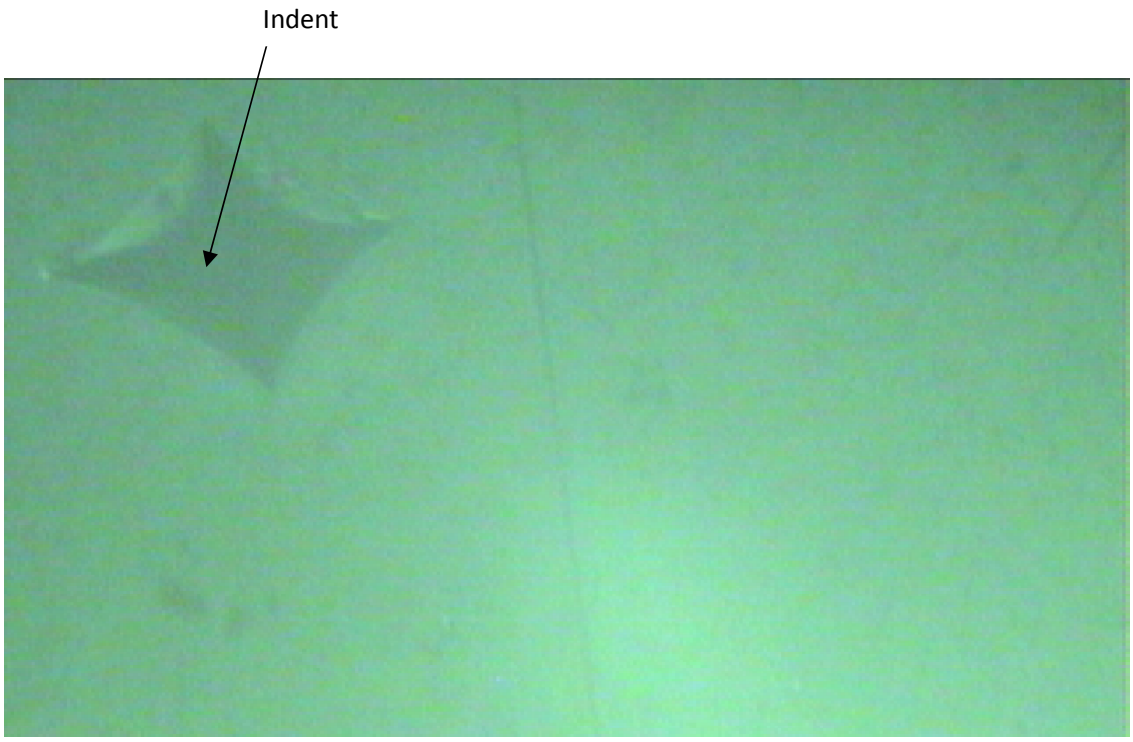

Fig.6.33 Indent shown in the image for micro-hardness estimation

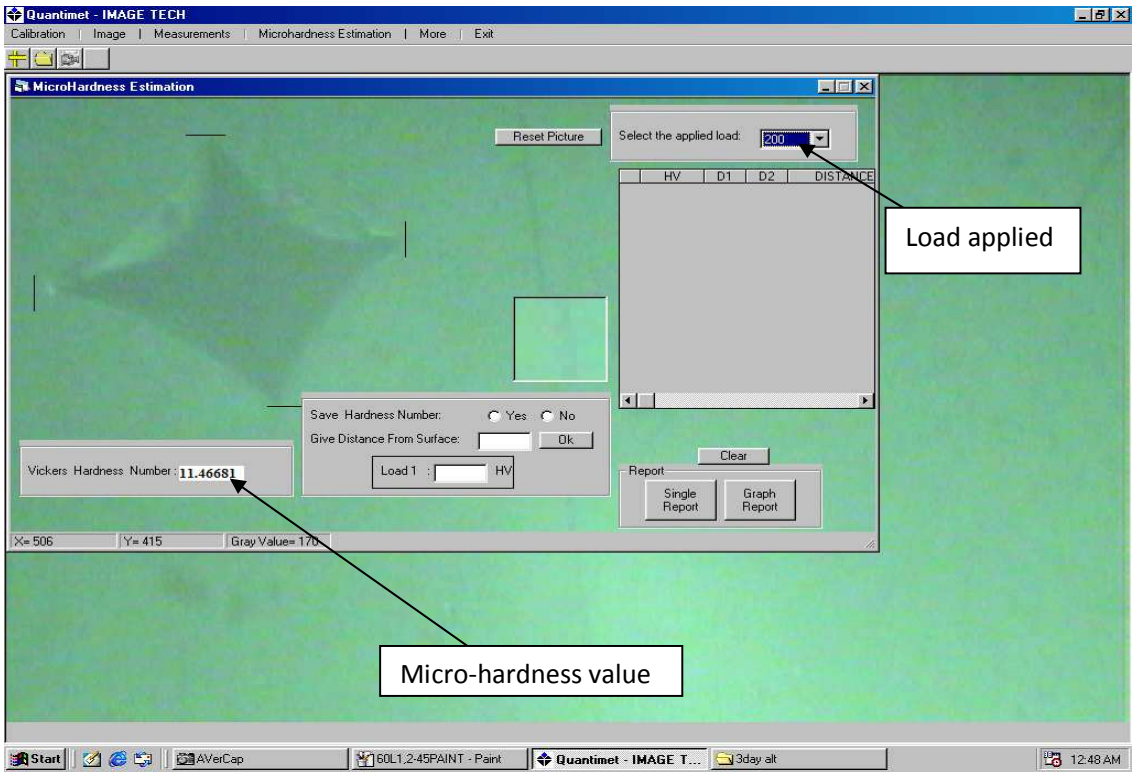

Fig 6.34 Image showing the micro-hardness value of the specimen

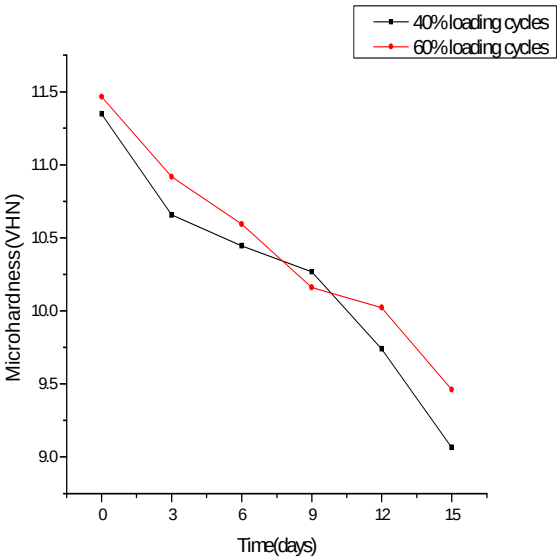

Fig. 6.35 For 45°C Bath (3-day alt.)

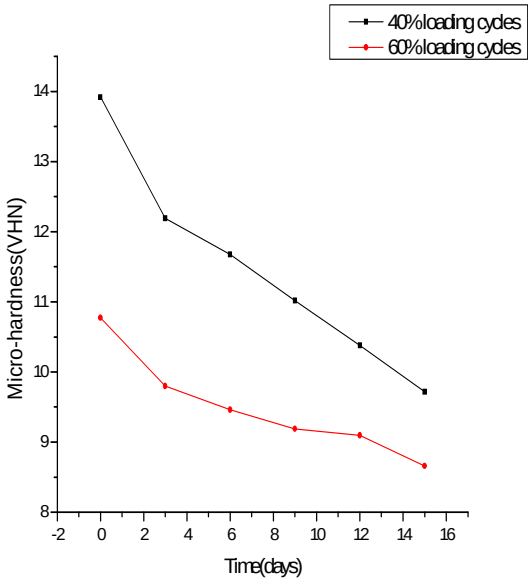

Fig. 6.36 For 55°C Bath (3-day alt.)

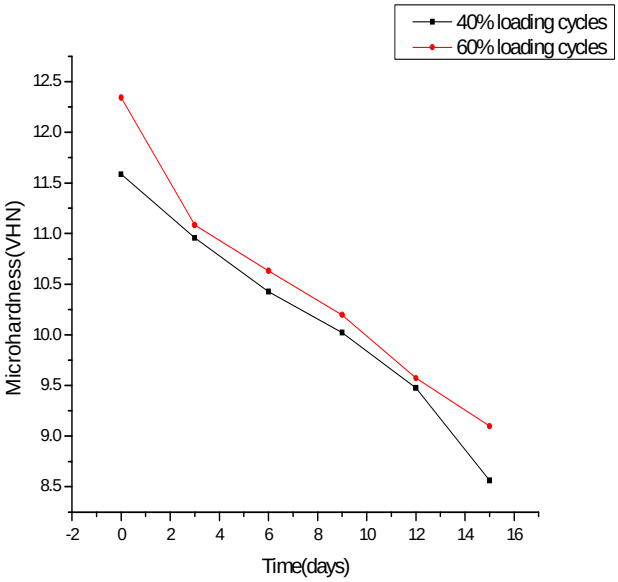

Fig. 6.37 For Natural Bath (3-day alt.)

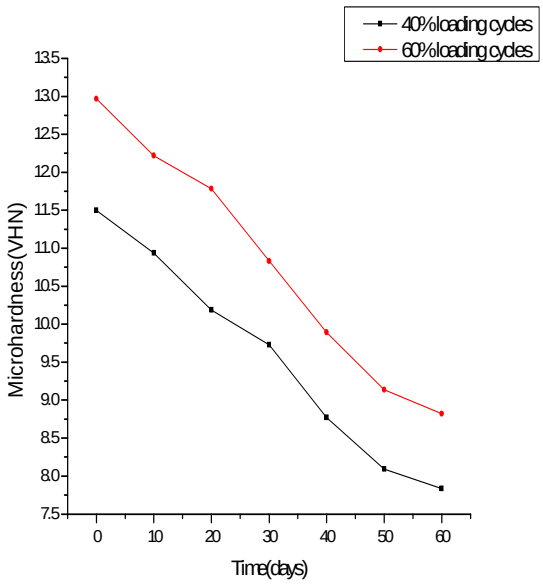

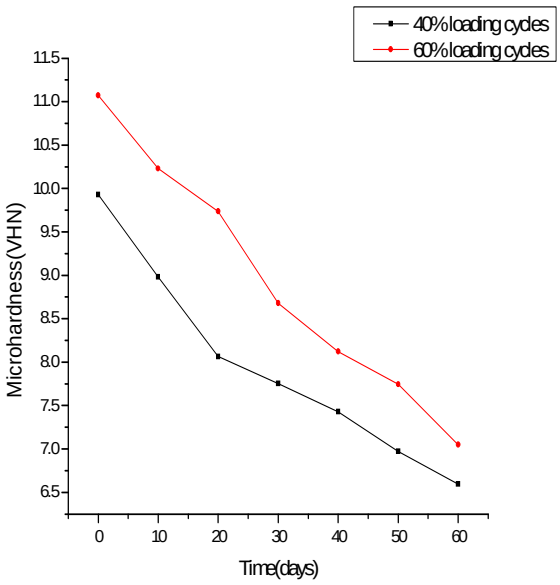

Fig. 6.38 For 45°C Bath **Fig. 6.39 For 55°C Bath**

Table 6.5 Discussion on micro-hardness change of the specimen (refer Fig. 6.35 to 6.39):

Loading (%)	**Slope (Rate of change of micro-hardness)**		**Drop (VHN)**	
	55°C bath	**45°C bath**	**55°C bath**	**45°C bath**
60	-0.06874	-0.069744	-4.12453	-4.04648
40	-0.0612	-0.0555	-3.66524	-3.33287

The above table 6.5 shows that the rate of decrease in the micro-hardness is more dominant in case of specimen dipped in bath with higher temperature (55°C) as compared to bath at lower temperature (45°C).

Also it is clear that at given time and temperature the specimen with higher loading cycles (60%) have higher drop in hardness as thus having higher rate of change as compared to specimen with lesser loading cycles (40%).

The time variation can also be discussed as it is clearly shown in the graph that the rate of micro-hardness decrease is higher in first month as compared to second month which is due to lesser diffusivity rate in second month as discussed earlier.

6.2.2 Scanning Electron Microscope (SEM) Readings

SEM micrographs are helpful in viewing the micro-structure of material, hence showing any changes in physical structure of material and showing any defects like cracks, voids generated after loading and hygrothermal degradation of the material. The setup is shown in Fig. 6.40.

These are also helpful in calculating the area fraction of fibre and epoxy in the given specimen and the changes occurring and for also calculating the circularity of the fibre in case of GFRP.

Fig 6.40 SEM Machine

(i)Initial specimen (refer Fig. 6.41 & 6.42)

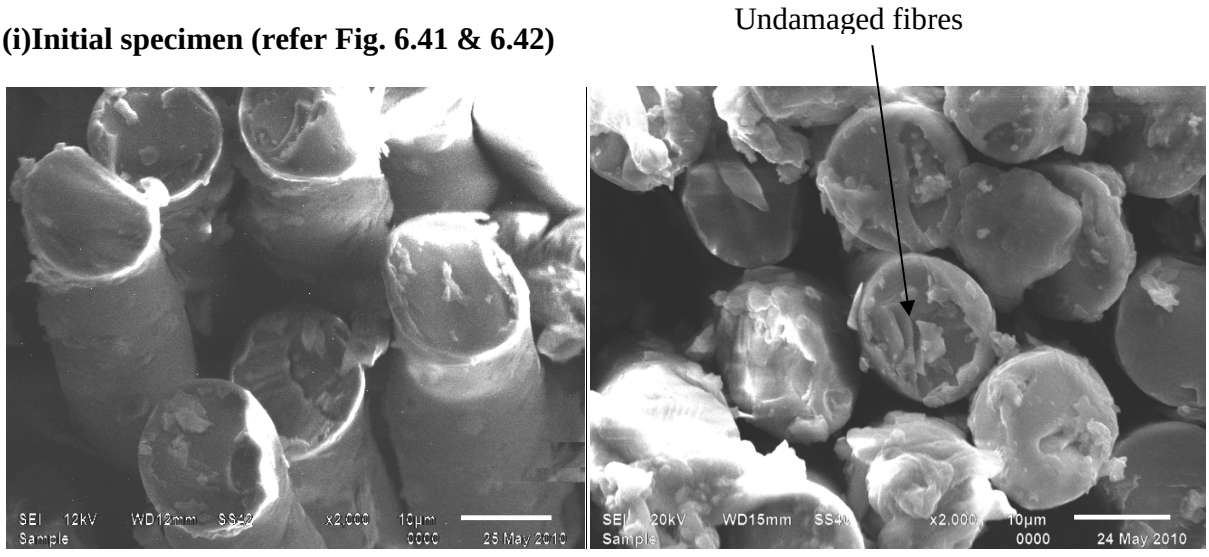

Fig 6.41 SEM micrographs of initial specimen at 2000X

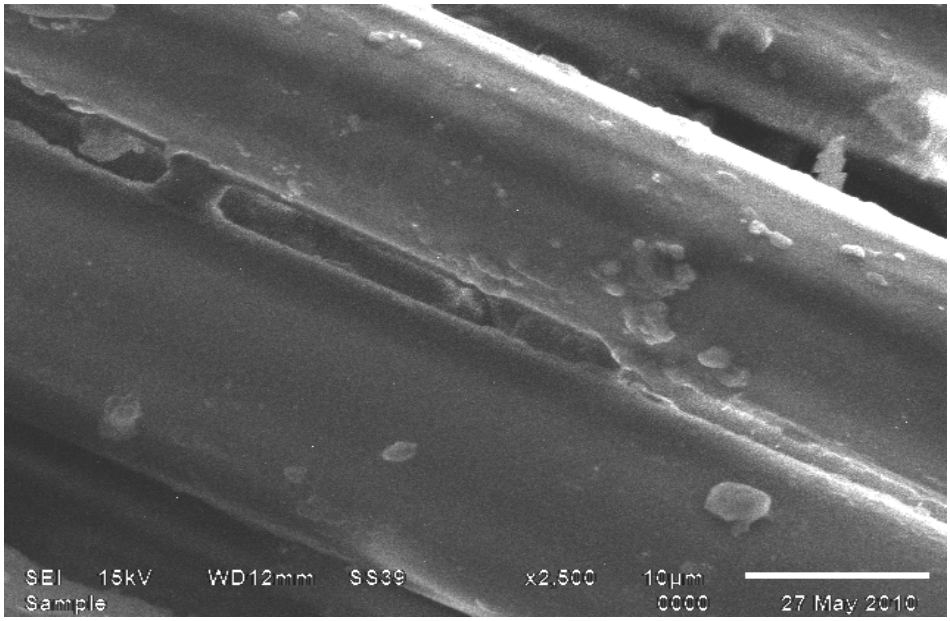

Fig. 6.42 Longitudinal fibres

(ii) After Fatigue loading (refer Fig. 6.43)

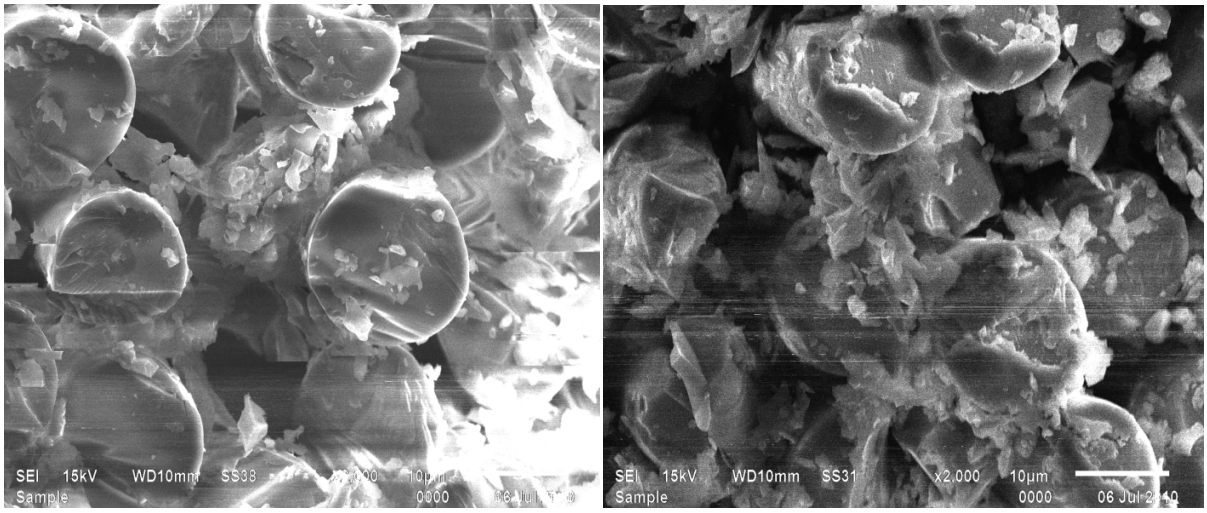

(a) **(b)**

Fig 6.43 SEM micrographs for (a) 40% loading cycles (b) 60% loading cycles

(iii)Pre-fatigued specimen after one month in water bath (refer Fig. 6.44 & 6.45)

(a)For 45°C temperature

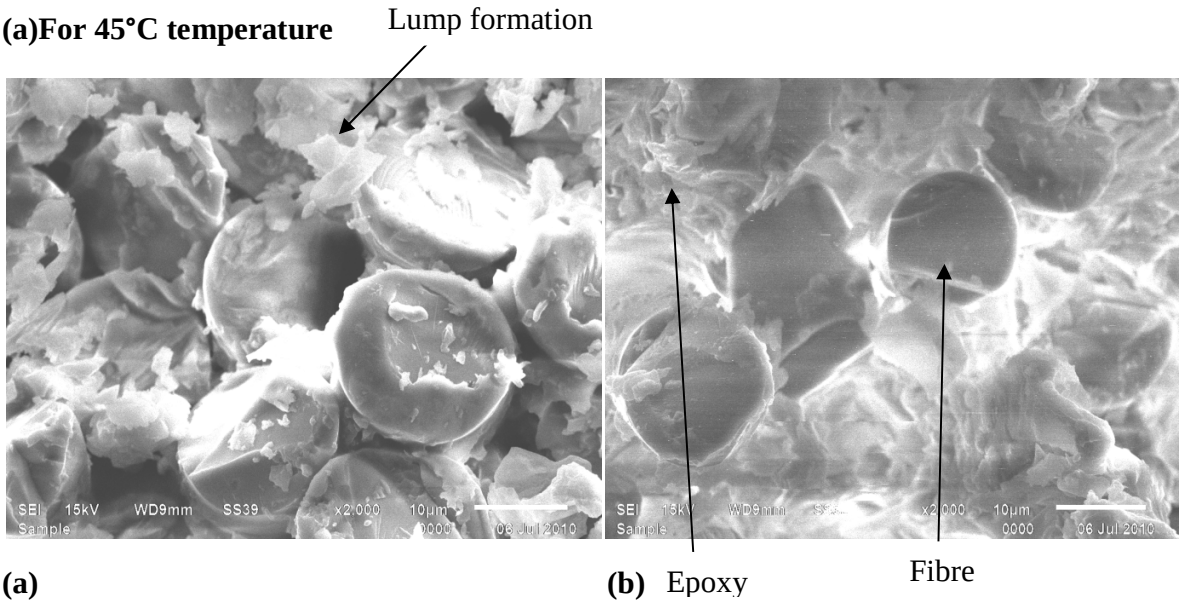

(a) **(b)**

Fig 6.44 SEM micrographs for (a) 40% loading cycles (b) 60%loading cycles

(b) For 55°C temperature

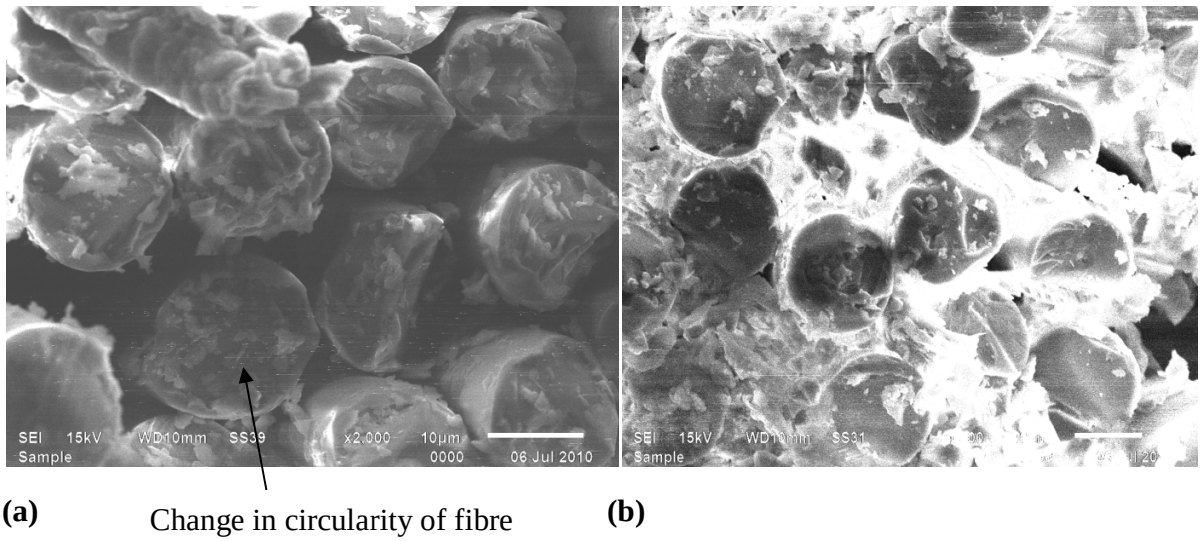

(a) **(b)**

Fig 6.45 SEM micrographs for (a) 40% loading cycles (b) 60% loading cycles

(iv) Pre-fatigued specimen after two month in water bath (refer Fig. 6.46 & 6.47)

(a)For 45°C temperature

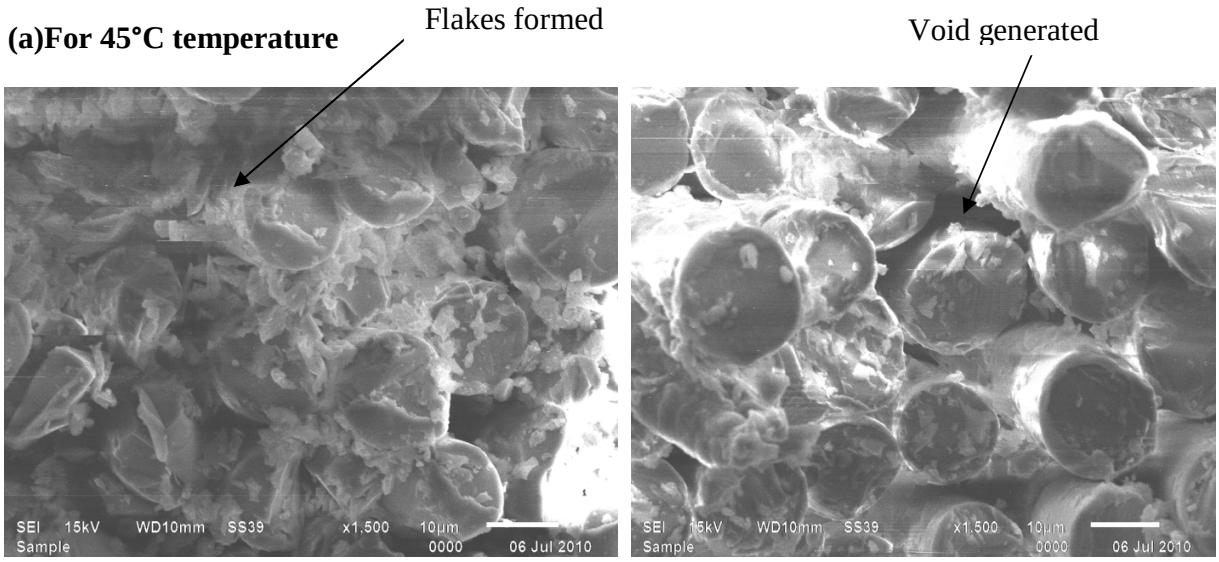

(a) **(b)**

Fig 6.46 SEM micrographs for (a) 40% loading cycles (b) 60% loading cycles

(b)For 55°C temperature

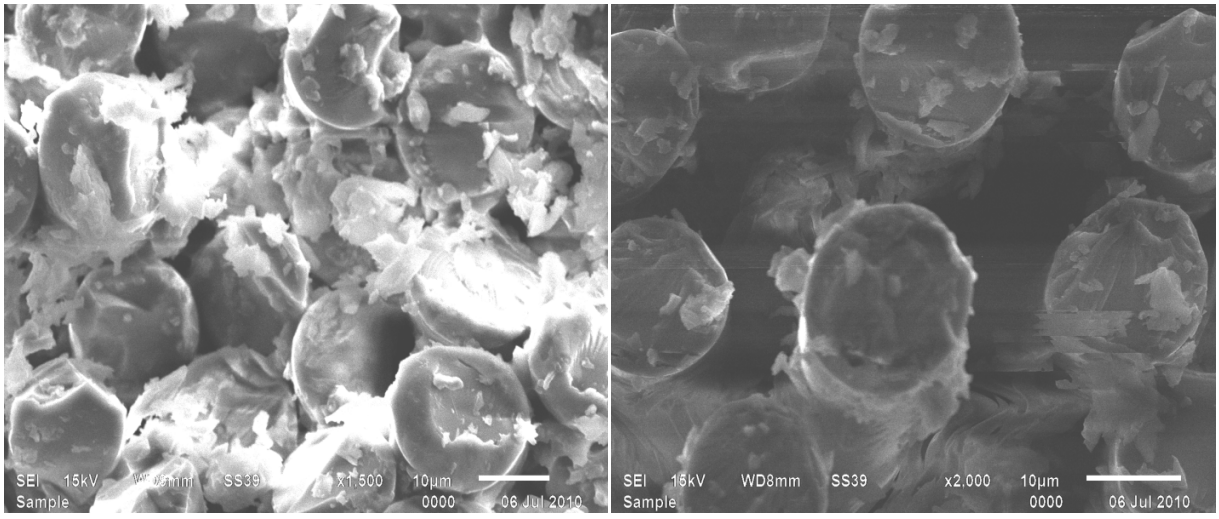

(a) **(b)**

Fig 6.47 SEM micrographs for (a) 40% loading cycles (b) 60% loading cycles

6.2.3 Area fraction and Circularity

Image Analysis by "IMAGE-J" Software for Calculating Area Fraction and Circularity:

The analysis of all the SEM images was done in order to compare the area fraction of both epoxy as well as of the fibre. The commercially available software Image-J was used for analysis of images. Image-J is open source software developed by National Institute of Health and considered as powerful for image analysis. Few representative images after analysis by software are shown from Fig.6.148 to Fig.6.154.

Procedure followed for analysis of the SEM images is explained below:

1) The image to be analyzed was opened using the software.

2) A line was drawn parallel to the 20µm line (shown on SEM images) using the Set Scale option. That distance was set equivalent to number of pixel (automatically counted by software).

3) As the scale was set, a line was drawn across fibre edges to measure the length of fibre.

4) To calculate the area fraction, firstly the image was converted to RGB color (a number of color options can be chosen, here Red/Green color option was chosen to fill the areas of SEM image)

5) After applying the above option the color of image changed (from the grey scale to chosen Red/Green), in which red color indicated the fibre area, green indicated epoxy and black was for voids. These areas were selected automatically by software according to the image contrast.

6) Using the Binary option and then selecting Make Binary, in the Procedure menu, the software converted the image to binary image.

7) To calculate the area fraction, firstly the option of measure area fraction in Set Measurement menu was activated. To measure the area fraction, the option Analyze →Measure was used. Area to be measured was selected by making a window around it and above mentioned Analyze option showed the results in a tabular form.

(i) Initial stage (refer Fig. 6.48)

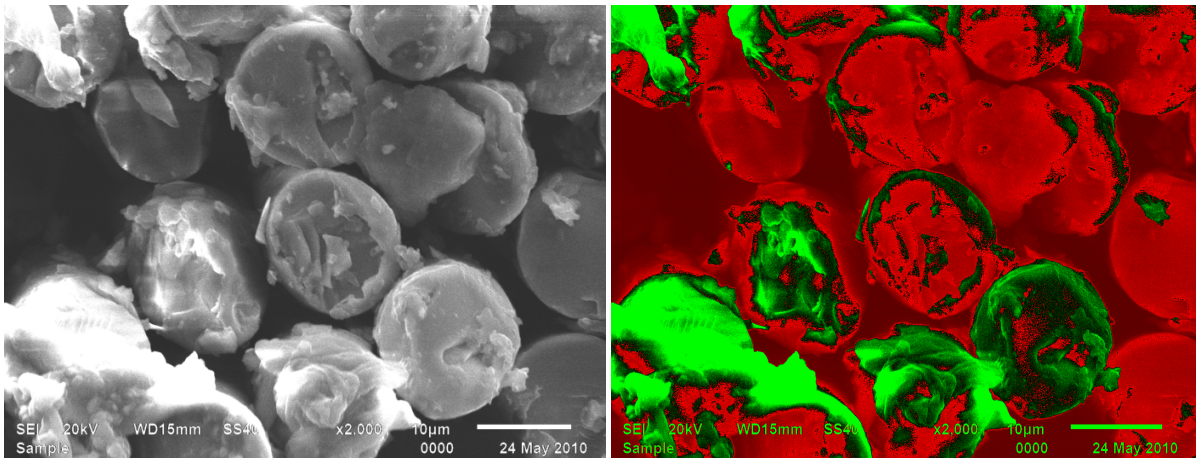

Fig.6.48 (Left) SEM image at Initial Stage, (Right) same SEM image by Image Analyzer

(ii) After Fatigue loading (refer Fig. 6.49)

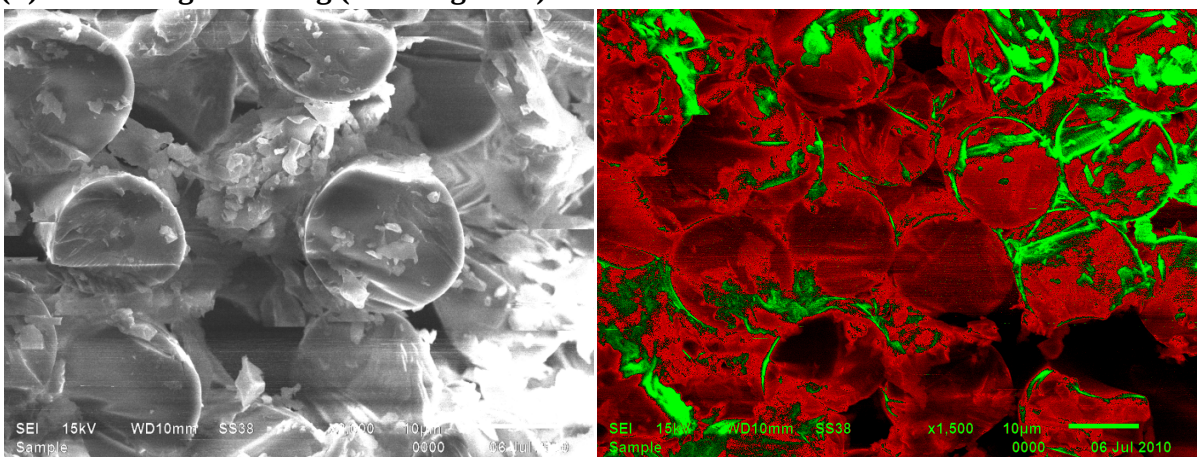

Fig.6.49 (Left) SEM image at 40% loading cycle specimen, (Right) same SEM image by Image Analyzer

(iii) After one month in water (refer Fig. 6.50 & 6.51)

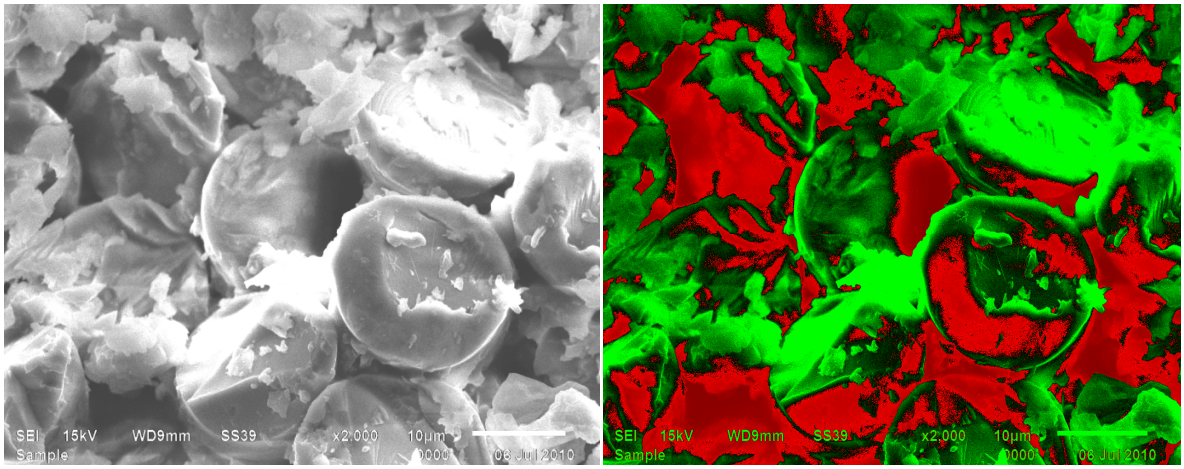

Fig.6.50 (Left) SEM image for specimen in 45°C bath, (Right) same SEM image by Image Analyzer

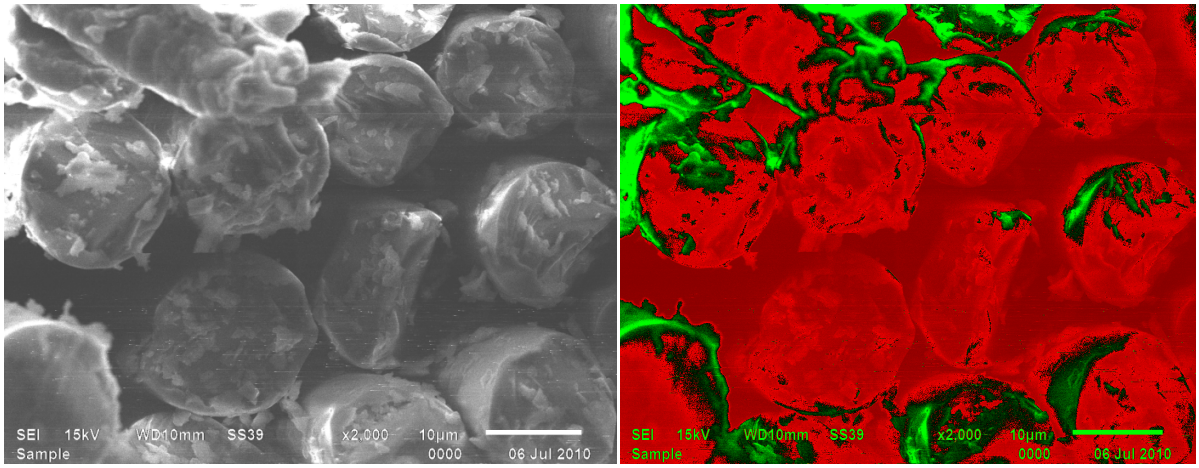

Fig.6.51 (Left) SEM image for specimen in 55°C bath, (Right) same SEM image by Image Analyzer

(iv) After two month in water (refer Fig. 6.52 & 6.53)

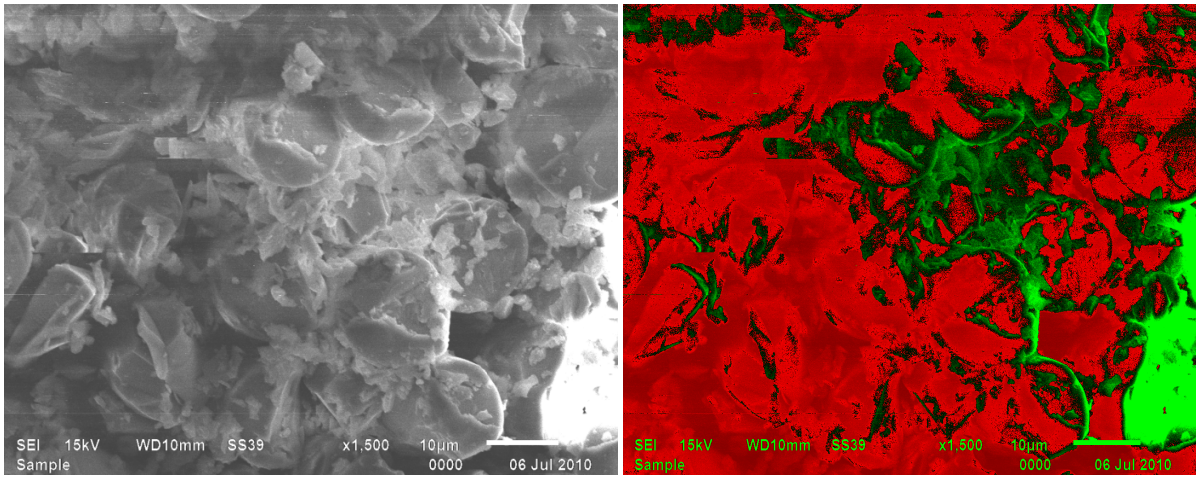

Fig.6.52 (Left) SEM image for specimen in 45°C bath, (Right) same SEM image by Image Analyzer

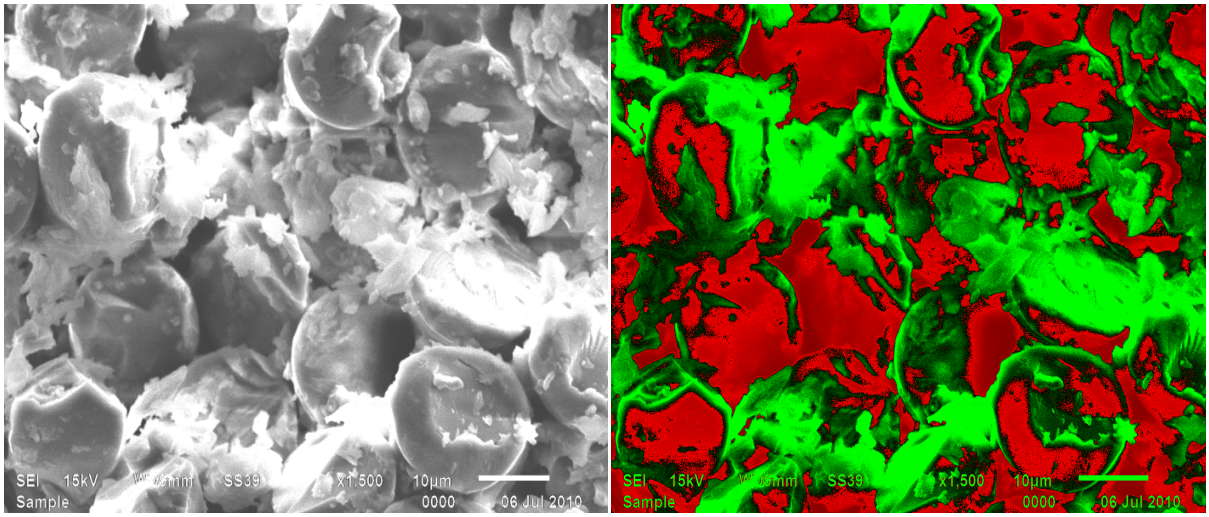

Fig.6.53 (Left) SEM image for specimen in 55°C bath, (Right) same SEM image by Image Analyzer

(a) Area fraction

After calculating the area fraction using IMAGE-J software, following results were obtained for specimen at different loadings and temperatures.

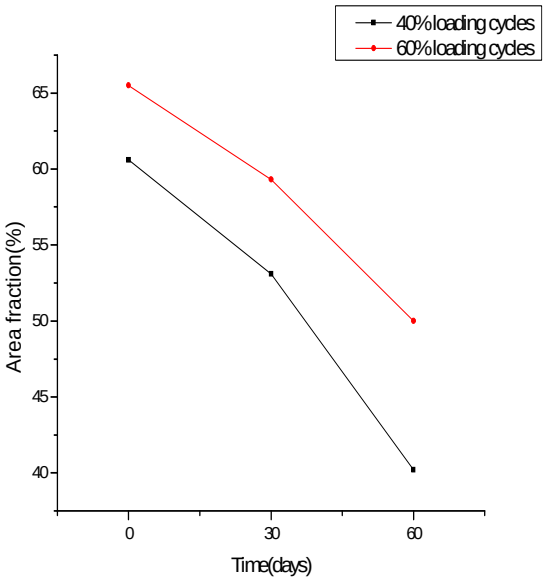

Fig. 6.54 For 45°C Bath (1500X)

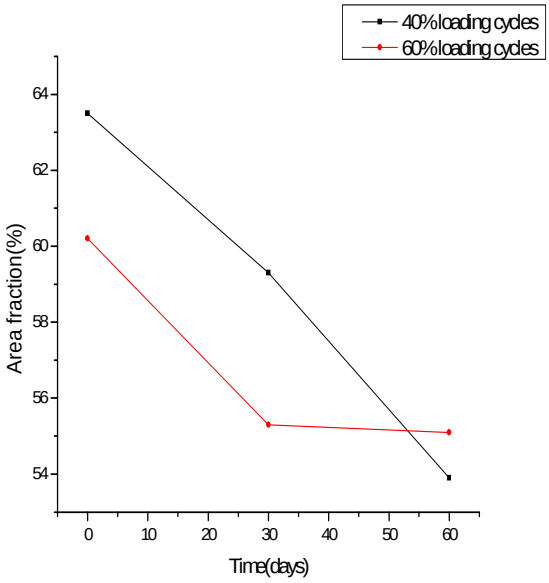

Fig. 6.55 For 45°C Bath (2000X)

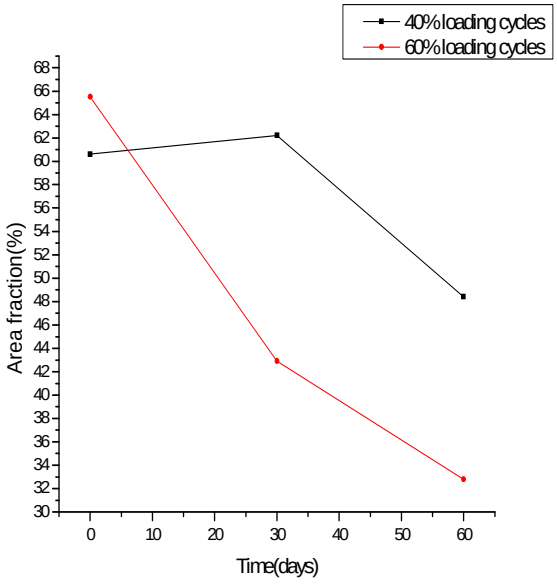

Fig. 6.56 For 55°C Bath (1500X)

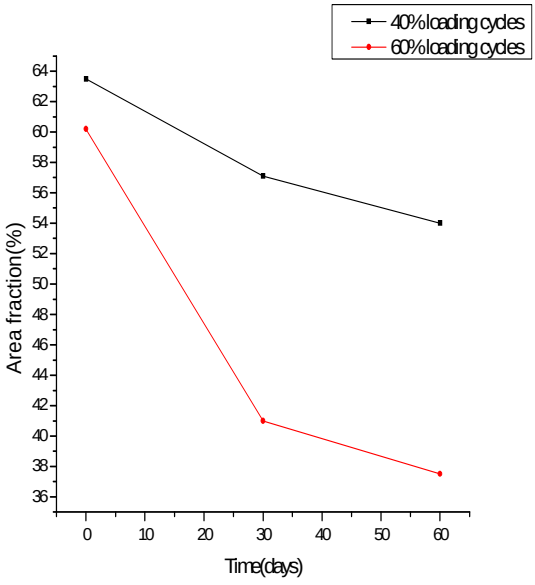

Fig. 6.57 For 55°C Bath (2000X)

Table 6.6 Discussion on area fraction change in fibres for the specimen (refer Fig. 6.54 to 6.57):

Loading (%)	Slope (Rate of change of area fraction)		Drop (%)	
	55°C bath	45°C bath	55°C bath	45°C bath
60	-0.37833	-0.085	-22.7	-5.1
40	-0.15833	-0.16	-9.5	-9.6

The above data in the table 6.6 shows a huge decrease in the fibre area fraction for 60% loading cycles specimen at 55°C bath after two month duration.

Thus, it can be clearly stated that at higher temperature and higher loading the decrease in area fraction of the fibre is also higher and the rate of this decrease is also higher compared to lower temperature and loading conditions.

The reason for this can be stated as more seepage of water in the more loaded specimen compared to less loaded ones and the higher temperature also plays a supporter for the same phenomenon.

(b) Circularity

The circularity of the fibre in the specimen can also be calculated by using IMAJE-J software. The procedure for that is given below:

(i) Either directly get the result by using the option Analyze-Measure and tick the option Shape Descriptors in Set Measurement.

(ii) The second method is to manually draw a circle over the fibre and aspect ratio would be shown on the above which is the x to y ratio and the circularity of the fibre, as shown in the Fig. 6.58.

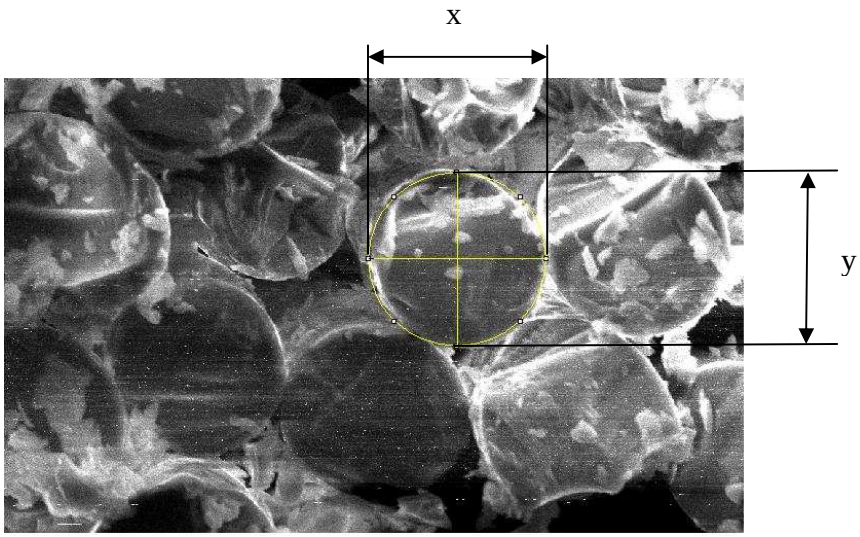

Fig.6.58 The circle drawn on the fibre gives the circularity by calculating x to y ratio

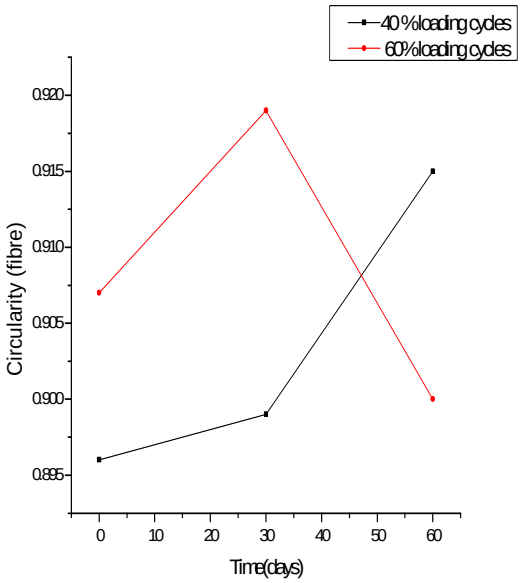

Fig. 6.59 For 45°C Bath (1500X)

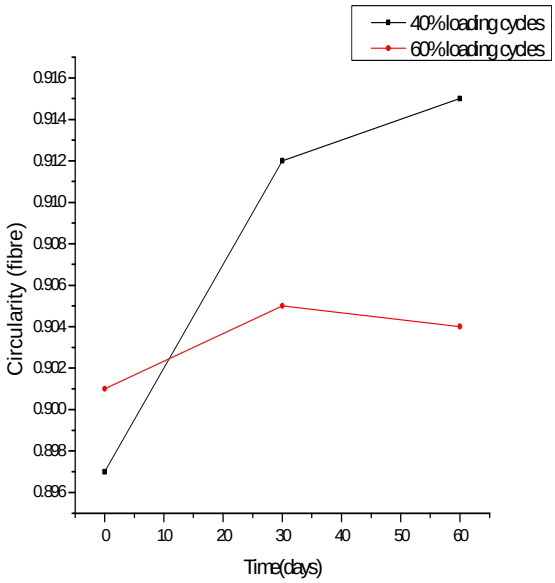

Fig. 6.60 For 45°C Bath (2000X)

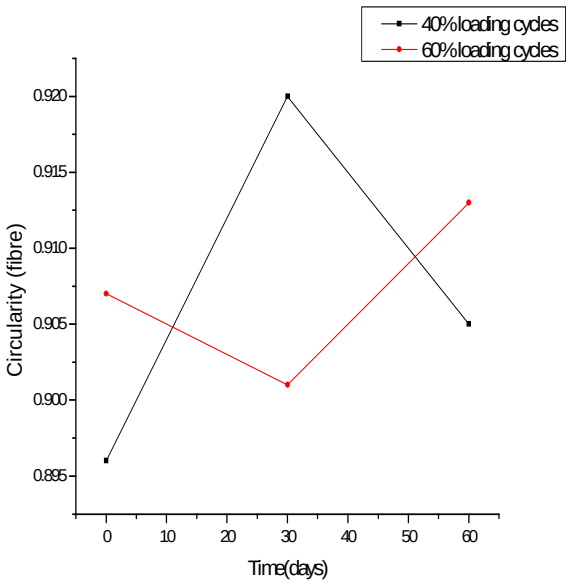

Fig. 6.61 For 55°C Bath (1500X)

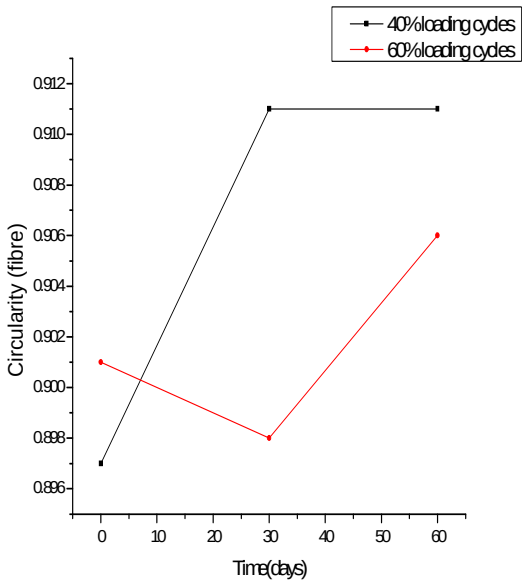

Fig. 6.62 For 55°C Bath (2000X)

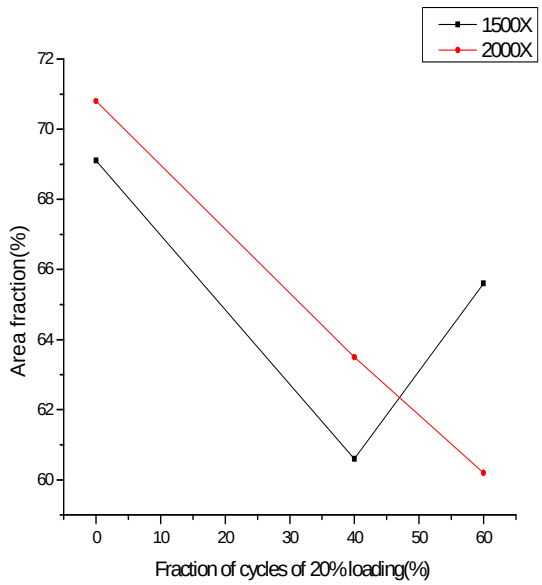

Fig. 6.63 Area fraction vs. loading

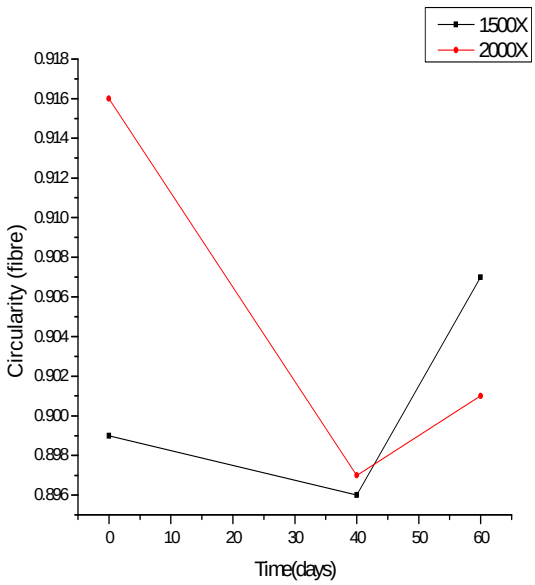

Fig. 6.64 Circularity vs. loading

Table 6.7 Discussion for circularity changes in fibres for the specimen (refer Fig. 6.59 to 6.64):

Loading (%)	Slope (Rate of change of circularity)		Drop	
	55°C bath	45°C bath	55°C bath	45°C bath
60	8.33E-05	0.00005	0.005	0.003
40	0.000233	0.0003	0.014	0.018

From the above data shown in table 6.7, it is clearly shown that not many changes are occurring in the circularity of the glass fibre for the given temperature, time and load conditions. The slight changes in the values are not monotonic in nature and are firstly decreasing and then increasing.

So, longer time periods and load and temperature variations are to be incorporated for getting satisfying results as no predictions could be made from the present results.

6.3 RELATIONSHIP BETWEEN MACROSCOPIC AND MICROSCOPIC BEHAVIOR

6.3.1 Relation between Ultimate tensile load and Micro-hardness (refer Fig. 6.65 to 6.68)

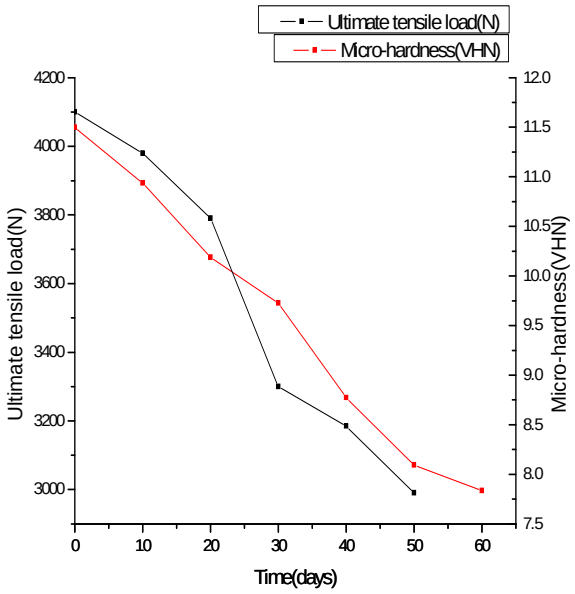

Fig. 6.65 For 40% loading cycles-45°C Bath

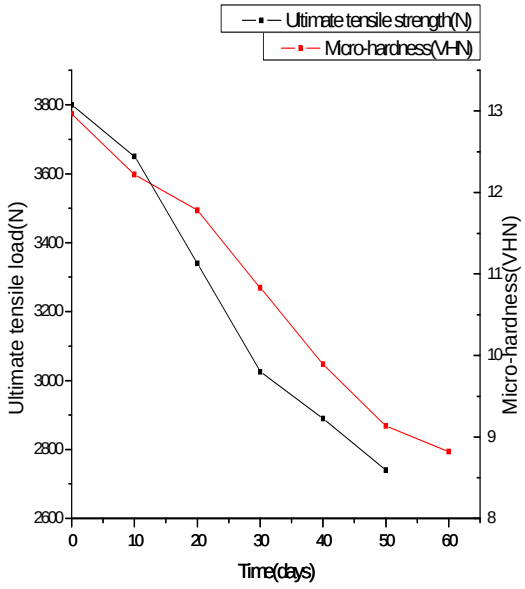

Fig. 6.66 For 60% loading cycles-45°C Bath

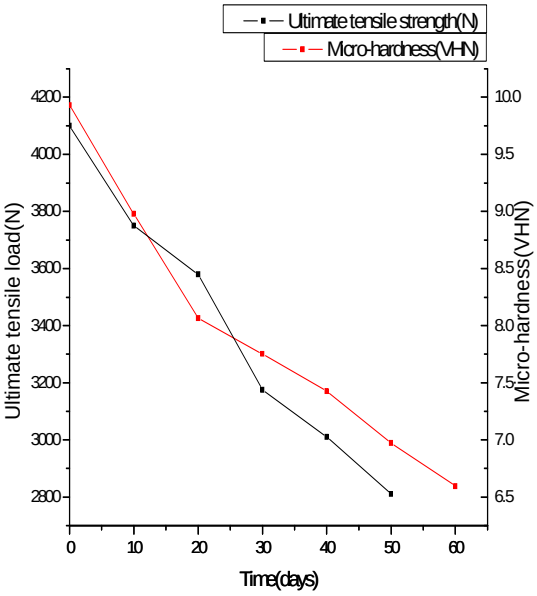

Fig. 6.67 For 40% loading cycles-55°C Bath

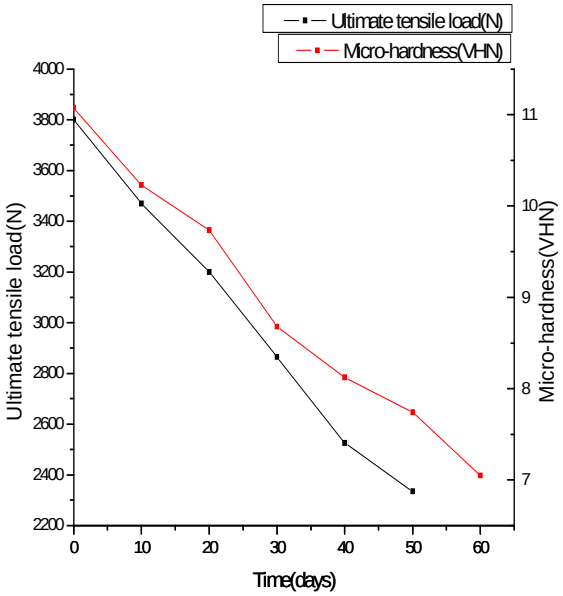

Fig. 6.68 For 60% loading cycles-55°C Bath

6.3.2 Relation between Weight gain and Micro-hardness (refer Fig. 6.69 to 6.72)

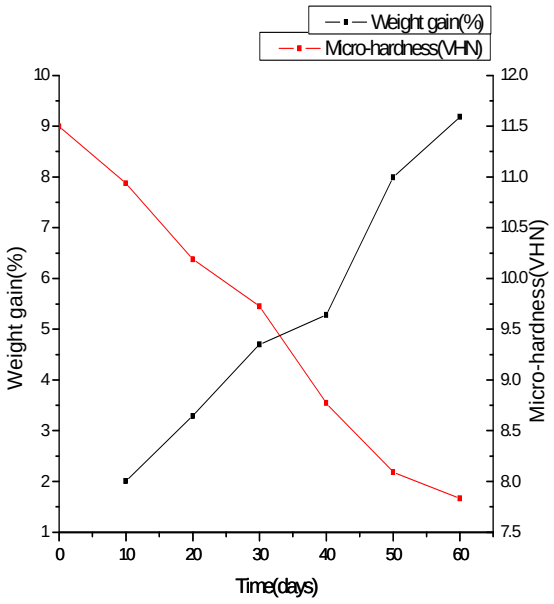

Fig. 6.69 For 40% loading cycles-45°C Bath

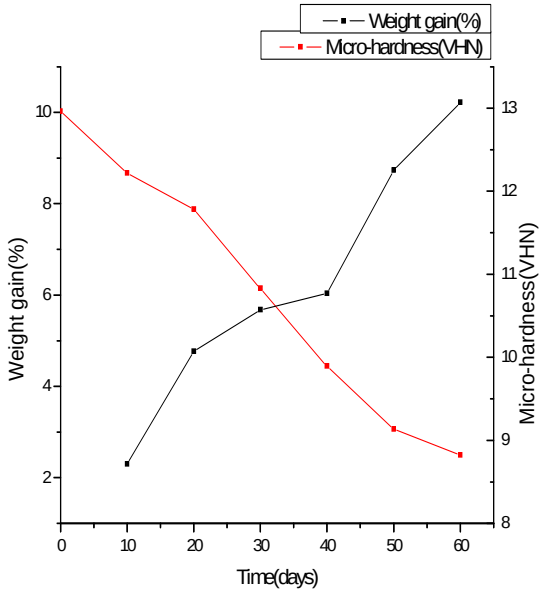

Fig. 6.70 For 60% loading cycles-45°C Bath

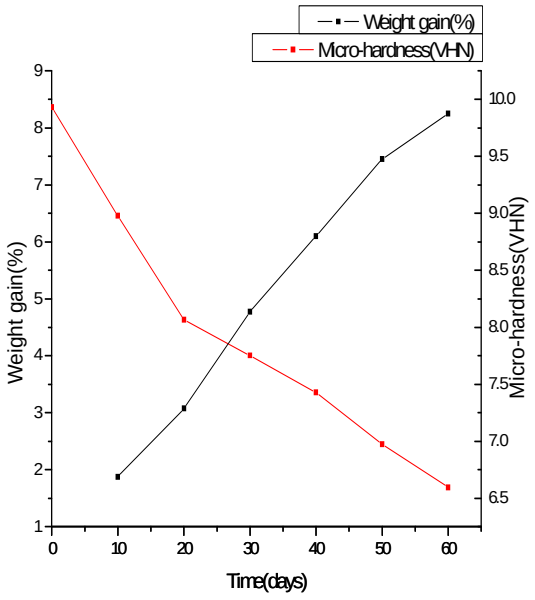

Fig. 6.71 For 40% loading cycles-55°C Bath

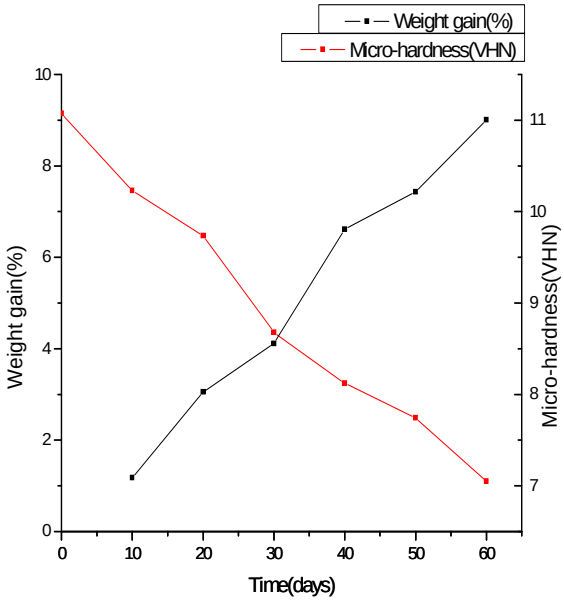

Fig. 6.72 For 60% loading cycles-55°C Bath

6.3.3 Relation between Capacitance and Micro-hardness (refer Fig. 6.73 to 6.76)

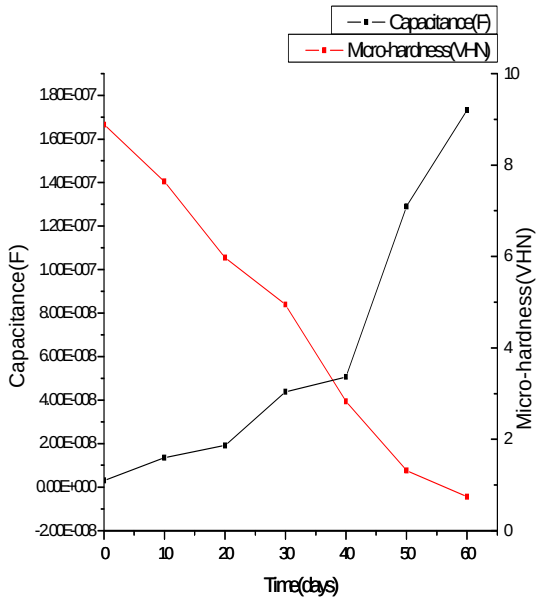

Fig. 6.73 For 40% loading cycles-45°C Bath

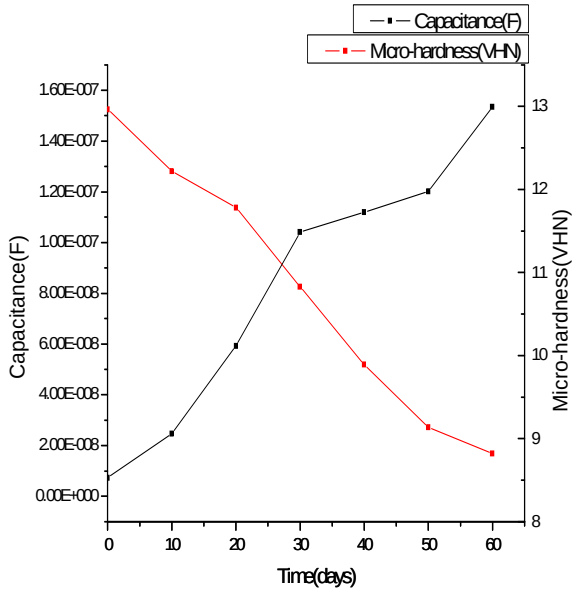

Fig. 6.74 For 60% loading cycles-45°C Bath

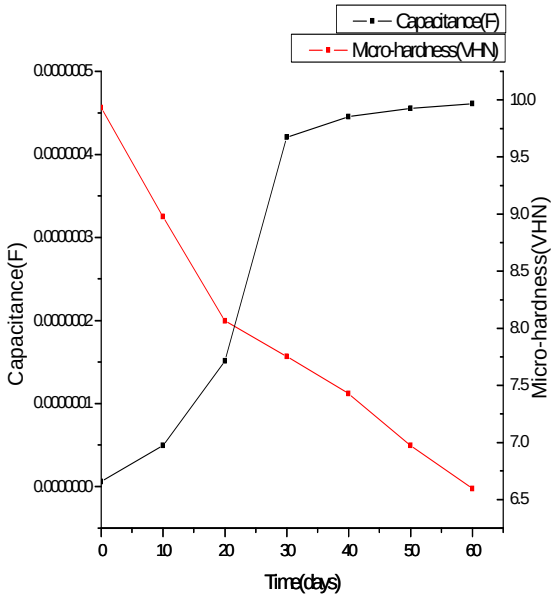

Fig. 6.75 For 40% loading cycles-55°C Bath

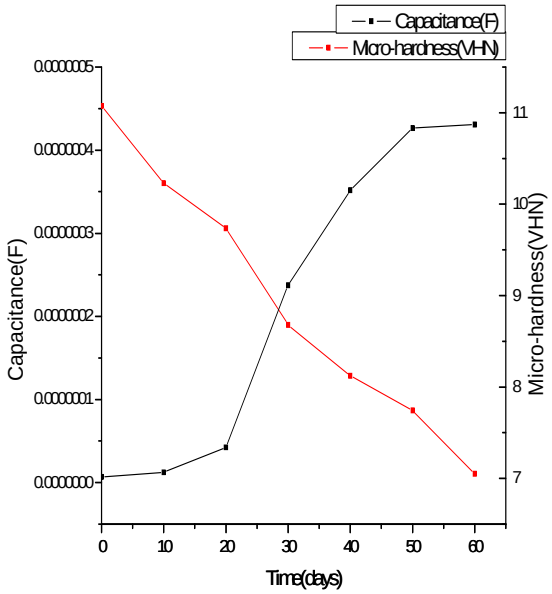

Fig. 6.76 For 60% loading cycles-55°C Bath

6.3.4 Relation between Ultimate tensile load and Area fraction (fibre) (refer Fig. 6.77 to 6.81)

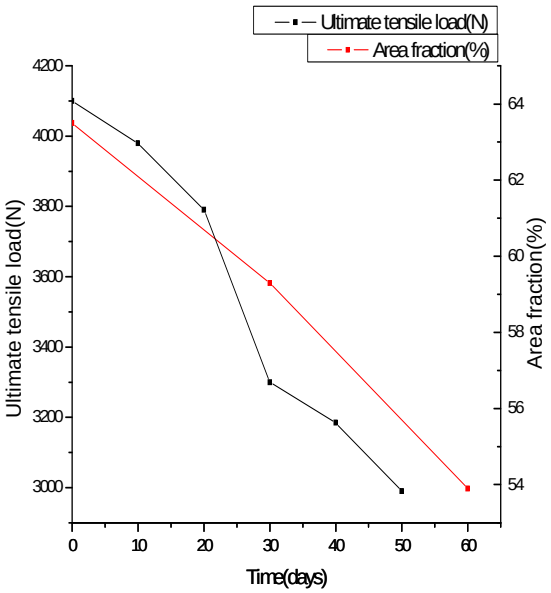

Fig. 6.77 For 40% loading cycles-45°C Bath

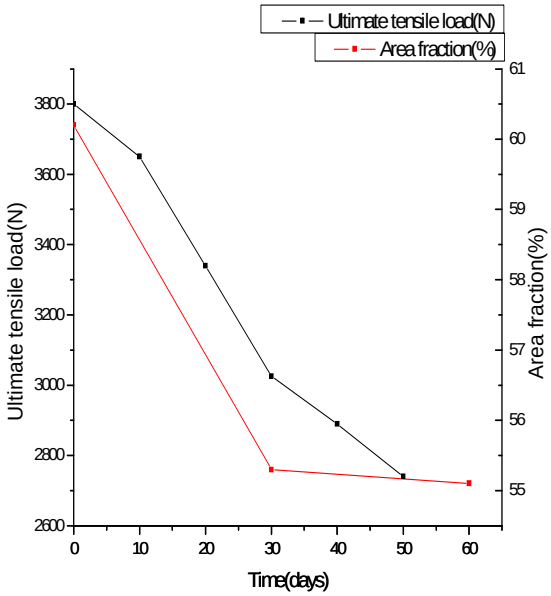

Fig. 6.78 For 60% loading cycles-45°C Bath

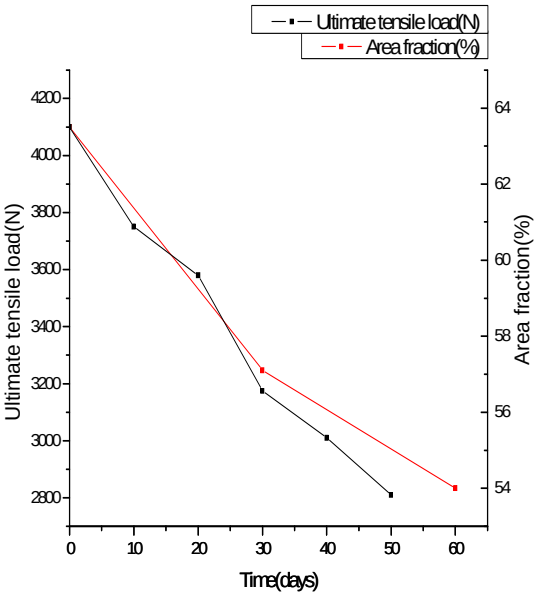

Fig. 6.79 For 40% loading cycles-55°C Bath

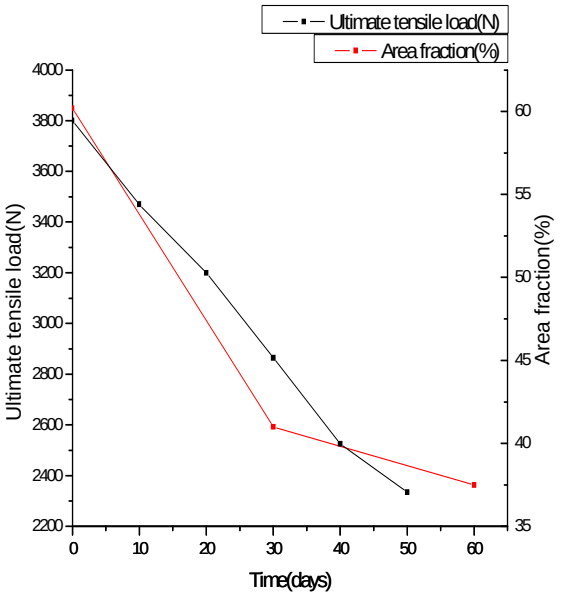

Fig. 6.80 For 60% loading cycles-55°C Bath

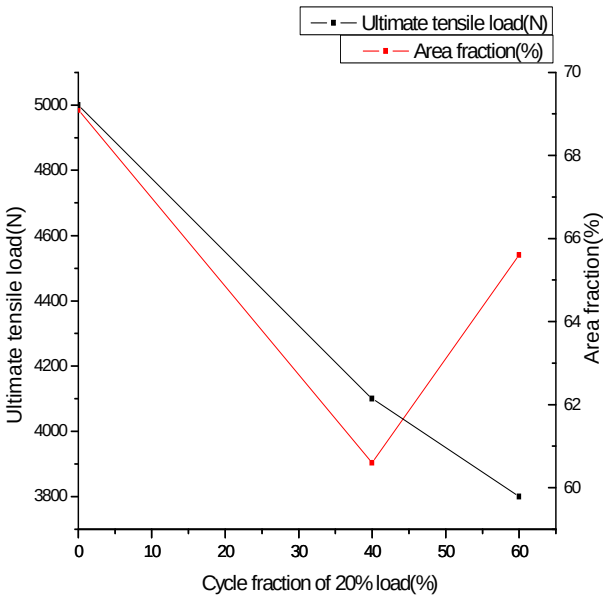

Fig. 6.81 Fatigue loading comparison

6.3.5 Relation between Diffusivity and Area fraction (fibre) (refer Fig. 6.82 to 6.85)

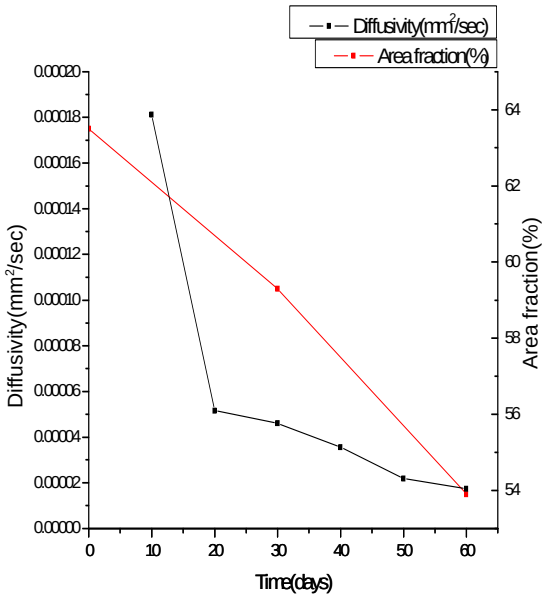

Fig. 6.82 For 40% loading cycles-45°C Bath

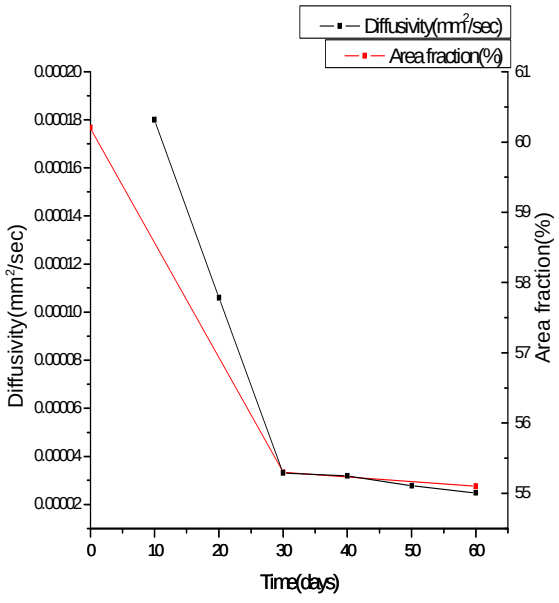

Fig. 6.83 For 60% loading cycles-45°C Bath

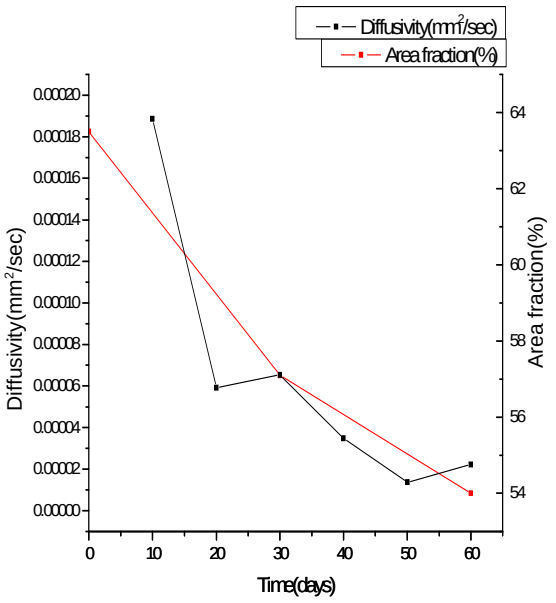

Fig. 6.84 For 40% loading cycles-55°C Bath

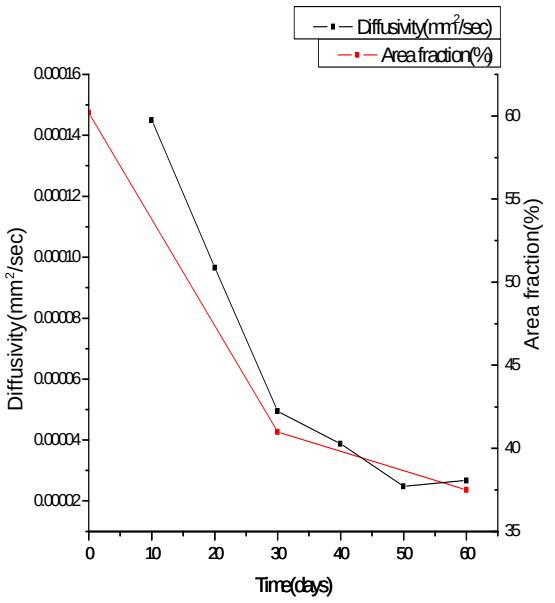

Fig. 6.85 For 60% loading cycles-55°C Bath

6.3.6 Relation between Capacitance and Area fraction (fibre) (refer Fig. 6.86 to 6.89)

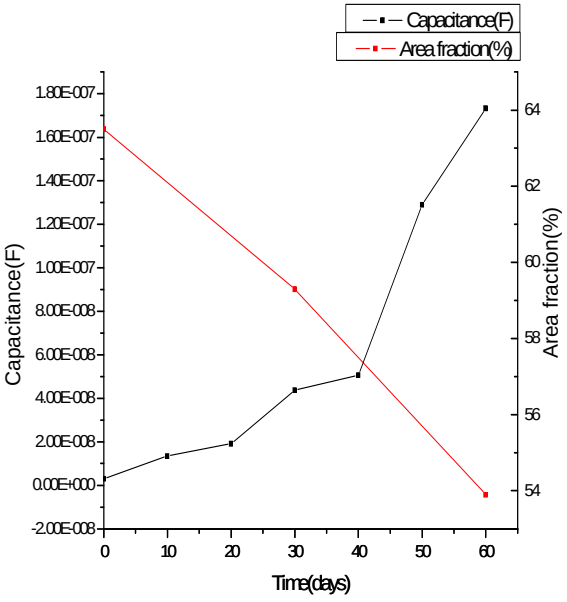

Fig. 6.86 For 40% loading cycles-45°C Bath

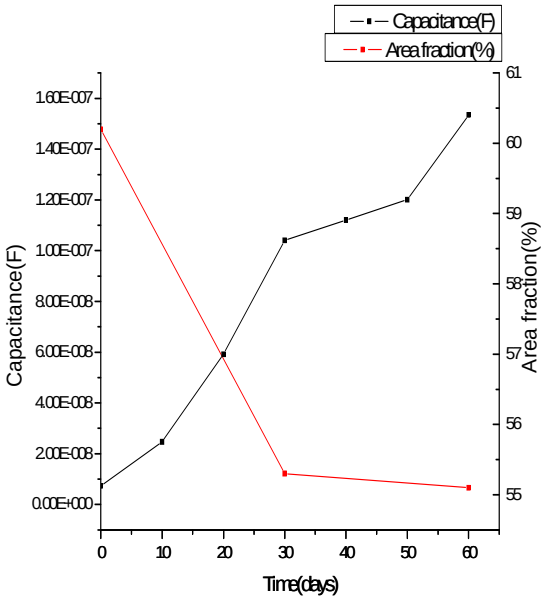

Fig. 6.87 For 60% loading cycles-45°C Bath

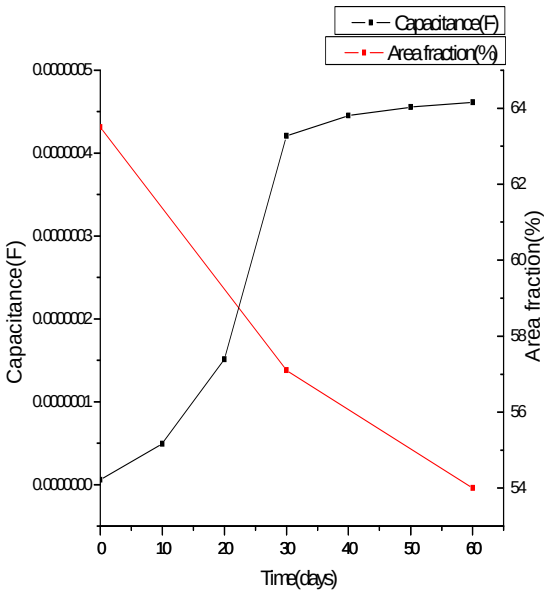

Fig. 6.88 For 40% loading cycles-55°C Bath

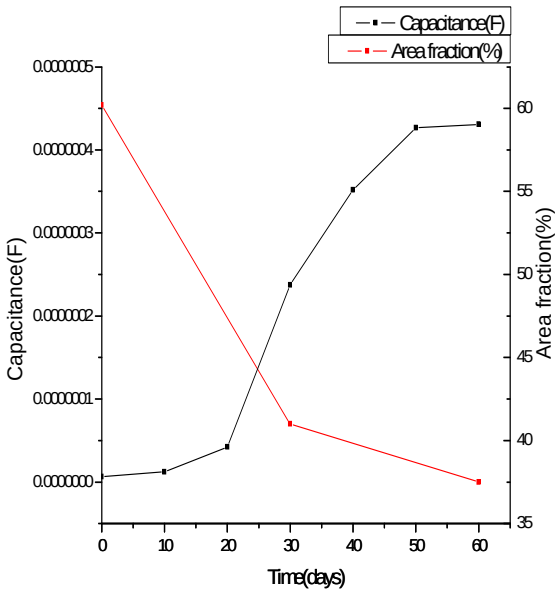

Fig. 6.89 For 60% loading cycles-55°C Bath

6.3.7 Relation between Weight gain and Area fraction (epoxy) (refer Fig. 6.90 to 6.93)

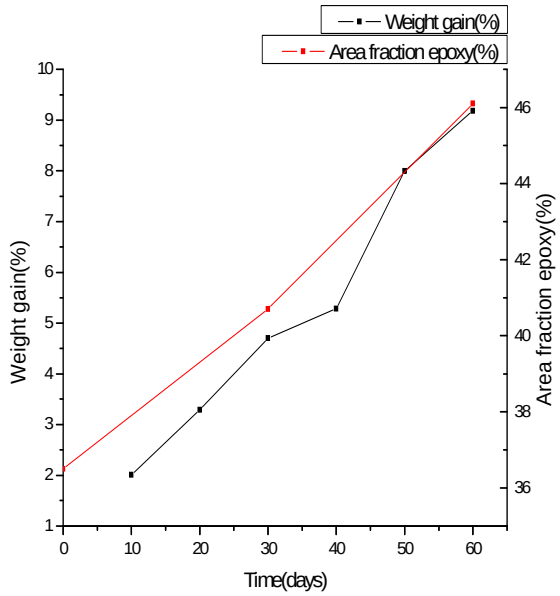

Fig. 6.90 For 40% loading cycles-45°C Bath

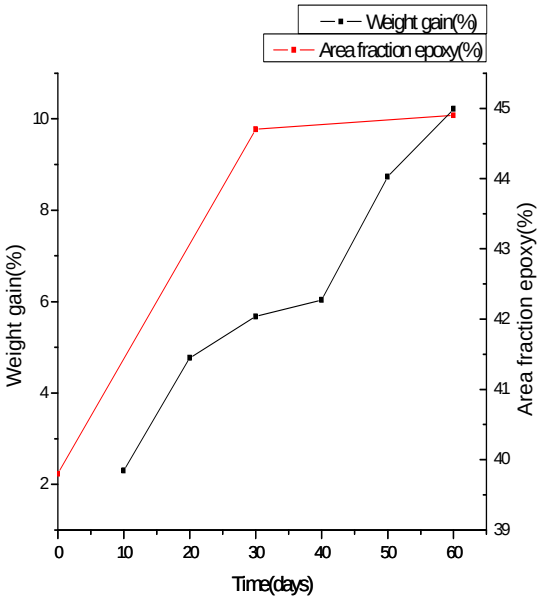

Fig. 6.91 For 60% loading cycles-45°C Bath

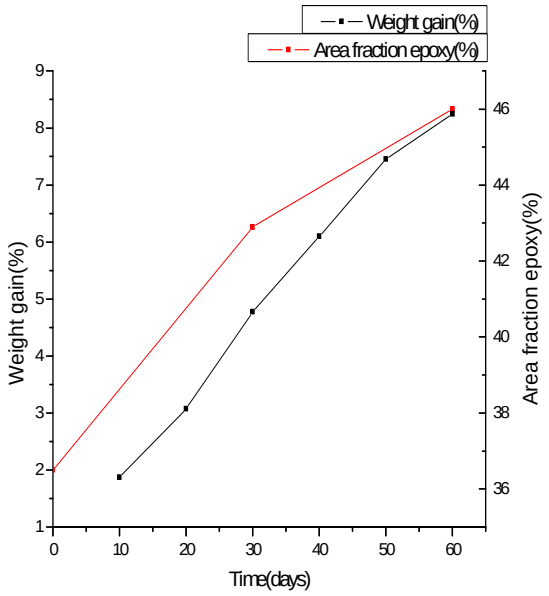

Fig. 6.92 For 40% loading cycles-55°C Bath

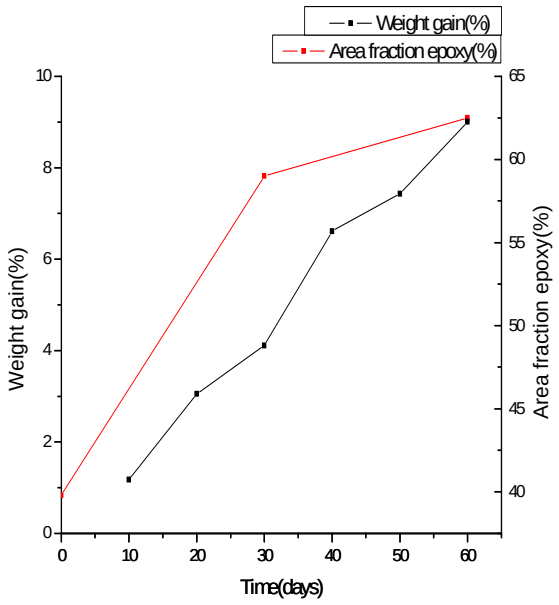

Fig. 6.93 For 60% loading cycles-55°C Bath

6.3.8 Discussion of results for relationship between macroscopic and microscopic properties:

1.) Discussion on the relation between Ultimate tensile load and Micro-hardness (refer Fig. 6.65 to 6.68):

The ultimate tensile load and micro-hardness are both decreasing with time and the nature of decrement is almost same up to the first month but there is a sharper decrease for ultimate tensile load for the second month but the weight gain percentage nature is almost similar.

2.) Discussion on the relation between Weight gain and Micro-hardness (refer Fig. 6.69 to 6.72):

The weight gain and micro-hardness show opposite characteristics to each other. While the weight gain is increasing with time, the micro-hardness is decreasing and the nature of change is found to be almost the same. For the first month the change for the entire specimen is less as compared to higher slope in the second month for both the specimen.

3.) Discussion on the relation between Capacitance and Micro-hardness (refer Fig. 6.73 to 6.76):

The capacitance is also following almost the same path as the weight gain and thus the capacitance is showing a continuous increase with time compared to the micro-hardness nature as discussed earlier.

4.) Discussion on the relation between Ultimate tensile load and Area fraction (fibre) (refer Fig. 6.77 to 6.81):

The ultimate tensile load and area fraction are both decreasing with time and the curves are almost of the same slope up to the first month and after that up to second month the area fraction is showing a lesser slope compared to the ultimate tensile load graph with increasing slope.

5.) Discussion on the relation between Diffusivity and Area fraction (fibre) (refer Fig. 6.82 to 6.85):

The diffusivity and area fraction are both showing a decrease in nature and the curves for both the properties are intersecting at many points showing a relation of similarity in their characteristics except for the specimen at 40% loading cycles at 45°C which is showing a lesser area fraction decrease for the first month.

6.) Discussion on the relation between Capacitance and Area fraction (fibre) (refer Fig. 6.86 to 6.89):

The capacitance and area fraction are both opposite in their behavior with respect to time. The capacitance as discussed in earlier discussions is directly related to the weight gain pattern which is clearly visible here. As the capacitance is increasing with time the area fraction of fibre for all the month and loading is decreasing with time.

7.) Discussion on the relation between Weight gain and Area fraction (epoxy) (refer Fig. 6.90 to 6.93):

The weight gain and area fraction of epoxy both are showing an increase with time but the area fraction of epoxy increment is much more pronounced as compared to the weight gain increase. This shows that with epoxy area fraction increasing the weight gain is also increasing which is due to more water seepage in the specimen and property of the epoxy to absorb more water and swell down easily as compared to fibre.

CHAPTER 7 CONCLUSION AND FUTURE SCOPE

7.1 CONCLUSION:

From the experiments conducted following conclusions have been drawn:

1) The trend of tensile strength for pre-fatigued GFRP specimen is seen to be continuously decreasing with time and this reduction is more pronounced in the second month as compared to the first month.

Also it is seen that with more fatigue cycles of specimen the rate of decrease of tensile strength is more as compared to the specimen with lesser fatigue cycles.

The temperature increment also indicates the accelerated degradation of GFRP specimen i.e. higher the temperature more is the rate of degradation.

2) Further investigation for properties of GFRP is done by measuring micro-hardness of the specimen which shows a slight decrease for the pre-fatigue load being applied but a much noticeable decrement for hygrothermally treated specimen and the minimum hardness is found to be of the specimen dipped in 55°C bath after two month time period.

3) The area fraction of the fibre and epoxy are analyzed using image analysis. The results show an increase in area fraction of the epoxy with increasing time showing a marked increase in second month for the entire specimen at different loadings and temperatures.

4) The change in circularity for the fibres is not much pronounced which is easily noticeable in SEM image of specimen. But some specimen immersed in water tank at higher temperature have shown chipping of edges completely with rest of periphery in quite a circular shape.

5) The percentage weight gain showed an increasing trend with time as expected in both the specimen immersed in water at 45°C and 55°C tank. The weight gain is slightly more in specimen at 55^{o}C compared to specimen at 45^{o}C.Its also seen that with time the diffusivity rate for each specimen is decreasing which is also expected, thus the rate of weight gain is decreasing with time.

6) The capacitance values for specimen is also increasing and following the same pattern as the weight gain trend which is the required criteria and expected result.

7) The study done on the relationship between macroscopic and microscopic behavior shows that the ultimate tensile load is decreasing with almost the same nature as the micro-hardness and the area fraction of fibre.

8) The weight gain and micro-hardness are related and show an opposite nature but its relation with area fraction of the epoxy shows similar nature with both curves intersecting at many points.

9) The diffusivity when compared with area fraction of the fibre show huge similarities in behavior to each other as they both are decreasing with time which are the expected results as the water seepage is decreasing due to saturation.

10) The capacitance is compared with both the micro-hardness and area fraction of the fibre which shows the same behavior with the both as for the weight gain.

7.2 SCOPE FOR FUTURE WORK:

1) The dynamic analysis for GFRP can be further extended with increasing loads applied for cyclic loading.

2) The duration of current experiment can be increased to see the effect in long term.

3) There is lot of scope of improvement in finite element modeling to simulate the results with more accuracy and study effect of various parameters with respect to time.

4) By changing the fibre orientation the change in results with respect to current experimentation can be compared.

REFERENCES

1. www.whitebuffalobeadsandstones.com & www.ia.ucsb.edu
2. www.wikipedia.com/Composite material.html
3. www.structsource.com/pdf/composite.pdf
4. www.emba.uvm.edu/iatridis/me257/Introduction.html
5. www.engr.sjsu.edu/sgleixner/PRIME/FRP.pdf
6. www.autospeed.com/composites.html
7. www.springerlink.com
8. www.sciencedirect.com

9. *www.engineer.tamuk.edu/departments/ieen/faculty/DrLPeel/Courses/Meen3344/Powerpoint_Files/ Chapter_16_avi.ppt*

10. American Institute of Aeronautics and Astronautics- Effects of Glass Fabric and Laminate Construction on the Fatigue of Resin Infused Blade Materials by Daniel D. Samborsky and John F. Mandell

11. A.Mukherjee, S.J. Arwikar (ACI Structural Journal) Title No. 102-S76 [2006]-Performance of externally bonded GFRP sheets on concrete in tropical environments Part I: Structural scale tests.

12. A.Mukherjee, S.J. Arwikar (ACI Structural Journal) Title No. 102-S82 [2006]-Performance of externally bonded GFRP sheets on concrete in tropical environments Part II: Micro structural tests.

13. Abhijit Mukherjee and S. J. Arwikar[2007]-Performance of Glass Fibre-Reinforced Polymer Reinforcing Bars in Tropical Environments-Part I: Structural Scale Tests.

14. Abhijit Mukherjee and S. J. Arwikar[2007]-Performance of Glass Fibre-Reinforced Polymer Reinforcing Bars in Tropical Environments-Part II: Micro structural Tests.

15. D. Olmos, R. Lo´pez-Moro´ n, J. Gonza´lez-Benito[2006]- The effect of the nature of glass fibre surface in the water absorption of glass fibres/epoxy composites was studied.

16. Beckry Abdel-Magid , Saeed Ziaee , Katrina Gass , Marcus Schneider [2005]- The properties of an E-glass/epoxy composite were examined before and after mechanical loading and moisture conditioning.

17. J.M. Ferreira, J.T.B. Pires , J.D. Costa , O.A. Errajhi , M. Richardson [2005]-Fatigue damage and environmental of polyester aluminized glass fibre composites.

18. Tong Yuanjian , D.H. Isaac [2007]- The low velocity impact and tension–tension fatigue behavior of glass fiber reinforced polyester resin composites have been investigated.

19. J.F. Laliberte´, C. Poon , P.V. Straznicky , A. Fahr [2002]- Fiber–metal laminates (FMLs) are a family of hybrid materials currently being considered for use in airframe structural applications.

20. Keiji Ogi , Tetsuro Shiraishi , Hideki Murayama [2006]- This paper presents effect of temperature and after-cure on fatigue fracture behavior in a glass fibre reinforced phenolic resin composite.

21. Ying Shan, Kin Liao [2002]- Unidirectional glass fiber reinforced and glass–carbon fiber reinforced epoxy matrix composite specimen were subjected to tension–tension fatigue in air and in distilled water at 25 °C.

22. Ashcroft, I. A., Abdel Wahab, M. M., and Crocombe, A. D. [2003]-Predicting degradation in bonded composite joints using a semi-coupled finite element method.

23. L.W. Davies, R.J. Day, D. Bond, A. Nesbitt, J. Ellis, E. Gordon [2006]- This paper assesses the use of the Quickstep method for the processing of an epoxy/carbon fibre aerospace material and compares this to equivalent composites produced using an autoclave process.

24. Botelho, E. C., Pardini, L. C., and Rezende, M. C. [2006]-Hygrothermal effects on the shear properties of carbon fibre/epoxy composites.

25. Tumino, G. Catalanotti, F. Cappello and B. Zuccarello[2002]- Experimental tests of fatigue induced delamination in gfrp and cfrp laminates.

26. V. M. Karbhari and S. Zhang [2002]- 2- and 4-layered specimen of E-Glass/Vinylester processing using resin infusion process.

27. Amit Sharma [2009]-Environmental degradation of GFRP in water and NaOH solution.

28. Leon L. Mishnaevsky Jr. [2004]-Three-dimensional numerical testing of microstructures of particle reinforced composites.

29. Benkhedda, A., Tounsi, A., and Adda bedia, E. A. [2007]-Effect of temperature and humidity on transient hygrothermal stresses during moisture desorption in laminated composite plates.

30. V.Alvarez & A.Vazquez [2005]-Effect of Hygrothermal History on Water and Mechanical Properties of Glass/Vinylester Composites**.**

31**.** E. Ahci , R. Talreja [2006]-Characterization of viscoelasticity and damage in high temperature polymer matrix composites.

30. www.selecindia.com/products.php?category=30

31.www.ab.com/industrialcontrols/products/relays_timers_and_temp_controllers/solid-state_relays.html

32. Abaqus User Manual-Getting started with Abaqus-Chapter3-Page3-4
33. www. Wikipedia.com/composites/frp